DSE - Looking for Water

Find groundwater using an autonomous, unmanned aerial vehicle by means of a low frequency electromagnetic field

B. Beijer	1518836	S. Nootebos	4023293
M. den Brabander	1356364	B.J.R. Smeets	1357107
C.D. Dieleman	1506897	V.F. Verschuure	1364383
T.A. Heil	4004876	J. Vink	1514105
A.M.C. Helmer	4020340		

Final Report

Design Synthesis Exercise

TU Delft Delft University of Technology

Faculty of Aerospace Engineering

Version 1.1, January 28, 2014

Change record

Table 1: Change record of the Final Report.

Issue	Date	Pages/sections affected	Brief description of change
0.1	20/01/2014	All	First issue, draft version
0.2	21/01/2014	All	Fixed errors after first quality check
1.0	21/01/2014	All	Fixed errors after final quality check, draft version for handing in
1.1	28/01/2014	Fixed grammar and spelling for all. Content changed or added in chapters: 2, 3, 4.1.1-4. 1.5, 4.4, 5.1, 5.3, 6, 7, 8, 8.7, 10, 11, 12, 13, 14.3; Appendices: D, E, G, H, K	Implemented comments after Final Review. Fixed errors after final quality check, final version for handing in and printing.

Preface

This report comprises the results of group 4 of the Design Synthesis Exercise in the fall of 2013, at the faculty of Aerospace Engineering of Delft University of Technology, Delft. The goal of this exercise is for the students to experience full-time work in a design team, having to meet strict deadlines and to get acquainted with the challenges that emerge during a design project. The team has assumed that the reader has a technical background and is familiar with the field of aerospace engineering. An analysis of the chosen design is performed in the main body of this report, a more extensive technical analysis can be found in the appendices.

We could not have written this report without the help of some other people. Therefore we would like to sincerely thank Joris Melkert, Sjoerd Dijkstra, Erik van der Putte, Artur Palha and Aleix Canet Sentis for their help, guidance and coaching. Furthermore the enthusiasm and advice of Erik van der Horst (MAVlab, TU Delft) was much appreciated and helped us a lot.

January 28, 2014

Group 4 of the Design Synthesis Exercise (fall 2013).

Contents

List of symbols

Symbol	Meaning	Value	Units
A	Aerofoil coefficient		[-]
A	Area		$[m^2]$
A, AR	Aspect ratio		[-]
a	Acceleration		$[m/s]$
B_r	Boom area		$[m^2]$
b	Wing span		[m]
C	Coefficient, 3D		[-]
C	Stability derivative		[-]
CP	Centre of pressure location		[m]
c	Chord length		[m]
c	Coefficient, 2D		[-]
$c_{m_{0.25}}$	Aerofoil moment coefficient at quarter chord		[-]
$c_{m_{LE}}$	Aerofoil moment coefficient at elading edge		[-]
$\bar{c}$	Mean aerodynamic chord		[m]
$\frac{d\epsilon}{d\alpha}$	Downwash derivative		[-]
D	Damping factor		[-]
D	Drag		[N]
d	Diameter		[m]
E	Young's modulus		[Pa]
E	Energy		[W]
e	Oswald factor		[-]
e	Span efficiency factor		[-]
$F_{A_{Y_t}}$	Aerodynamic side force in turn		[N]
F	Force		[N]
g	Gravitational acceleration	9.81	$[m/s^2]$
h	Altitude		[m]
I	Moment of inertia		$[m^4]$
I	Rotational inertia		$[kgm^2]$
I	Conductivity		[S/m]
k	Spring constant		[N/m]
L	Lift		[N]
L'	Lift per unit span of aerofoil		[N]
L_{A_t}	Aerodynamic rolling moment in turn		[Nm]
l	Length		[m]
M	Moment		[Nm]
m	Aircraft mass		[kg]
N_{A_t}	Aerodynamic yawing moment in turn		[Nm]
n	Load factor		[-]
P	Power		[W]
P	Force in x-direction		[N]
P	In-plane force due to boom stress		[N]
P_{crit}	Critical buckling force		[N]
p	Angular velocity over x-axis		[rad/s]
Q_1	Steady-state pitch rate		[rad/s]
Q	Force in y-direction		[N]
q	Dynamic pressure		[Pa]
q	Shear flow		[N/m]
q_{s_0}	Closed section shear flow		[N/m]
R	Radius		[m]
R	Force in Z-direction		[N]
RC	Rate of climb		[-]

Symbol	Meaning	Value	Units
Re	Reynolds number		[-]
R_1	Steady-state yaw rate		[rad/s]
r	Distance to obstacle		[m]
S	Surface area		[m^2]
S	Shear force		[N]
s	Change in length		[m]
T	Thrust		[N]
T	Torque		[Nm]
T_s	Torque on cross-section		[Nm]
t	Time		[s]
V	Velocity		[m/s]
W	Aircraft weight		[N]
X	x-coordinate		[m]
x	x-coordinate		[m]
y	y-coordinate		[m]
z	z-coordinate		[m]
α	Angle of attack		[rad]
β	Side-slip angle		[rad]
Γ	Circulation over aerofoil		[m^2/s]
γ	Flight path angle		[rad]
δ	Control surface deflection		[rad]
ϵ	Downwash angle		[rad]
η_0	Arm from horizontal shear force to moment point		[m]
η_r	Arm from boom horizontal force to moment point		[m]
η	Location of aileron		[m]
η	Efficiency		[-]
θ	Camber line slope		[rad]
$\ddot{\theta}$	Pitch acceleration		[rad/s^2]
λ	Taper ratio		[-]
μ	Viscosity of air		[-]
ρ	Air density	1.225	[kg/m^3]
Φ	Bank angle		[rad]
ϕ	Bank angle		[rad]
σ	Normal stress		[N/m^2]
τ	Shear stress		[N/m^2]
ξ	Angular resolution		[°]
ξ_0	Arm from vertical shear force to moment point		[m]
ξ_r	Arm from boom vertical force to moment point		[m]
ψ	View angle		[rad]

Subscripts	Meaning
C	centrifugal
A	aircraft
a	aileron, available
$A-h$	Aircraft minus horizontal tail
cruise	in cruise condition
ac	aerodynamic centre
b	basic
br	brake
c	cone
cg	centre of gravity
D	drag of wing
d	drag of aerofoil
e	elevator
eff	effective
g	gravity
h	horizontal stabiliser

Subscripts	Meaning
i	impact, inner, induced
j	propulsive
L	lift of wing
l	lift of aerofoil
m	moment
N	normal force of wing
n	nosecone
o	outer
p	parachute, propulsive
r	rudder, required, root, rubber
s	spring
t	total, turn
stall	for stall condition
TO	take-off
v	vertical stabiliser
w	wing
x	in x-direction / about x-axis
xp	centre of pressure
y	in y-direction / about y-axis
z	in z-direction / about z-axis
α	(with respect to) angle of attack
0	maximum
∞	freestream

List of abbreviations

AACS	Attitude and Altitude Control (Sub)System
CAS	Collision Avoidance (Sub)System
CCD	Charge-coupled Device
c.o.g.	centre of gravity
EASA	European Aviation Safety Agency
EU	European Union
FAA	Federal Aviation Authority
FBS	Functional Breakdown Structure
FEM	Frequency ElectroMagnetics
FFD	Functional Flow Diagram
FPP	Flight Plan Processor
GPS	Global Positioning System
GSA	Ground Sample Area
HLDs	High-Lift Devices
HP	Horse Power
IMU	Inertial Measurement Unit
IR	Infrared
ISA	International Standard Atmosphere
NAS	National Airspace System
PIC	Pilot In Command
RPM	Revolutions per Minute
SAC_EC	Special Airworthiness Certificate - Experimental Category
SM	Safety margin
SRTM	Shuttle Radar Topography Mission
SSC	System Status Check
UA	Unmanned Aircraft
UAV	Unmanned Aerial Vehicle
UAS	Unmanned Aerial System
USA	United States of America
WPAN	Wireless Personal Area Network

Division of contents

Table 4 contains the division of the content in this report by the team members involved.

Table 4: The division of contents for the final report.

Name	**Responsible for**
B. Beijer	Performance analysis, cost analysis, sensitivity of design, electrical systems, communication flow diagram, resource allocation and budget breakdown, verification and validation of performance, design optimisation
M. den Brabander	Structural analysis, verification and validation of structural analysis, configuration and layout, take-off and landing design (including all calculations), CATIA modelling of the take-off system, manufacturing and assembly, D&D-logic plus Gantt chart, autopilot systems and sensors, discussion and recommendations
C.D. Dieleman	Abstract, requirements, aircraft external systems, data handling & communication flow, take-off and landing performance, cruise performance, manoeuvring performance, risk analysis and mitigation, cost breakdown structure, cost estimation, FFD, FBS, aerodynamic analysis, verification and validation of aerodynamics, editing
T.A. Heil	Configuration and layout, measurement methodology, take-off and landing, electrical block diagram, sensitivity analysis, design optimisation, design decision justification, data exchange management, conclusion
A.M.C. Helmer	System functions, Configuration and Layout, Operations and logistics (including calculations), Non-CATIA illustrations, Control and Stability analysis
S. Nootebos	Quality control, Aircraft geometry, Sustainable Development Strategy, Performance and limitations, Aerodynamics analysis, Verification and Validation of Aerodynamics
B.J.R. Smeets	Structural analysis, structural analysis verification and validation, configuration and layout, take-off and landing design, manufacturing assembly and integration, CATIA modelling of the vehicle, UAV regulations, conclusion
V.F. Verschuure	Aircraft geometry and structure, Aircraft internal and external systems, Data handling and communication flow, Performance and limitations, Performance analysis, Quality control
J. Vink	Introduction, Preface, Control & Stability, Control & Stability verification and validation, Sensitivity analysis, Market analysis, Compliance matrix, Regulations, Design optimisation

Abstract

A lack of water to meet daily needs is a reality for one in three people around the world (WHO, 2009). Not only is this currently a huge problem, but also globally the problem is getting worse as cities and populations grow and the needs for water increase in agriculture, industry and households. Over the last few years several solutions have been developed to pump and desalinate water, but one part of the problem still persists; no one knows where to look for water.

At the faculty of Civil Engineering and Geosciences an instrumentation package is being developed to map groundwater with the use of Frequency Electromagnetics (FEM), but current solutions that can carry this package are either expensive (helicopters) or unpractical (handheld/walking). To solve this problem a purpose-build vehicle has been designed. This report covers the characteristics and specifications of that vehicle and elaborates on the design choices that were made leading to this design. Previous steps of the design process can be found in the Project Plan [1], the Baseline Report [2] and the Mid-term Report [3].

The top level requirements state that the final design has to carry the FEM measurement package, perform measurements with an acceptable resolution and should be operable in a foolproof way in all kinds of environments. Also, the vehicle has to comply with UAV regulations that apply. Preferably, it costs less than €10,000 and flies autonomously.

The designed UAV is called the *SkyDowser* and is a small aircraft with top mounted wings and a combustion engine in the front that drives a propeller. It has a T-tail and a fuselage, which is sized to house the avionics. The wing span is 3.5 m, the length of the fuselage is 2.0 m and the entire aircraft weighs only 12.5 kg. The measurement package is located in the wing, with the measurement coils 2.4 m apart.

The aircraft is mainly constructed out of fibreglass-composite and has easily detachable wings and tail for easy transportation. Moreover, the wings, containing the measurement package, can be used as a handheld device for more resolved measurements.

The SkyDowser takes off with the use of a catapult system with elastic bands and lands using a parachute. This makes the UAV suitable for take-off and landing in any type of environment.

The UAV can scan over 29 km^2 per day using one litre of gasoline per day. It flies autonomously, based on (predefined) waypoints and has a stereoscopic camera system on board to detect and evade obstacles. The unit price of the UAV is estimated at €6,500, not taking into account the development costs of the SkyDowser. Including the development costs the scan price is approximately €7 per square kilometre.

In order to construct the final design, analyses were performed in the fields of aerodynamics, performance, structures and control & stability. Next to the analyses, a technical risk assessment was performed to detect the largest risks and mitigate them and an analysis has been made to check the sensitivity of the design to changes in important parameters.

A market analysis and cost breakdown structure were made to give insight in the costs of the project. The project will require a total investment of €18.1 million to operate 100 UAVs for 5 years, with 180 operational days per year. An analysis of the future development concludes the design project. Future development will include more extensive technical analyses, prototype testing and manufacturing. Finally, interesting design options have been identified and are mentioned as future recommendations.

Chapter 1

Introduction

"Water is an essential resource for life and good health. A lack of water to meet daily needs is a reality today for one in three people around the world. Globally, the problem is getting worse as cities and populations grow, and the needs for water increase in agriculture, industry and households." [4]

In recent years, multiple systems have been developed at Delft University of Technology that can pump and desalinate groundwater. However in interior regions, where no sea water is available for desalination, the remaining challenge is to locate these underground water reservoirs. The faculty of Civil Engineering and Geosciences is developing an instrumentation package that can detect groundwater, carried out at the request of Sjoerd Dijkstra, CEO of the Winddrinker. Current instruments are either expensive to operate, or unable to scan large areas. This new instrumentation package is able to overcome these drawbacks if carried by a cheap and reliable aircraft. Therefore mr. Dijkstra has requested the design of an unmanned aircraft that can carry the instrumentation package. This project aims to design such an aircraft. The aircraft should be able to scan at least 10 square kilometres per day and provide a stable measurement platform such that accurate measurements can be taken. The objective of this project can be described as: *Develop an unmanned aerial measurement platform capable of finding ground water in remote areas, within a budget of preferably €10,000, by 9 students in 10 weeks time.*

In this report the aircraft that has been developed will be discussed. The requirements of the mission will be discussed in chapter 2. The requirements from regulations are also included. In chapters 3 and 4 the configuration and layout of the aircraft will be explained. For each part of the design it will be explained why this specific solution was chosen. Furthermore, in chapter 5 the performance and limitations of the design will be discussed. Chapter 6 then shows the sensitivity of the design to certain changes.

In the following chapters, important characteristics of the aircraft are discussed. The approach towards manufacturing and assembly is explained in chapter 7. The operational characteristics of the design are described in chapter 8. Furthermore an overview of mass, power and fuel budgets is given in chapter 9. Also the possible technical risks and the plan to mitigate these risks is discussed in chapter 10. Based on the configuration and system description explained earlier, the sustainable development strategy is presented in chapter 11.

Chapter 12 gives the cost breakdown structure. Finally a market analysis is performed, of which the results are shown in chapter 13. In chapter 14, the compliance of the design with the requirements as discussed in chapter 2 is evaluated. Finally the conclusion of this project is presented, as well as a discussion on the results.

Supporting calculations for the decisions made in this report can be found in the appendices.

Chapter 2

Requirements

As stated in the Project Guide[5] *"the ultimate goal of this project is to develop an UAV(...)"*. However, the total project also has a clear final goal: Be able to scan the Earth's land surface within a reasonable time to find underground water and contribute to the world's need for drinking water.
To meet these goals a number of requirements were set at the beginning of the project. These are divided in top level requirements and additional detailed requirements. The additional detailed requirements are not hard constraints, but they should be a guideline and can bring the final goal closer if they are met. There are also measurement requirements, stated under one of the top level requirements. These are requirements that follow from the way the measurement package works.

Top level requirements:

- The UAV must carry a measurement package consisting of:
  - Three coils
  - A processor
  - A battery
  - Two inclinometers
  - A magnetometer
  - An altimeter
- The measurement package must be able to perform measurements at an resolution of at least 10 m, see section 8.7 for details. This can be done by:
  - Placing the coils a minimum of two meters apart.
  - Not flying faster than 30 m/s.
  - Fly at a fixed, low altitude above the ground, with a maximum of 30 m.
  - Ensure that the receiver coils are on the same axis as the transmitter coil and have the same orientation.
  - Ensure that the difference in twist angle between coils should not be more than 3°.
- A calibration measurement must be performed.
- The UAV should be foolproof.
- The UAV should be able to operate in all kinds of different climate circumstances.
- The UAV should be able to take off and land in all kinds of environments and in remote areas.
- The UAV should comply with worldwide UAV regulations.

Additional detailed requirements:

- The UAV should have a unit price of €10,000 or less.
- The UAV should scan at least 10 km^2 a day.
- The UAV should fly as autonomously as possible.
- The UAV should be able to fly for two hours continuously or more.
- The UAV should be easy to manufacture and should have a modular design for easy maintenance.

Not all of these statements are hard constraints, but they form a reference for some of the design factors. During the final design phase some of the design choices were based on these requirements.

Next to the requirements set by the customer, there also are requirements set by UAV regulations. These regulations are discussed in appendix B on page 70. An overview of the requirements on the design due to regulations is given here.

- The UAV has to be within visual line-of-sight (VLOS) of an observer.
- The UAV has to be within a maximum distance from the observer of 500 m.
- A observer needs to have the ability to manually control the UAV, in case of emergencies.

- The UAV velocity should not exceed 36 m/s.
- The UAV operating mass should not exceed 150 kg.

The UAV will have to comply with these regulations to assure that missions can be performed anywhere around the world.

Chapter 3

Introduction of the SkyDowser

Now that the requirements for the aircraft have been stated, the results of the design analysis are presented in this section. Here, the final version of the UAV is presented; the SkyDowser. In figure 3.1 the SkyDowser can be seen, including the main internal systems. A summary of the aircraft characteristics is presented here, for a clear overview of the capabilities of the SkyDowser.

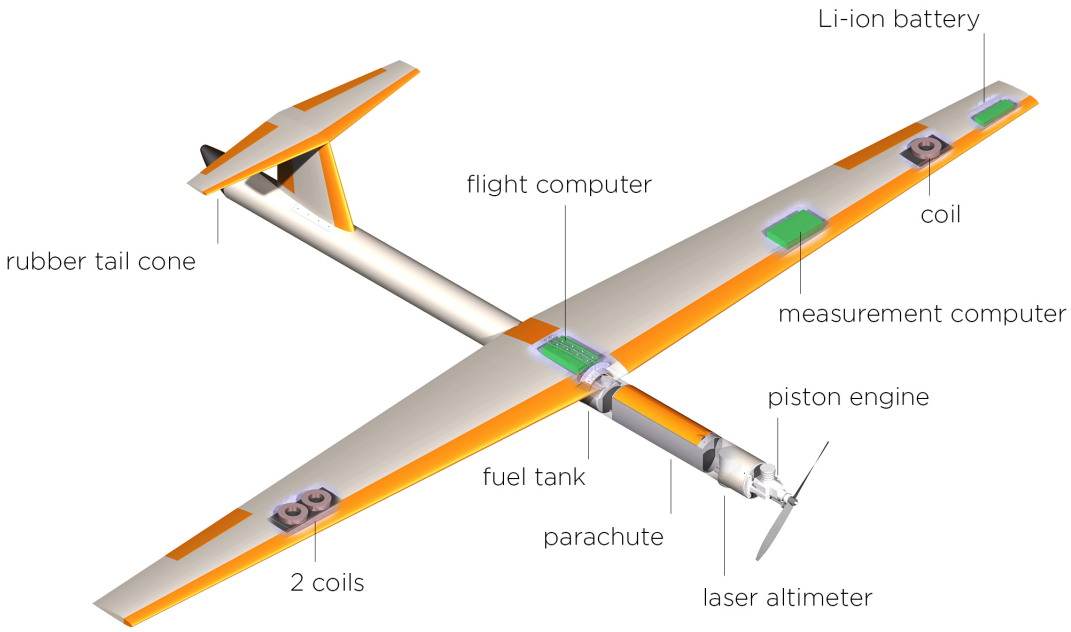

Figure 3.1: Overview of the final design of the SkyDowser, including main internal systems.

The SkyDowser has a mass of 12.5 kg, and a wingspan of 3.5 m to produce sufficient lift to carry this mass. Launched from a catapult, the SkyDowser can be operated from nearly every terrain. A piston engine propels the aircraft, flying at a cruise velocity of 25 m/s. At this speed it is capable of flying 720 km per day, on a single fuel tank of 1.7 L. With the use of the coils in the wings, the SkyDowser scans an area of 29 km^2. At the end of its mission the SkyDowser lands using an on-board parachute. It lands on a rubber tail cone, to protect the fibreglass aircraft against impact damage. The unit cost of the SkyDowser is €6,500, not taking into account development cost). With development cost taken into account, the unit price of the SkyDowser is €18,500, resulting in an operational cost of approximately €7 per scanned km^2.

In this part the detailed results of the analysis of the SkyDowser is presented, explaining the reasoning behind all design choices.

Chapter 4

Configuration & layout

In this chapter the configuration and layout of the SkyDowser is elaborated. Here mostly results are discussed, and justification of the design choices made. First the aircraft geometry is discussed, followed by the main systems. Next both the internal and external systems of the SkyDowser are discussed, providing a clear overview of the system configuration. Finally, the data handling and communication flow is presented.

4.1 Aircraft geometry & structure

4.1.1 Wing

The SkyDowser generates its lift using the wing that acts as a lifting surface. The fairly common NACA-2412 aerofoil has been used as a profile throughout the entire wing, see figure D.1 on page 74. It is an aerofoil with a simple geometry that performs well at low speeds. It has a high lift coefficient (1.94) at high angle of attack, sufficient drag capabilities and is easy to manufacture because of the lack of a double camber line or even reflex camber. Because of the low operating altitude the deposit of dust and insects can influence the performance of the wing. Also, the chosen aerofoil is relatively insensitive to roughness on the aerofoil. There are some aerofoils that have better drag capabilities. For instance the NACA $63_1 - 412$ has a so-called drag bucket which gives the profile a low drag for a range of range of lift coefficients. This is interesting for aircraft with high fuel fractions. However, since the aircraft has a small fuel fraction, this more complicated aerofoil, which increases the manufacturing cost, is not worth the gain in drag performance, hence the chosen NACA-2412 is suitable.

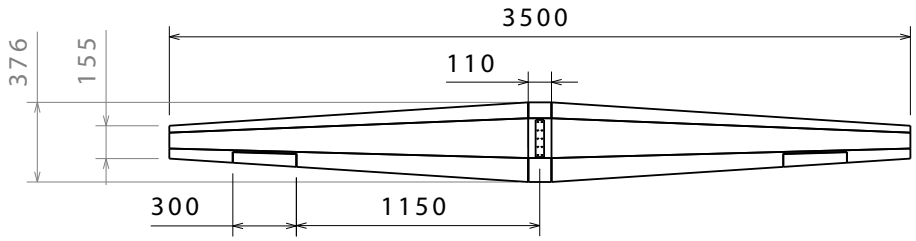

Figure 4.1: Top view of the main wing. Dimensions are in mm.

For a particular aerofoil the surface of the wing is mainly determined by the weight and the velocity of the vehicle. From the aerodynamic simulations in appendix D.1 (page 73) it was determined that a surface of 0.92 m^2 is necessary for a design lift coefficient of 0.4. This design lift coefficient was chosen to keep the wing size low enough to keep the weight at a reasonable level. For aerodynamic reasons, both a large aspect ratio and span are desirable, but due to the frequent transport in cars, handling qualities limit the wing span. Furthermore the structure gets heavier when elongating the wing. The compromise has resulted in a span of 3.5 m. With an aspect ratio of 13.3 this comes down to an average chord length of 0.26 m. To ensure a low induced drag, a taper of 0.4 has been chosen. The consequential dimensions have been depicted in figure 4.1.

The wing has no sweep, since this is only beneficial at higher operating velocities and only increases the manufacturing costs of the structure. Next to that sweep increases the stall velocity, thus the take-off and

landing speed. This means the launching system needs to provide a higher velocity, increasing its complexity, thus it's cost. Also, the probability of a failed launch increases, because of the increases speed. The same goes for winglets; they offer no significant advantage at these low velocities and thus only add structural weight.

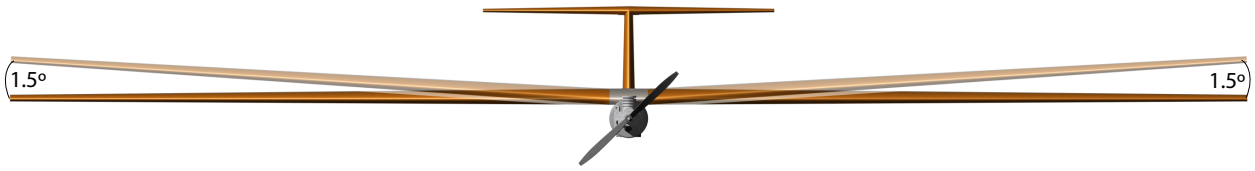

Figure 4.2: Deflection angle of the wingtip.

The load bearing structure in the wing is a wing box, which contains some of the electronics and the coils. See figure 4.2. Since the angle between the coils must not exceed 3° (1.5° upwards and 1.5° downwards), a closed structure is chosen, since a closed structure performs well under torsion. Another advantage is that control surfaces can easily be connected to the rear spar of the wing box. Since bird strikes are very likely at only 30 metres altitude, the risk of damaging the load bearing structure needs to be avoided. This is why a D-nose structure is also abandoned. The upper and lower parts of the wing box do not have extra skin on top, which effectively means that a double spar solution with load bearing skin is used. To prevent failure in buckling, stringers are required. Over part of the wings length, 4, 2 and 1 stringer(s) are placed subsequently. This option resulted in a lighter option than increasing the wing box thickness. The wing is top mounted with respect to the fuselage. The main reason for this is increased stability in lateral direction, since the centre of gravity is positioned below the aerodynamic centre of the wing. See figure 4.3 on page 111 for an overview of this.

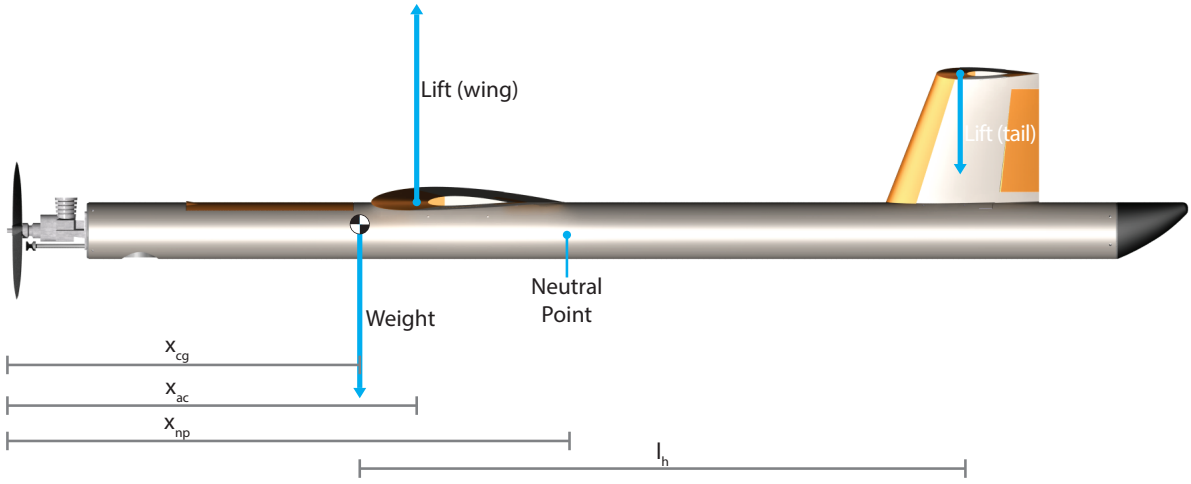

Figure 4.3: Free Body Diagram of the aircraft in cruise. Forces are not to scale.

To be able to roll the aircraft during flight, ailerons have been placed on the trailing edge of the wing. The rolling moment, which they can produce, varies linearly with distance from the centre of gravity, so they have been placed as far outboard as possible, keeping in mind that the local structural elements should be able to cope with the loads induced by the control surface. Also, the lifting efficiency of the wing decreases towards the wingtip, thus placing ailerons at the very tip is not possible. The ailerons have been sized for an evasive manoeuvre. In case the vehicle approaches an object, that is too high to fly over, a turn needs to be initiated to avoid crashing into the obstacle. The calculations can be found in appendix F.2.2 on page 88. High-lift devices (HLDs) have not been implemented since they are generally expensive, heavy and can be avoided by using a sufficiently large wing and take-off velocity. This saves in structural weight and costs, which is favourable.

4.1.2 Empennage

The main part of the empennage consists of the T-tail. The vertical part of the T-tail provides lateral stability and the top mounted horizontal part gives longitudinal stability. The dimensions of the T-tail are shown in figure 4.4. It is beneficial to have the horizontal stabiliser at the top of the tail and not directly attached to the fuselage, such that in this position the horizontal tail is not affected by the wake of the main wing during all flight conditions. The height of the rudder is designed as such that the horizontal stabiliser will not be in the wake till 14° angle of attack. A symmetrical aerofoil with a NACA-0012 profile, as depicted in figure D.2. The horizontal stabiliser produces negative lift, which is needed to counteract the moment of the lifting force of the main wing about the centre of gravity in x-direction of the aircraft. Since this is a symmetric aerofoil the stabiliser must be placed under a negative angle of attack to ensure a negative lift force. The downside of having a tail with negative lift is that the surface of the main wing needs to be larger with respect to the wing of a tandem wing configuration.

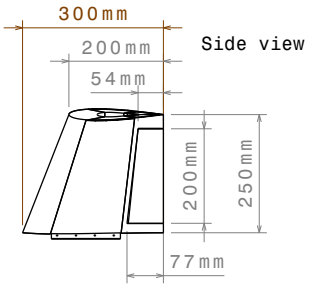

Figure 4.4: Side view of the vertical stabiliser, with the horizontal stabiliser mounted on top.

Horizontal stabiliser

The horizontal stabiliser has been sized using the scissor-plot method, as described in appendix F.1 on page 87. The centre of gravity and tail surface have been chosen such that the SkyDowser is very stable. Because of this, the manoeuvrability decreases, since a larger force is needed to generate a sufficiently large pitching moment. With the measurement system in mind, a stable aircraft is preferred over a controllable, but less stable one, since the measurements have to be done at a constant height and velocity. A technical drawing of the result is displayed in figure 4.5.

In order to longitudinally control the aircraft during all flight situations, elevators have been placed on the horizontal stabiliser. Whereas for regular aircraft these are sized to provide rotation at take-off [6], the elevators of the SkyDowser have been sized for a vertical evasive manoeuvre (similar to the ailerons for a horizontal evasion), since the vehicle is launched by catapult at an angle of 15°. As will be discussed in section 5.1 the vehicle needs to be able to climb 30 m in 110 m horizontal distance. To perform this climb a climb angle of 15° is needed. In order to fulfil this requirement, the size of elevators has been determined. The calculations regarding the horizontal stabiliser can be found in appendix F.2.1 on page 88.

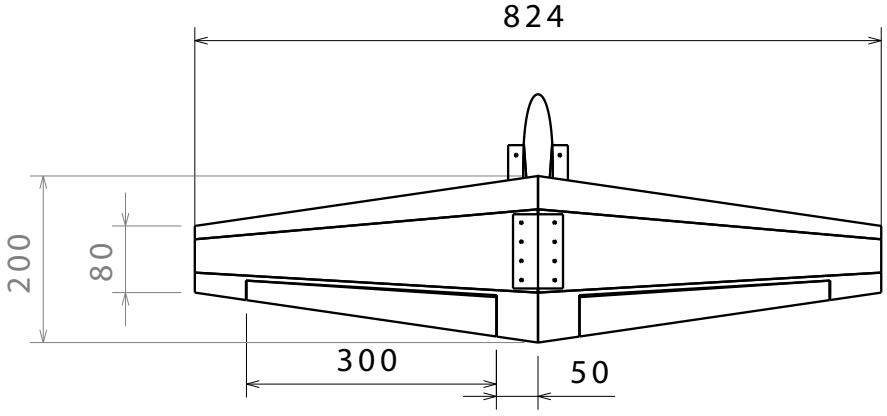

Figure 4.5: Top view of the horizontal stabiliser. Dimensions are in mm.

Vertical stabiliser
The vertical stabiliser is sized mainly based on two drivers: the necessary height to assure the horizontal tailplane will not lie in the wake of the main wing (figure 4.6) and to provide a suitable vertical surface for the rudder. The second driver is implemented as a check after the dimensions of the rudder have been determined. The rudder can be sized for different requirements. For remote controlled and model aircraft the most critical flight condition is the coordinated turn [6]. Such a turn is achieved by deflecting both the aileron and rudder. Therefore, the rudder of the SkyDowser has been sized for this flight condition. The coordinated turn has a couple of advantages, such as no slipping, constant turn radius and constant turn rate. It is achieved by using a simultaneous deflection of the rudder and the ailerons. The final dimensions of the vertical stabiliser and rudder can be found in figure 4.4.

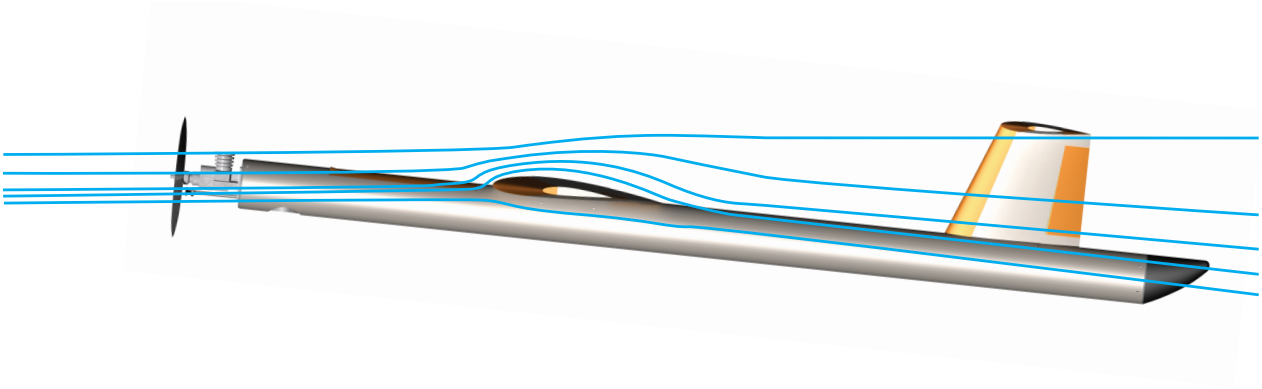

Figure 4.6: Impression of the wake of the wing and its effects on the horizontal tail for $\alpha = \alpha_{max}$.

4.1.3 Fuselage

The fuselage consists of a circular tube with a diameter of 0.11 m and a length of 2 m. The circular tube provides good resistance against cross-winds, which influences the stability and controllability of the aircraft. Furthermore the frontal area is kept as small as possible by using this type of cross-section, ensuring good drag characteristics. The tube is made of fibreglass, a light-weight material that is easy to manufacture and maintain. Also, the use of a metallic material is not possible, since this interferes with the measurement equipment.

4.1.4 Propulsion system

The aircraft operates at velocities ranging from a minimum velocity of 15 m/s to a maximum of 36 m/s set by regulations. For this range of velocities a propeller engine is an efficient type of propulsion system. For the SkyDowser, a Saito FG-30B Gasoline [7] engine with 2.8 HP has been used to drive a two-bladed propeller. This is an off-the-shelve available engine that weighs 1.1 kg and operates at a RPM range of 2,000-10,000. The power varies by changing the RPM setting of the engine. The calculations regarding the complete propulsion system can be seen in appendix E on page 81. The propeller engine is placed at the nose of the fuselage. This increases the longitudinal stability, since the distance between the centre of gravity and the aerodynamic centre is increased. Also, the engine operates in an undisturbed flow, increasing propeller efficiency.

Another advantage of this engine is that it uses regular petrol as fuel, that is available world-wide. To lubricate the engine 5 percent of oil must be added. Oil is also widely available and easy to add to common petrol.

4.2 Aircraft internal systems

4.2.1 Fuel tank

The maximum fuel capacity of the fueltank is 1.7 l and is stored inside the fuselage. This tank is located inside the fuselage and positioned at the centre of gravity (x-direction) of the aircraft. It is depicted in figure 4.7. Since fuel is burned during flight, the mass of the aircraft decreases. With the fuel tank located at the

centre of gravity, the decrease in fuel does not affect the longitudinal stability during flight. A fuel pump system is needed including hoses to provide the engine with fuel during all flight conditions.

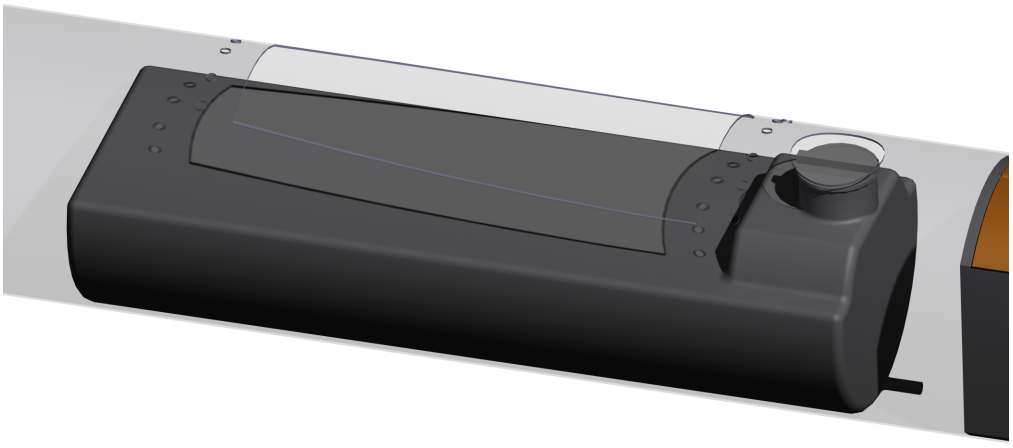

Figure 4.7: View of the fuel tank inside the fuselage.

4.2.2 Avionics

To fly autonomously the SkyDowser uses the open-source *ArduPilot Mega* as autopilot system[8]. All data from flight measurement devices are controlled by this on-board system. To determine the aircraft's relative position to the Earth, the Global Positioning System (GPS) is used and linked to the autopilot. A GPS system can also provide the altitude of the aircraft, but the accuracy of the GPS system is limited to a few metres[9]. To solve this problem a laser altimeter provides accurate altitude data for the autopilot. This altimeter is preferred over a radar system because of the relative low weight and cost. Acoustic altimeters where also excluded due to the small range (< 30 m). The laser altimeter can be found just behind the engine. The autopilot with GPS and gyroscope are found above the fuel tank within the wing box. This 3-axis gyroscope measures the roll, pitch and yaw angle such that the attitude of the SkyDowser is known continuously during flight. Finally the pressure measurements from the Pitot tube and static port give the airspeed. The ground speed is determined using the GPS system. All control surfaces are controlled by an integrated fly-by-wire system and actuated by servomotors. This system saves weight compared to a hydraulic control system, since control cables are not needed.

To be able to fly completely autonomous a collision avoidance system is added to the SkyDowser. The technique of stereoscopic image processing is used to create a depth map in the heading direction of the aircraft. The system consists of two cameras, each of them placed at the wingtips. The distance between the cameras is 3.5 m. The collision avoidance system gives input to the autopilot so the flight path can be changed. This can either be done by climbing to clear the object or by a climb together with a turn. If both options are not possible due to limitations of the aircraft, the autopilot will make a turn of 180° to avoid collision. These manoeuvres are discussed in detail in section 5.3 on page 20.

4.2.3 Measurement package

The measurement package consists of the following components;

- three cylindrical coils with a diameter of 8.5 cm and a height of 1.5 cm
- a power source
- two inclinometers
- a magnetometer
- a GPS sensor

In figure 4.8 all components can be seen as placed in the wing. The small height allows the coils to be placed inside the wing with a maximum distance of 2.4 m apart and their weight acts as bending relief for the wings. The inclinometers are positioned next to the coils, so they can accurately determine the orientation

of the coils. The processing unit and storage are placed in the wing as well, next to the autopilot. In this way the wing can be detached from the fuselage and can be used to perform handheld measurements. Since one wing needs to house two coils and the other wing one coil, the centre of gravity in y-direction needs to be balanced. This is done by placing the two coils more towards the longitudinal body axis of the wing.

Concerning the determination of the location of a measurement the GPS sensor of the SkyDowser is used. The accuracy of GPS is limited to a couple of metres, which constraints the applications of the measurement data. For example, it could not be used to determine during flight the exact place where the customer should drill.

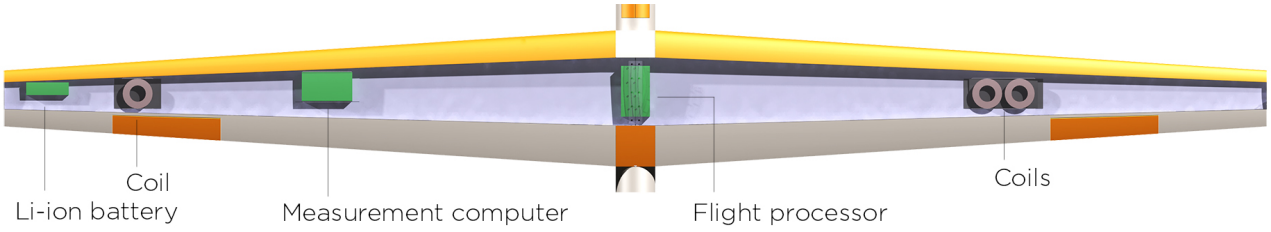

Figure 4.8: Planform showing the components of the measurement package.

4.2.4 Generator and battery pack

The electrical system consists of the components that are shown in appendix K on page 113. The average electrical power consumption of all components is estimated to be 32 W during cruise. If a battery was chosen to provide energy for all electrical components during the complete mission a battery of at least two kilograms. This estimated mass is based on the specific energy data of a Lithium-ion battery [10]. In order to prevent the use of this battery a generator has been included in the design. The generator adds a budgeted mass of 40 grams in total to the SkyDowser due to a transmission system and an electric motor which only weighs 20 grams and is able to provide maximum power of 75 W [11]. The generator is connected to the propeller shaft via a belt. The main engine uses an extra fuel mass of 0.11 kg over the entire mission to provide sufficient electrical power. In order to still have the electric systems available when the generator fails, a small battery pack (1.6 Ah at 11.1 V) is installed next to the autopilot, which is able to power the on-board electronics for thirty minutes. Although at a higher cost, the use of a generator instead of only batteries saves 1.6 kg in total mass. This leads to savings in fuel consumption, lowering the operational costs and thus compensates for the added manufacturing cost.

4.2.5 Landing system

A parachute system is used to ensure a safe landing at the end of its mission. Since the SkyDowser must be able to land in all kinds of environments and in remote areas, a conventional runway landing approach is not an option. The size of the parachute is 4.7 m^2 and made of a Spectra and Kevlar material [12]. The parachute weighs 0.7 kg and has a volume of 2.3 l when folded and is positioned in a casing just in front of the main wing. The place of the parachute is critical since its position relative to the centre of gravity defines the attitude of the SkyDowser when the parachute is deployed. The casing is closed by two flaps and are hold together by a pin system. To deploy the parachute the pin system is released and two air scopes (figure 4.9) ensure that the flaps are opened. A pilot chute catches the free stream airflow and brings the main parachute in operation. The maximum force caused by the parachute is 1.8 kN, which is considerably lower than the landing force due to the slower energy dissipation. Landing on the nose is not preferred, because the propeller engine is placed at the front of the SkyDowser.

In figure 4.10 the impact phase is shown including a close-up of the rubber tail cone. A horizontal impact on the surface would damage the fibreglass fuselage structure, since the thickness is only 0.8 mm thick. Therefore the SkyDowser will land on its tail where a rubber cone is placed to dampen the impact. After impact the SkyDowser will tip over. To ensure that the horizontal tail does not damage due to tipping over, the tail cone is slightly bended upward. Due to this shape the aircraft will land on the bottom fuselage after impact. The force at impact is calculated to be 5.5 kN acting on the fuselage. This means the fuselage will reach 6% percent of its compression limit and 23% of the critical buckling load, when incorporating the dampening of the tail cone. All calculations for the landing system can be found in appendix I.2 on page 105.

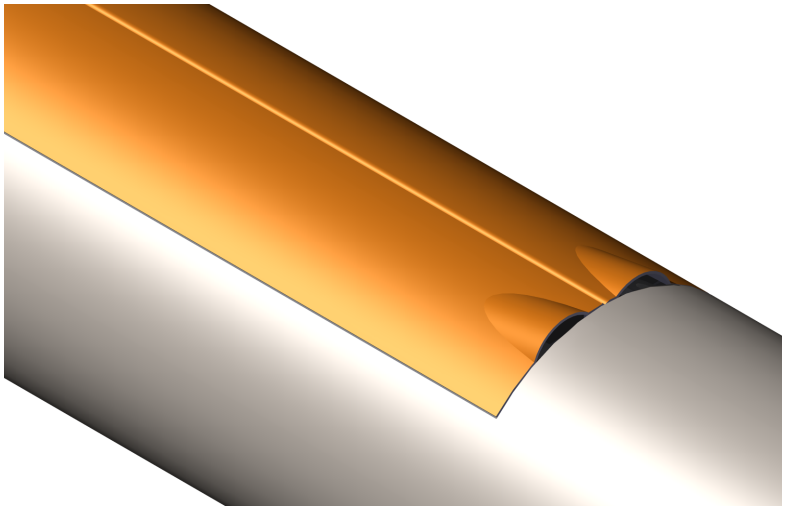

Figure 4.9: Parachute housing; two flaps wit air scopes.

4.3 Aircraft external systems

There are two main external systems: the launch system and the ground system. Both systems, their layout and the design choices leading to this final design are described in this section.

4.3.1 Launch system

Since the aircraft must be able to take-off at any kind of surface in remote areas, the take-off system is a difficult problem. Vertical take-off would be the most suitable for the problem, but since the aircraft has lifting surfaces this is not possible. Short take-off is then the best possible solution. Since the operating terrain can be rough, uneven and scattered with rocks or other obstacles, the use of a landing gear is also ruled out. Lastly, hand launch can not be used due to the high mass of the aircraft and the large dimensions. This means an external system has to be used.
It was chosen to use a catapult system that uses elastic bands to launch the aircraft. The system is visualised in figure 4.11. This system can easily be put together, is easy to operate, manufacture and maintain, is relatively compact and allows for a short take-off. Therefore it meets all requirements set for the mission. More importantly, it is a safe system to use. The system is designed to make sure that the UAV reaches a velocity of 16 m/s, 125% of the stall speed. Therefore the rail has a length of 4.5 metres and uses 14 elastic bands. In order to transport the system, it consists of two parts that can easily be assembled at the take-off site. The total mass of the system is 13 kg. The calculations can be found in appendix I.1 on page 105.
The choice for this system also brings some consequences. Since there is an external system. The take-off will take extra time, since the system has to be assembled before launch. The extra system will also add extra weight and volume to the total amount of systems that have to be brought along when deploying the aircraft. Besides this, a launch site has to be found where the UAV has enough space to climb to a safe altitude. The choice for elastic bands as tensioning device will mean that these ropes have to be protected against radiation from the sun. Therefore a coating will have to be used to protect the elastic bands. Finally it is necessary to bring spare elastic bands for the case where one band breaks.

4.3.2 Ground station

The ground system gives the pilot on the ground the possibility to control and follow the SkyDowser. Since the *ArduPilot Mega* software is used as autopilot system (see section 4.2.2), the UAV can communicate with the ground station. The choice for this software leaves the option open for a ground control unit, since the software is able to run on both Android tablets and laptops. However, since a laptop will give the best performance it is recommended to use this. The laptop will then be used to monitor the flight control system and change the flight path if necessary while the aircraft is in the air. Since the pilot needs to be in direct line of sight, the monitoring can also be done by direct sight, but the monitoring system of the software provides a very good overview of what the aircraft is doing and what outputs its sensors are providing. To receive the signal being sent by the UAV, a WPAN connection will be set up between the laptop and the

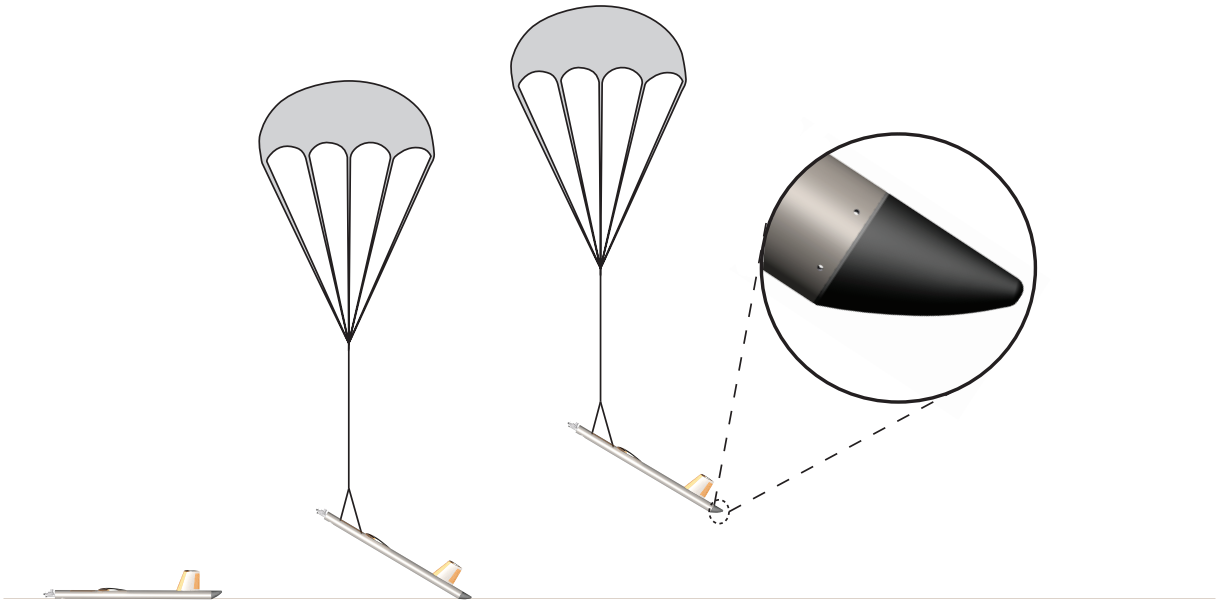

Figure 4.10: View of the landing of the SkyDowser on rubber tail cone.

UAV using a WPAN (similar to Wi-Fi) antenna that can be connected to the laptop through USB. This WPAN antenna uses a frequency of 2.4 GHz, which is legal to use all around the world and has a range of 1.5 km [13]. This system also supports a remote control to control the UAV if the autopilot is disabled. This can be used as manual override if the aircraft does not behave as designed or the pilot wants to take control of the SkyDowser for any other reason.
A consequence of this design choice is that sufficient power needs to be brought along to power the laptop and the remote control. A spare battery for both is a necessary good. In case of emergency the car battery can be used to power the ground station.

4.4 Data handling & communication flow

The data handling and communication flow visualises all communication elements in blocks and the data or commands with arrows, connecting the blocks. The communication flow is visualised in appendix N.2 on page 125.

4.4.1 On-board computer

This section describes the subsystems of the on-board computer. It contains the following major subsystems: Attitude and altitude control (AACS), Flight plan processor (FPP), System status check (SSC) and Collision avoidance subsystem (CAS).

Attitude and altitude control system
The AACS handles the stability and control of the SkyDowser and maintaining the altitude. According to the information stored in the flight plan the attitude and altitude control system activates actuators to change the attitude of the aircraft. The actuators are used to change any kind of control surfaces for roll, pitch and yaw movement and provide their own feedback to the system, based on the voltage running through the actuator. If the flight altitude deviates from the measurement height the angle of attack is changed to climb or descend to 30 m. A direct relation is established between the collision avoidance system. This system can directly interrupt the attitude and altitude control system if a possible collision is detected.

Flight plan processor
The flight plan processor is the major part of the on-board computer and supervises the programmed route and provides the AACS with commands to adjust this route. The GPS sensor, pitot tube and static port sensor provide the flight plan processor with its position, ground speed and airspeed. The FPP then performs

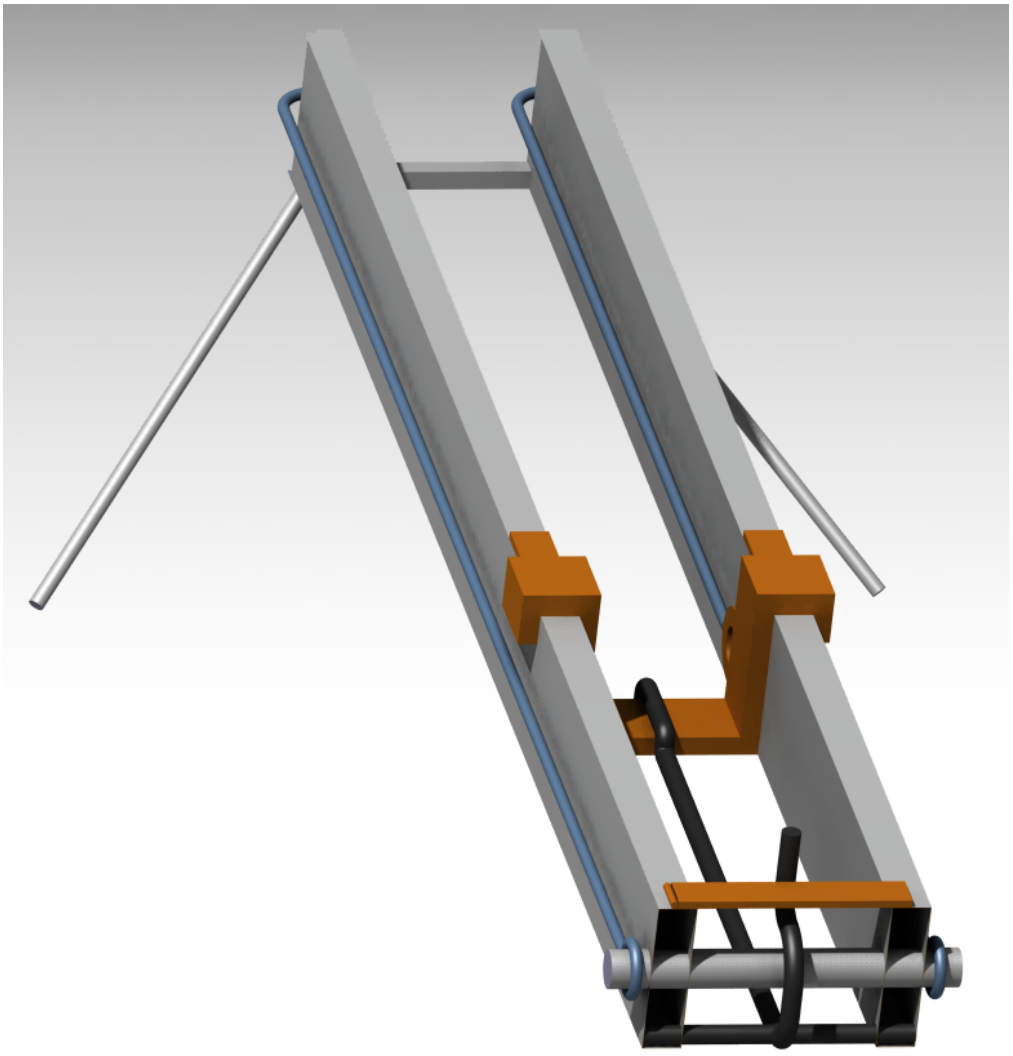

Figure 4.11: The catapult used for launching the SkyDowser.

all calculations needed to change the control of the aircraft and gives feedback to the AACS. In this way there is a constant interaction between the FPP and the AACS. The communication processor connects the ground station system with the FPP, in order to manually change the flight plan during the flight.

System status check
All errors, energy levels, power levels, sensor data and status are controlled in the system status check. All data outputs to the communication processor for further usage and to the flight plan processor such that the SkyDowser can abort its mission if the system detects an error.

Collision avoidance system
The images from the cameras are analysed by a processor to detect any nearby objects that the aircraft could collide with. The system is supported by the altimeter. When a nearby object in the direction of flight is detected, or the altitude is too low, the system commands the AACS directly to change the heading and/or altitude of the aircraft. Furthermore the system can directly command the propulsion system to change the amount of thrust.

4.4.2 Other data handling & communication systems

Propulsion system
The AACS or CAS sends the required thrust level to the propulsion system. The fuel tank/battery sensor provides the system with the amount of energy left. The propulsion system commands the power regulator, which regulates the engine setting. The power level of the engine is registered and provides feedback to

the propulsion system. A temperature sensor is used to register the internal temperature of the propulsion system and communicates with the status check system.

Measurement equipment system
The measurement equipment receives input from the flight plan processor. This input consists of an on/off switch and the measurement instrument settings. These settings consist of the frequency for which the measurements are conducted. This setting is set into the flight plan beforehand, but can be changed during the flight.

Electrical power system
The electrical power system consists of a battery and a small generator, powered by the engine. The battery communicates with the SSC by providing energy level and temperature data.

Ground station
A ground controller or supervisor can provide the ground data transfer system with a flight plan and payload settings using a direct wifi link. During flight the ground station processor, a laptop, can upload changes to the flight plan manually, by using an up-link system of the ground antenna. Using a down-link the system status, flight position and measurement data can be transferred to the ground station. The position of the ground station is determined using a GPS system. The UAV can use the position of the ground station to land near it when the mission is aborted in case of emergency.

4.5 Electrical block diagram

The electrical systems are powered by the electrical power system, the power provision and power conversion of these systems are visualised in the Electrical Block Diagram found in section N.1 on page 124. It shows the operational voltage and power consumption of the different components. The generator is powered by the engine, after which a voltage regulator passes a constant 12 V on to the battery. The engine's ignition system is powered through the 5 V circuit, the battery has to be fully of partially charged before take-off.

Chapter 5

Performance & limitations

The performance and limitations of the SkyDowser are presented in consecutive order of the mission phases; take-off, cruise and corresponding manoeuvres, and finally the landing phase. For each phase the performance characteristics and corresponding limits are shown. The calculations done to obtain these characteristics can be found in appendices D to I (pages 73 to 105).

5.1 Take-off and climb performance

The first phase of the aircraft's mission is the take-off; which will be performed with the help of a catapult. In figure 5.1 this take-off phase is presented, clearly showing the path of the SkyDowser up to cruise altitude. This allows for a very short take-off length of 4.3 m, such that no conventional runway is needed. Without the need for this conventional runway, the SkyDowser can be launched from virtually every terrain. In order to perform a safe take-off, a take-off velocity 1.25 times higher than stall velocity $V_{\text{stall}} = 12.8$ m/s is used; $V_{\text{TO}} = 16$ m/s.

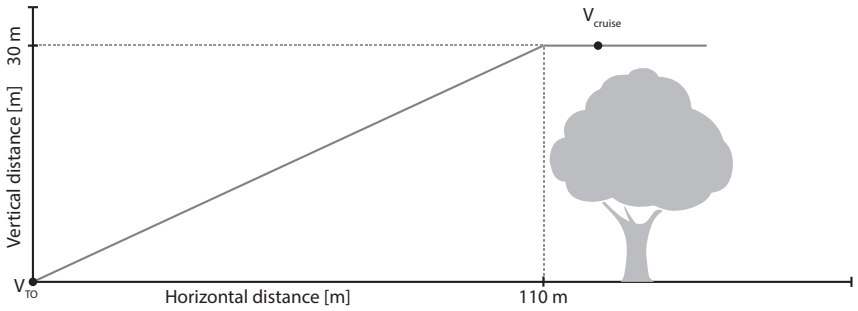

Figure 5.1: Visualisation of the take-off path including clearance of obstacles.

Next, the aircraft starts the climb to cruise altitude, with a climb angle of 15°. Within 110 m, the cruise altitude of 30 m is reached, and the aircraft continues it's mission in a steady, horizontal flight. When the cruise altitude is reached, the velocity is increased to the cruise velocity of 25 m/s. The cruise altitude is set at 30 m because then the SkyDowser will be able to scan a wide Ground Sample Area (GSA) at an acceptable resolution whilst clearing most obstacles. A higher altitude is not desired, since the measured ground response decreases with the ratio $1/r^3$, where r is the altitude, if the same strength of the magnetic field is used. The measurement methodology is elaborated in section 8.7 on page 37. The cruise velocity of 25 m/s was chosen because it is within UAV regulations (see appendix B on page 70) and is also a safe speed to operate at this altitude. Flying at this velocity forms a good compromise between range and obtained resolution of the measurements.

5.2 Cruise performance

When the SkyDowser reaches its cruise altitude the lift over drag ratio equals 25.7. During cruise (in windless) conditions the fuel consumption is approximately 30 gr/km^2. With a mission duration of 8 hours and a cruise velocity of 25 m/s the corresponding range of the aircraft is 720 km. The SkyDowser has to carry 1.3 kg of petrol (including reserve fuel of 0.5 kg) on board such that it will have enough fuel to complete the mission in all allowable weather conditions. The aircraft is safe to perform the mission up to wind velocities of 5 bft.

Due to the lift force that acts on the wing during cruise, the wingtip will deflect 11 mm. This amount of bending causes no problems for the measurement equipment to perform accurate measurements.

The SkyDowser is statically stable, as shown in table J.2. The aerodynamic centre is placed aft of the centre of gravity, because the tail of the SkyDowser produces a negative lift force. This way, the amount of control inputs to keep the aircraft longitudinally stable is minimised.

5.3 Manoeuvring performance

The SkyDowser will make a lot of turns and must provide a stable measurement platform. The relation between the turn radius, velocity and load factor can be seen in figure E.5 on page 85. At cruise velocity, the turn radius is 22 m and gives a load factor of 3. This enables the aircraft to fly a route where it can scan "lanes" of 30 m width, with a spacing of 14 m in between. More details on this flight path can be found in section 8.4 on page 32. To generate enough lift for this steady coordinated turn, the lift generated will have to be 3 times higher than that in steady cruise condition. This means that the lift produced is then 90% of the maximum lift that can be produced.

Evasive manoeuvres
In case of a detected object that has to be avoided, the SkyDowser can either perform a (sharp) turn (see figure 5.3), climb (figure 5.2) or a combination of these to avoid the specific object. Preferably the SkyDowser will climb over the object. If this is not possible a combination of climbing and turning should be used (see figure 5.4). Finally if this too is not possible, a sharp 180 degree turn should be made. From the point where the actuators are moved, the SkyDowser can climb 35 m within a horizontal distance of 150 m, or make a 180 degree turn within 45 m from an obstacle. Further details of the collision avoidance system are given in section 8.8 on page 39 and appendix I.4, on page 107.

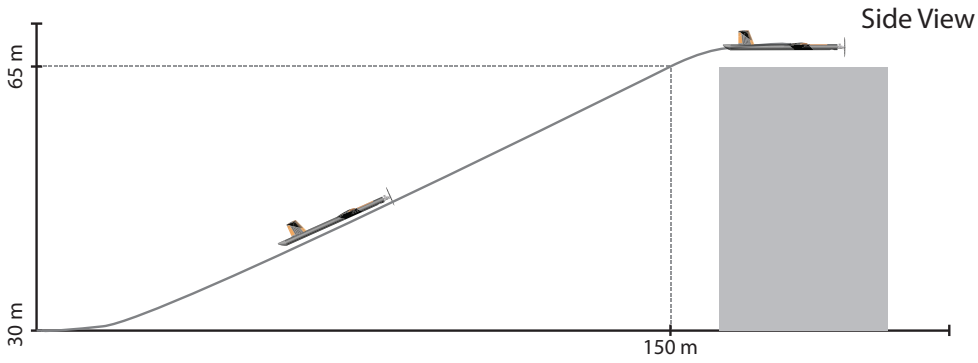

Figure 5.2: Evasion of an object smaller than 65 metres using a climb.

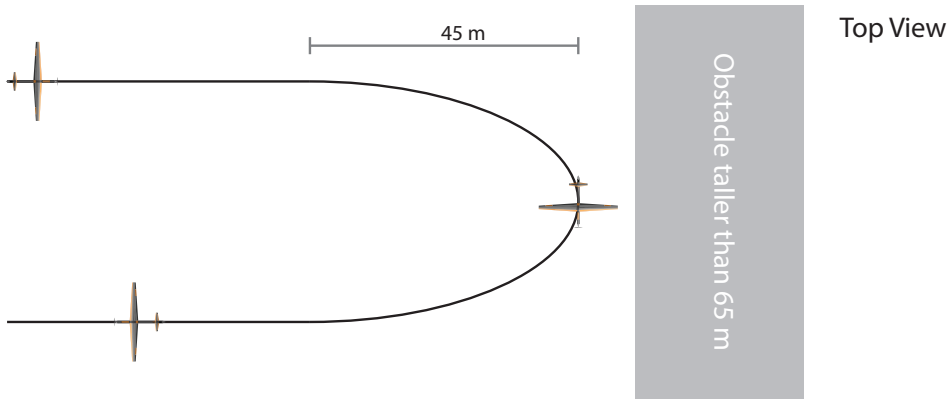

Figure 5.3: Evasion of an object taller than 65 metres using a sharp turn.

At cruise velocity the aircraft is able to climb with an angle of 16.5 degrees at a rate of 6.4 m/s. The aircraft can perform its steepest climb at a velocity of 15 m/s with a climb angle of 16.5 degrees. The rate of climb and climb angles for all velocities can be found in appendix E on page 81.

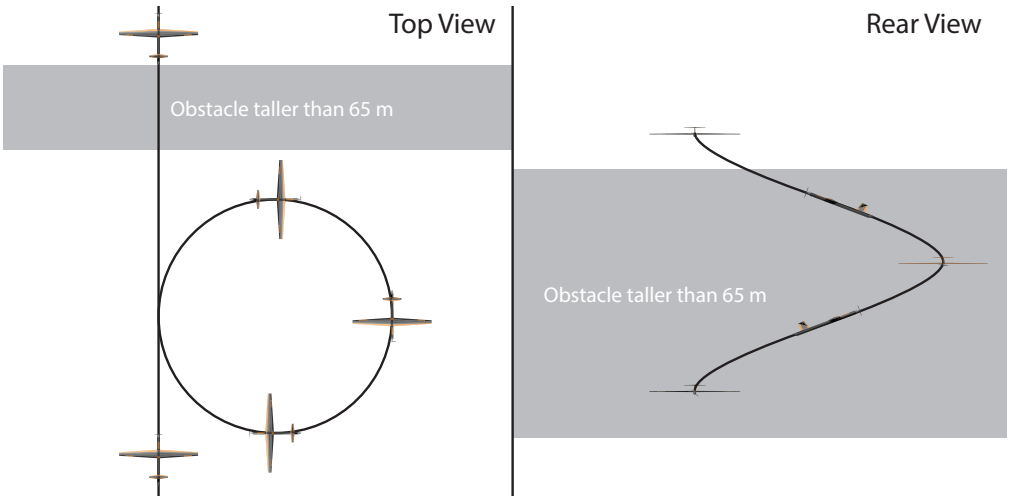

Figure 5.4: Evasion of an object taller than 65 metres using a combination of turning and climbing.

In case the collision avoidance system determines that the SkyDowser has to avoid the object by climbing over it is not possible, a sharp turn is initiated. In figure 5.3 this manoeuvre is shown. Since the response time is below one second for the aircraft to have a bank angle of 70 degrees, an object can be avoided at any time when it is detected 45 metres in advance. The aircraft shall perform a climbing turn for 360 degrees and try if the object can be evaded once again.

Structural performance
At the maximum limit load factor of 4.7, which is determined in appendix E.5 on page 84, the structure in the wings will reach 13% of its yield loads. This load factor occurs when performing a steep pull-up motion at high velocity, which during normal operations does not occur. To prevent buckling of the top skin, longitudinal stiffeners have been added. Under these maximum loads the wingtip has an upward deflection of 58 mm, at an angle of 2.5°. Note that measurements cannot be performed when the deflection angle between the coils is larger than 3° (see chapter 2 on page 5). So when the deflection of one wing exceeds 1.5°, measurements cannot be performed. Also, the wingtip is twisted 1° at maximum load factor, which is below the set limits for the measurement equipment. During cruise, wing deflection and tip twisting is not a problem.

Stability
The SkyDowser is also dynamically stable for input deflections of the different control surfaces. The Phugoid motion, the aircraft response to a step input on the elevator, has a time to half-amplitude of approximately 45 seconds. A step input on the rudder will result in a Dutch roll motion that has a time to half-amplitude of the roll angle of about 42 seconds. After an input on the ailerons that makes the SkyDowser roll 45°; it's original attitude is restored after 4 minutes with a time to half amplitude of approximately 42 seconds. Note that the SkyDowser uses an autopilot, such that the dynamic stability is further enhanced because of active controls. The aforementioned dampening times can be further decreases because of this active dampening. More details on the control and stability of the aircraft can be found in appendix F, starting on page 87.

5.4 Landing performance

The final phase of the mission is the landing phase; during which the aircraft will perform a safe landing using a parachute system. For ee chapter 8.3). When the aircraft approaches the landing coordinates, the parachute hatch is opened via an electric servo, and a pilot parachute is deployed. This pilot parachute ensures the main parachute is properly deployed from it's container, causing the aircraft to abruptly slow down. It then start it's descend, at a maximum velocity of 4.4 m/s. From cruise altitude, the aircraft touches down after 7.4 seconds. The impact of this landing is dampened since the SkyDowser lands on its rubber tail cone. The force of impact at landing is then 5.2 kN, causing the fuselage to reach 6 % of its compression limit and 23 % of its critical buckling load.

Chapter 6

Sensitivity of design

It is likely that during the finalisation of the design or during operation of the aircraft, some changes of main system parameters will occur. In this chapter the effects of such changes will be discussed, determining the sensitivity of the design to a change in a main system parameter. First two different scenarios will be discussed, changes during the final design of the aircraft and changes during operations. Next the results of the analysis will be discussed in section 6.3.

6.1 Change in design

Changes during the design phase may occur, to test the feasibility of the design, important parameters are changed to determine their effect on the design. Note that the range of 720 km will be maintained during this analysis.

Increase of component mass

In the final design phase it is common that some components or systems turn out to be heavier than anticipated. Especially heavy components e.g. wings or empennage may pose a threat to the feasibility. Should the aircraft be unable to fly as a result of a small weight increase, then the design has a lower degree of feasibility. To evaluate this for the SkyDowser, a significant weight increase in a major system component is simulated. The mass of the aircraft's lift generating surfaces (wing and tail) contribute to about 35% of the total mass of the aircraft. For the purpose of this sensitivity analysis, it is assumed that the mass of the structure of these lifting surfaces increases with 50%. This can be caused by manufacturing reasons like a higher minimum thickness.

Table 6.1: Change in aircraft parameters due to increase in wing-mass.

Configuration	**Mass [kg]**	V_{stall} **[m/s]**	**Range [km]**	**Fuel used [kg]**
Initial configuration	12.54	12.7	720	0.79
+50% wing mass	15.36	12.8	720	0.93
Change [%]	22.5	0.6	0.0	17.7

The effects on the design are shown in table 6.1. The mass of the aircraft increases rapidly. Due to the heavier wing more lift is required, leading to a larger wing surface. This larger wing, again, leads to an increase of the wing mass. This process is called the *snowball effect* of mass increase in an aircraft, and is visualised in figure 6.1.

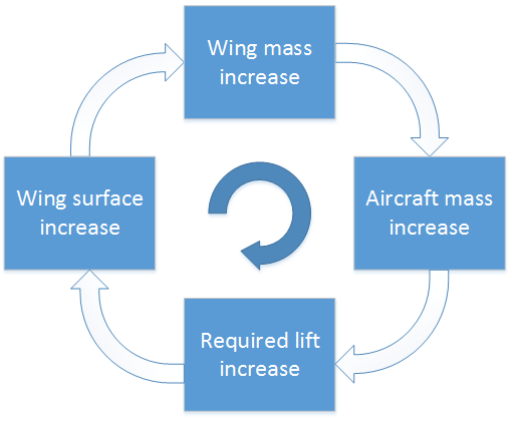

Figure 6.1: Visualisation of the *snowball effect*.

6.2 Change during operations

Next to changes that alter the design, changes can also arise during operations, the design itself remains unchanged. A versatile aircraft can easily cope with these changes, which is an advantage for the client. To evaluate the feasibility and versatility of the SkyDowser, several scenarios are simulated. First two unintentional changes are simulated.

Increase in drag

Current values for the parasite drag (C_{D_0}) have been based on literature, as is discussed in appendix D starting on page 73. Since this is an important factor in the total drag force, and thus in the thrust required, this parameter is increased by 50%. Table 6.2 shows the effects on the design. In this analysis the total mass of the aircraft is kept constant, the total mass comprises a full fuel tank. When the fuel used increases, the amount of reserve fuel in the aircraft is reduced.

Table 6.2: Change in aircraft parameters due to increase in parasite drag.

Configuration	Mass [kg]	V_{stall} [m/s]	Range [km]	Fuel used [kg]
Initial configuration	12.54	12.7	720	0.79
+50% parasite drag	12.54	12.7	720	0.88
Change [%]	0.0	0.0	0.0	11.4

Decrease in lift coefficient

The lift coefficient is an important aerodynamic parameter for the design. Should the aerofoil be less effective than calculated, the design will be greatly influenced. For the purpose of this sensitivity analysis it is assumed that the effective lift coefficient is only 90 % of the calculated value. Table 6.3 shows the effects on the design.

Table 6.3: Change in aircraft parameters due to decrease in lift coefficient.

Configuration	Mass [kg]	V_{stall} [m/s]	Range [km]	Fuel used [kg]
Initial configuration	12.54	12.7	720	0.79
-10% lift coefficient	12.54	13.4	720	0.80
Change [%]	0.0	5.3	0.0	1.3

Additional payload

Lastly two intentional changes are made. The aircraft is currently equipped with a payload that can be used to measure groundwater levels. However, it would be a major advantage if the aircraft can be fitted with additional measurement equipment, for example (infra-red) cameras. In total four kilogramme of extra payload will be simulated, in steps of one kilogramme. The first 2 kg are fitted inside the fuselage, just behind the fuel tank. The last 2 kg are fitted underneath the fuselage at 0.5 m behind the engine, where no additional parasite drag has been taken into account. The reason for this is that centre of gravity of the aircraft should stay within controlability and stability limits. The results of the simulated additional payload is summarised in table 6.4.

Table 6.4: Change in aircraft parameters due to additional payload.

Configuration	Mass [kg]	V_{stall} [m/s]	Range [km]	Fuel used [kg]	Fuel change [%]
Initial configuration	12.54	12.7	720	0.79	
Additional payload					
1 kg in fuselage	13.54	13.2	720	0.82	3.8
2 kg in fuselage	14.54	13.7	720	0.86	8.9
2 kg in fuselage, 1 kg outside	15.54	14.2	720	0.90	13.9
2 kg in fuselage, 2 kg outside	16.54	14.6	720	0.95	20.3

Additional fuel

The versatility of the design greatly depends on the range of the aircraft. If the amount of fuel that is carried can be increased, the range of the aircraft can be increased. This would make the aircraft suitable for a wide variety of applications, for example aerial surveillance missions. To simulate this, 2 kg of additional fuel is fitted inside the wing-box. Table 6.5 shows the effects on the design. Note that 100% of the fuel is used to examine the change in range.

Table 6.5: Change in aircraft parameters due to additional fuel.

Configuration	Mass [kg]	V_{stall} [m/s]	Range [km]	Fuel used [kg]
Initial configuration	12.54	12.7	1198	1.30
Additional fuel	14.54	13.7	2914	3.30
Change [%]	15.9	7.9	143.2	153.8

6.3 Feasibility analysis

In this section the results of the sensitivity analysis are elaborated, starting with the changes during design, followed by the changes during operation.

Increase of component mass
Increasing the weight of the wing and empennage with 150% (due to manufacturing reasons) causes a significant *snowball effect* in the aircraft's total mass. The two changed systems caused the need for a larger wing surface given a unchanged stall velocity of 12.7 m/s. The increase in wing surface itself causes the total system mass to increase. A design equilibrium was established where the wing mass increased with just over 75% whereof 25% is caused by the snowball effect. The fuel consumption increased with 17.7%. Because the propulsion system has sufficient power to cope with the increased drag no changes to the propulsion system had to be made. The reserve fuel is sufficient for compensating the increased fuel consumption. The degree of feasibility of the design is marginally influenced by unforeseen changes in component mass.

Increase in drag
Increasing the parasite drag (due to increased roughness caused by wear or manufacturing reasons) causes a significant increase in fuel consumption. Given a constant range and cruise velocity the fuel consumption increased 11.4% with an increase of 50% in parasite drag. Because the propulsion system has sufficient power to cope with the increased drag, no changes to the propulsion system had to be made. The reserve fuel is sufficient for compensating the increased fuel consumption. The degree of feasibility of the design is uninfluenced by changes in parasite drag.

Decrease in lift coefficient
Decreasing the lift coefficient of the wing (due to manufacturing reasons or operational wear). The stall velocity is a critical parameter and is increased with just over 5% with a decrease of 10% in maximum lift coefficient. An increase of 1.3% in fuel consumption is not a threat for the feasibility. The reserve fuel is sufficient for compensating the increased fuel consumption. The degree of feasibility of the design is marginally influenced by a unforeseen decrease in lift coefficient.

Additional payload
Increasing the mass of the aircraft (due to adding additional payload) causes a increase in stall velocity and an increase in fuel consumption. The reserve fuel is sufficient for compensating an increased fuel consumption, as the configuration with 4 kg additional payload still has 0.35 kg of reserve fuel. This configuration has a stall velocity of 14.6 m/s which is 15% higher. When the additional payload of both 3 and 4 kg is added, the launch system has to be adjusted. Since the stall velocity has increased with respect to the initial configuration the take-off velocity should also be increased. In order to achieve this, two more elastic bands should be added to the catapult. This ensures the SkyDowser reaches 125% of the stall-velocity at take-off. The degree of feasibility of the design is marginally influenced by adding additional payload up to 4 kg.

Additional fuel
Increasing the fuel mass with 2 kg (due to adding additional fuel) causes an increase in stall velocity, range and fuel consumption. The fuel mass is increased with 154% which results in an increase of 143% in maximum range, from approximately 1200 km to 2900 km. The fuel consumption per km increases marginally and the increased stall velocity from 12.7 m/s to 13.7 m/s is still low enough for launch using the existing system. The degree of feasibility of the design is largely enhanced by an increase of fuel mass.

Chapter 7

Manufacturing, assembly & integration plan

This chapter discusses the integration of all components to form one coherent entirety. A lot of the main components will be bolted to each other, for easy maintenance and modularity. For every bolt and nut, a pressure ring will be used to prevent damage to the structural components. In some cases, extra material will function as load transfer and/or protection. This will be specifically stated for those cases.

7.1 Wing structure

The choice was made to keep the wing box intact, since it is subjected to the largest forces. In order to be able to attach wing properly to the fuselage, a cut-out is made in the fuselage. The wing box and fuselage will be attached using bolts and nuts, allowing for easy assembly and dis-assembly. The tensile loading on the bolts will reduce fatigue life, to limit this effect, the bolts will be preloaded. The loading on the bolts is far below 50% of the yield strength, thus fatigue causes no imminent problems. The bolts are to be replaced during the scheduled maintenance. A softer material will be attached on the inside of the fuselage, to ensure the bolts and nuts do not damage the fibreglass fuselage. Since this extra layer does not have to carry significant loads, but only transfers the load to the fuselage and wing box, a 1 mm thick layer of polymer is chosen, to keep the structure lightweight. Rivet nuts are attached to the structure so the wing can be mounted by fastening bolts from the outside. The fuselage consists of a prefabricated fibreglass cylinder, to keep costs at a minimum. The two parts of the wing will also be attached using a patch of overlapping material, which will be made of fibre glass to withstand the loads. By bolting only the wings together, excluding the fuselage, the wing can be used as a portable measurement platform, for pinpointing drilling locations. The wing and fuselage assembly is depicted in figure 7.1. It is envisioned that the wing box will carry all loads, the other wing parts only have an aerodynamic function. All parts will have to be tailor-made, they cannot be purchased prefabricated. An overview of the estimated cost of all the wing components can be found in chapter 12 on page 47. The front and the rear of the wing will be attached to the wing box using glue. The ailerons are directly connected to the wing box, using bolts and nuts.

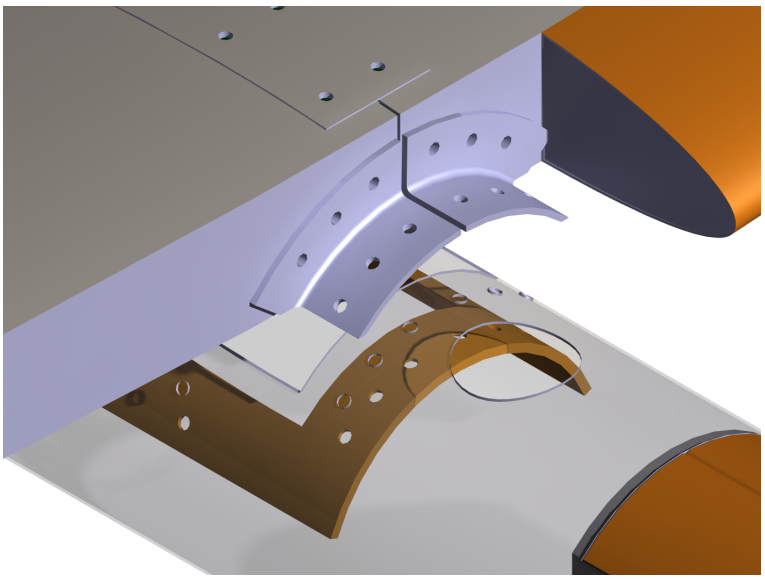

Figure 7.1: Assembly of wing to fuselage.

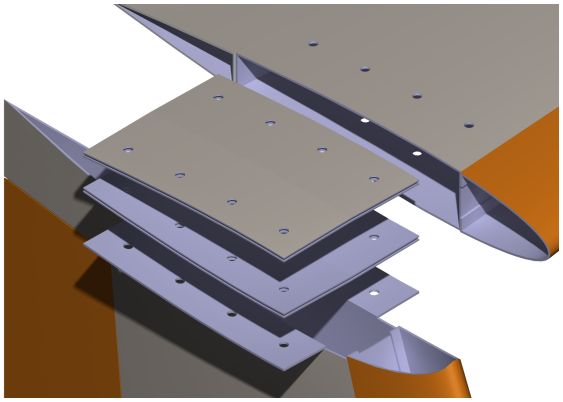

Figure 7.2: Assembly of horizontal tail to vertical tail.

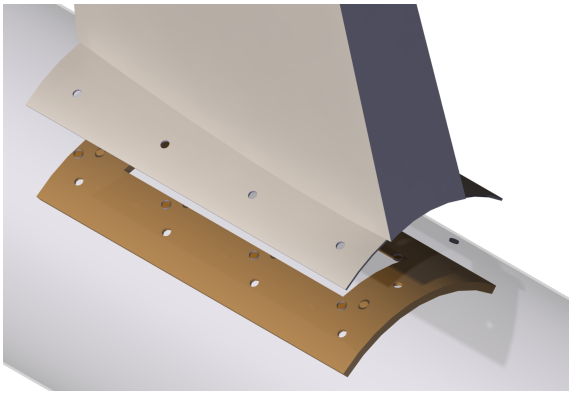

Figure 7.3: Assembly vertical tail to fuselage.

7.2 Empennage structure

The empennage consists of three parts that need to be assembled. The vertical tail and two parts of the horizontal tail. The horizontal tail consists of two parts, because this is easier for manufacturing. An extra layer of polymer material will be placed on the inside of the wing box of the horizontal tail, as well as a fibreglass layer on the top. These pieces will be bolted together, combining the two wing boxes. The horizontal tail will be bolted to the vertical tail, as shown in figure 7.2. The horizontal tail in its turn, is connected to the fuselage much in the same way the main wing is. The fuselage will have an internal layer of polymer, through which the tail will be attached with bolts and nuts. This is depicted in figure 7.3. The rudder is directly connected to the wing box of the vertical tail, as are the elevators to the horizontal tail. Again, all parts need to be custom made.

7.3 Parachute structure assembly and manufacturing

The parachute hatches will be connected to the fuselage using hinges. They can be closed manually, once the UAV has been recovered. The parachute itself will be connected to an aluminium structure placed in the fuselage. This structure will be able to carry the loads caused by drag of the chute and momentum decrease of the UAV. The structure that is used for this is shown in figure 7.4. A plastic container in which the parachute is stored will make sure the parachute does not get stuck or move during flight. This container will be made of a thin, but rigid plastic polymer, since it only carries the mass of the parachute, which is 0.7 kg.

7.4 Engine mounting

The engine has four prefabricated holes, through which bolts can connect it to the fuselage. In order to do so, the fuselage will have an aluminium cap in the front, which is bolted to the fuselage. This is depicted in figure 7.5.

7.5 Fuselage and wing internals

Most of the electronic systems can be found in the wing. The fuselage will however contain the generator (which together with the engine functions as generator) and the laser altimeter. These are placed between the engine and the parachute compartment. They are easily accessible by removing the engine. The electronics in the wing are spread over the wing's length. The coils, inclinometers and cameras for collision avoidance are placed outward. To allow for easy access to these components, an inspection hatch is placed here. The processing unit, storage, batteries and other sensors are placed towards the fuselage. To be able to retrieve the measurement data after the mission has been performed, a cable lengthens the USB-connectivity of the storage to one of the inspection hatches of the coil and camera. If the other electronic systems need to be accessed, the wing will have to be removed. However this is most likely already the case during transport of the vehicle.

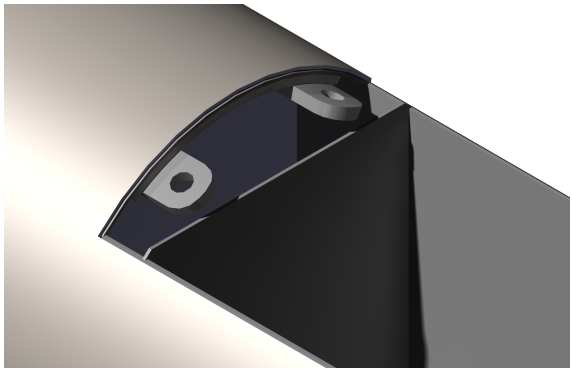

Figure 7.4: Strengthened parachute mounting in the fuselage.

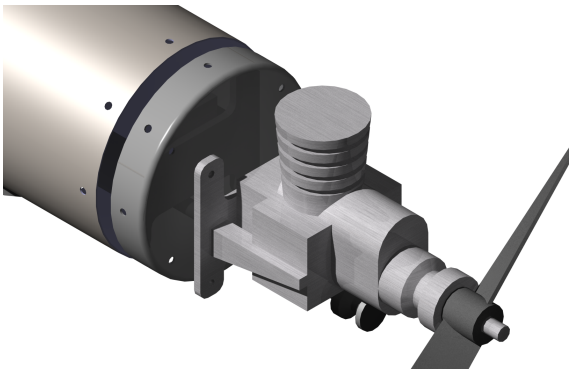

Figure 7.5: Engine mounting system to fuselage.

Chapter 8

Operations & logistic concept description

8.1 Transport

Since the vehicle is to operate in a lot of different and remote places, it needs to be easy to transport. The modular design allows the wings and, if necessary the tail, to be taken off so the aircraft can be transported in no more than four main parts; the fuselage, a 2.0 m long cylinder with a diameter of 11 cm, two trapezoidal wings with a length of 1.75 m and maximum width (at root chord) of 0.38 m and possibly the tail with a height of 32 cm and a width of 82 cm, as shown in figure 8.1. In this way the vehicle can be transported by a jeep-like car or SUV. Taking apart the vehicle is done by removing a couple of screws, as shown in figures 7.1 and 7.3 (see page 27). Even more, the entire SkyDowser can be fitted in a skibox, that can easily be place on top of a jeep or normal car. Also the catapult, which is used for take-off, can be separated in three parts to allow easy transport. Due to the range of the aircraft, the operator is advised to also use the car for following the vehicle.

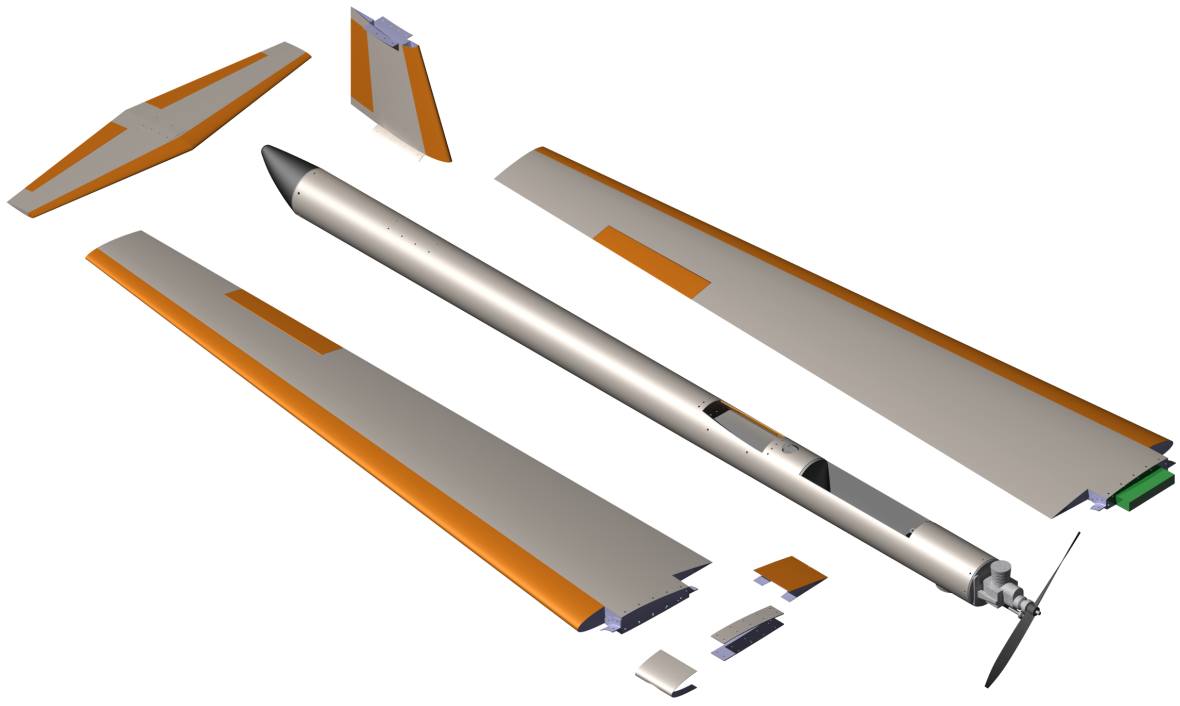

Figure 8.1: Disassembled SkyDowser for easy transport.

8.2 Fuel

The piston engine of the SkyDowser uses a mixture of gasoline and oil. For each 20 litres of unleaded gasoline (at least 91% octane), one litre of 100% synthetic oil for 2-stroke engines needs to be added. The manufacturer

of the engine recommends using Evolution Oil (EVOX1001Q) and stresses that it is important to use high quality oil, since it minimises the inevitable carbon buildup in the exhaust valve. [7]

This high octane, unleaded gasoline is widely available in Africa [14]. Although it is currently unknown what the availability of this specific Evolution Oil in Africa is, it is expected that 100% synthetic oil for 2-stroke engines also is widely available in Africa.

8.3 Take-off & landing

Both the take-off and landing systems have been designed to be as simple and flexible as possible, since the operation locations are expected to be remote and diverse. The catapult to launch the UAV is shown in figure 4.11 on page 17. The SkyDowser is positioned on the slide, at the base of the launch rail. The operator locks the slide, and tensions the elastic bands over the lower side of the launch rail. After starting the engine and testing the propulsion system, the SkyDowser is released by pulling the launch lever. By making sure that the SkyDowser is placed on the sled after it has been tensioned, the system is fail-safe, and the risk of losing the aircraft is minimised.

Landing is performed by means of a parachute, as described in section 4.2.5 on page 14. The parachute is deployed mid air, while entering the landing site. The placement of the system is in front of the centre of gravity, causing the aircraft to descent and land tail down, as visualised in figure 8.2. The horizontal distance, which the SkyDowser will travel with the parachute deployed from an altitude of 30 m is around 65 m, taking into account a wind velocity of 8 m/s deadwind. This system can be used in any terrain, as long as there is room for the SkyDowser to land. The parachute can also be used as a fail-safe system during the mission. Finally, for a safe landing the minimum deployment height is estimated to be 15 meters. However, here it is assumed the descend will take place from the cruise altitude of 30 metres.

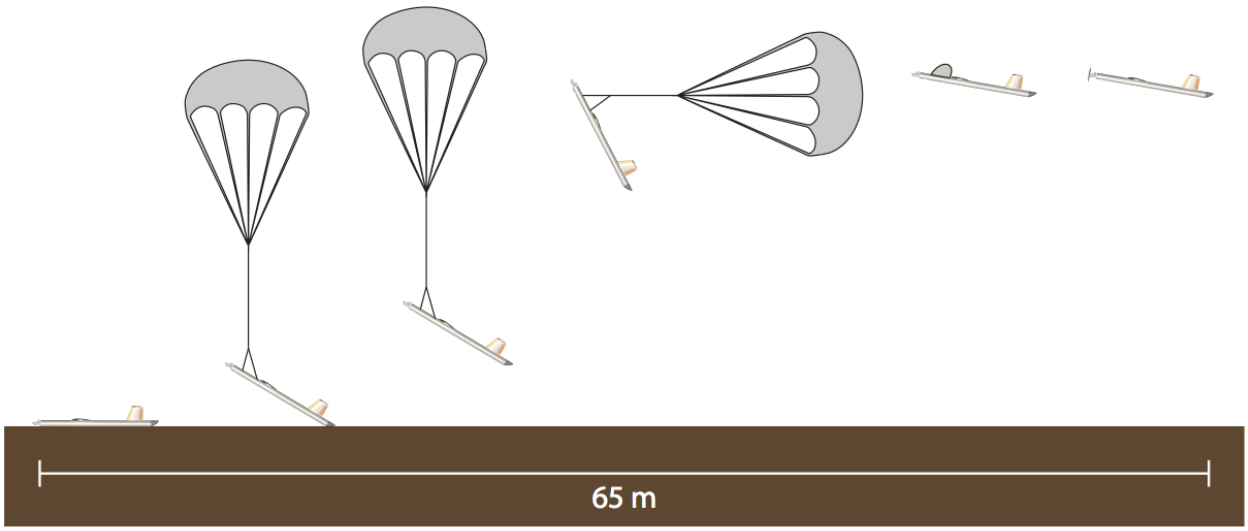

Figure 8.2: Process of deploying the parachute and landing the SkyDowser. Parachute is not to scale.

8.4 Optimal route

Flying an optimal route is necessary to maximise the scanned area. Since the vehicle is not able to measure during a turn, but does use fuel, theoretically the most optimal route would just be a straight path with a 720 kilometre length. This is however, undesirable, since in most cases the area to be scanned is somewhat rectangular shaped. Nevertheless, it is efficient to avoid turns as much as possible. From this follows the principle of flying *lanes*. The longer these lanes are, the more area can be scanned.

As discussed in section 5.3 on page 20, at cruise velocity, the UAV is limited to a turn with radius 22 m. Assuming a swath width of 30 m, a stroke of width 14 m is left between the lanes. All these concepts have been illustrated in figure 8.3. However, the swath width is not an absolute value, since a highly conductive object at a distance higher than 15 m would completely overrule the measurement of water directly under the SkyDowser. The swath width is strongly dependent on the conductivity of the material in the ground and is therefore hard to quantify.

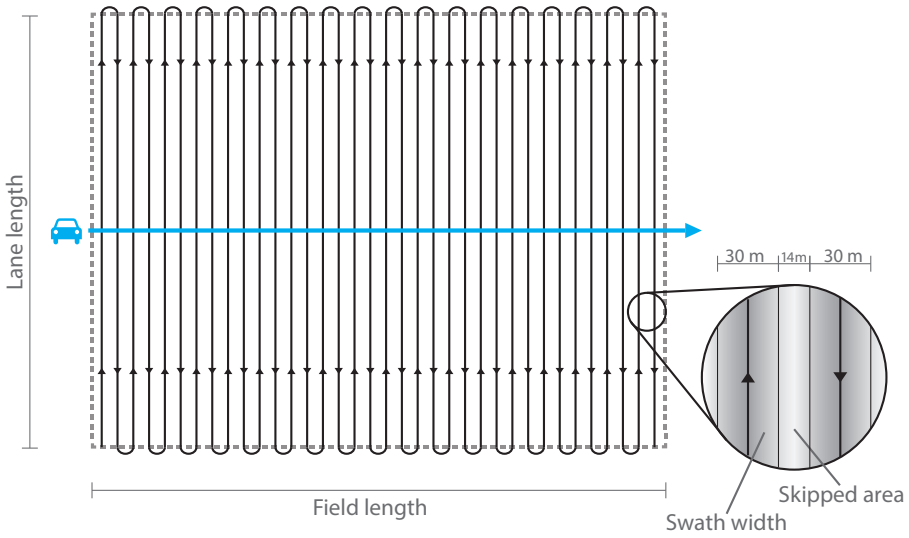

Figure 8.3: Optimal route for a rectangular area. Swath width is not an exact figure, it depends on the contents of the soil. The arrow represents the path of the operator.

A couple of other limitations pose restriction to the routing:

- **500 m line of sight:** European regulations require the UAV to stay within a line of sight of, and no more than 500 m away, from the operator. These regulations are not implemented in Africa, but nevertheless the client has requested to incorporate this regulation in the design.
- **More than 100 m between the car and UAV:** Since the highly conductive car severely distorts the measurement of the FEM equipment, the operator should always keep a distance of at least 100 m[15] between the car and the SkyDowser, as illustrated in figure 8.4.
- **Breaks for the observer:** Considering the SkyDowsers endurance of 8 hours, it is undesirable to let the observer drive constantly. He/she will need a (short) break from time to time. Since the UAV flies continuously, the observer cannot take a long break during the day, but is subjected to many short ones.

Taking all the limitations in account, the optimum with respect to the break of the observer, is when the length of the lane is about 800 m. Consequently the lateral distance between the observer and the SkyDowser is always between 100 m and 300 m (measured perpendicular to the lanes). Assuming that the car can move with 35 km/h, this will give the observer around 3.5 minutes pause, alternating with 30 second drives. For the full range of the aircraft, this corresponds to a field length of over 29 km. The schematic of following the aircraft has been illustrated in figure 8.5. The calculations can be found in appendix I.3 on page 106.

The data link allows to communicate the velocity of the operator to the SkyDowser. The autopilot can adjust its flight parameters in order not to break with the 500 m line of sight or the 100 m margin distances. In case that the operator wants to take a longer break, the SkyDowser can loiter around until the operator starts moving again. Due to visibility issues, it is however advised to always have the SkyDowser in front of the operator.

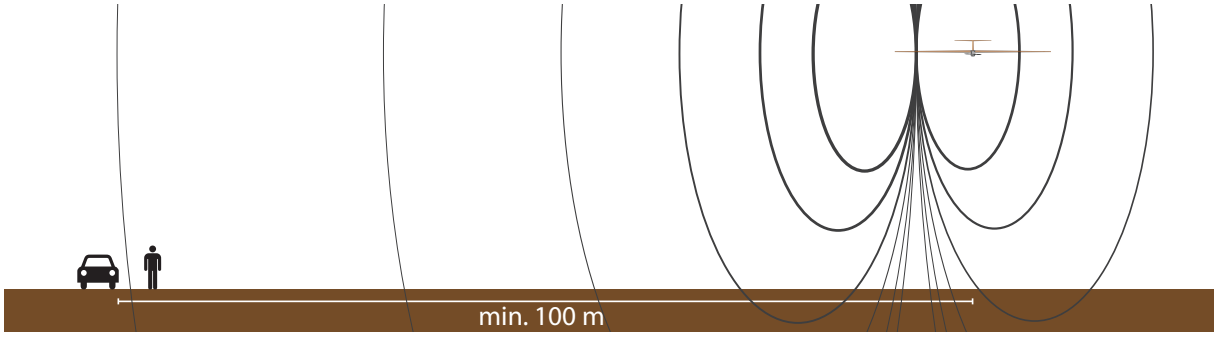

Figure 8.4: Minimum distance between car and the SkyDowser, necessary to avoid distortion of the measurement. The UAV is not to scale. Note that the coil is placed in the wing, not the fuselage.

If areas have a larger length than 800 m, it is recommended to divide the area in sub-areas with a 800 m lane length. Also for smaller areas it is still advisable to minimise the number of turns. Assuming a rectangular area, this implies that the lanes should be parallel to the long side of the area (in a similar fashion as the flight path in figure 8.3).

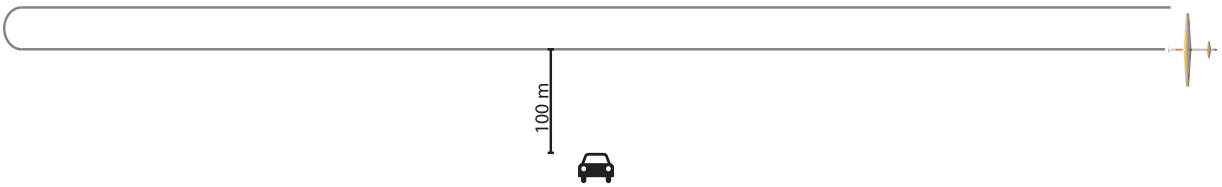

(a) The car should keep a distance of at least 100 m.

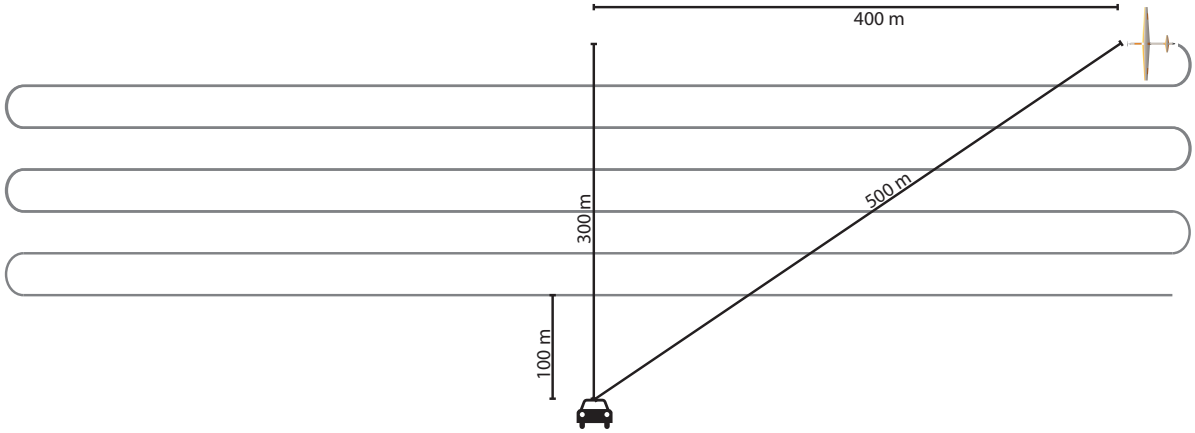

(b) The maximum lateral distance to the vehicle is 300 m. When the SkyDowser is 300 m away, the car should approach the vehicle.

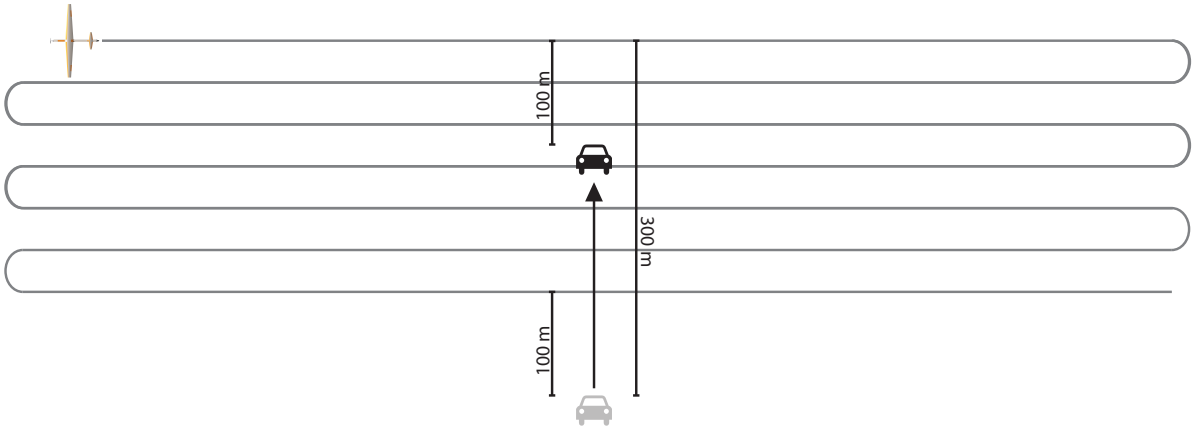

(c) The car should stop again where it is 100 m from the SkyDowser and wait until the distance to the aircraft is again 300 m.

Figure 8.5: Process of following the vehicle, top view.

Finally, the optimisation also depends on the take-off and landing point, but since infinitely many different combinations are possible, this is left to be determined on a case-to-case basis.

8.5 Operation in extreme environments

In some areas, the terrain may be challenging for the car, which hinders it in achieving the velocity necessary to follow the SkyDowser. In this case, it is advised to leave the car behind and have the operator go by foot. The minimum distance between the operator and SkyDowser can now be decreased to 50 m, due to the reduced conductive material of the operator with respect to the car. Using the Pythagorean theorem, the lane length is determined to be 994 m ($2 \cdot 497$ m), as illustrated in figure 8.6. The velocity of the operator should now be 3.7 km/h in order to keep a constant distance to the path of the SkyDowser. However, if the operator cannot travel this fast, or needs a break, this change in velocity can be communicated automatically to the SkyDowser via the data link. The SkyDowser can either fly slower or loiter around until the operator is ready to go. As with the car, it is advised to have the SkyDowser follow the operator, but to always keep the SkyDowser in front of the operator. The battery of the laptop / tablet is limited to a couple of hours at most (especially together with the WPAN router). It can, however, be elongated by carrying a separate battery.

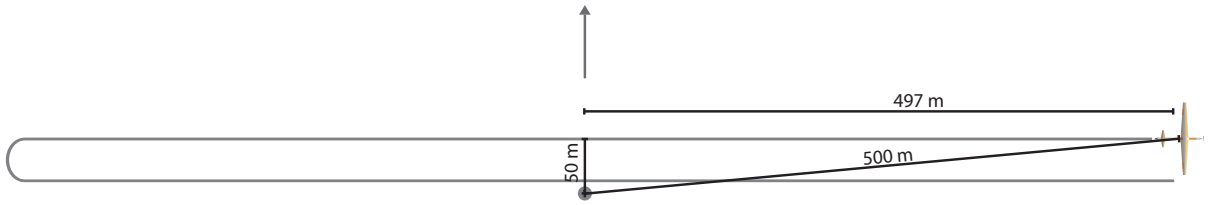

Figure 8.6: Route and distances for the case where the operator travels by foot. Grey dot represents operator and the arrow his direction.

8.6 Route planning

The planning of the route is done on the ground station, which is either a laptop or tablet as described in section 4.3.2 on page 15. The Mission Planner Software[8], allows the user to enter waypoints, which the vehicle can follow. The user interface of the software is shown in figure 8.7. The flight plan is sent to the SkyDowser using the WPAN of the ground station. The software does not allow entering of areas as described in section 8.4. A plug-in for the software should be created, where the scan area can be defined. This is however, beyond the scope of this project. A recommendation would be to include a function where certain areas within the scan area can be excluded, in order to avoid mountain- or forest-like areas or areas with many known obstacles.

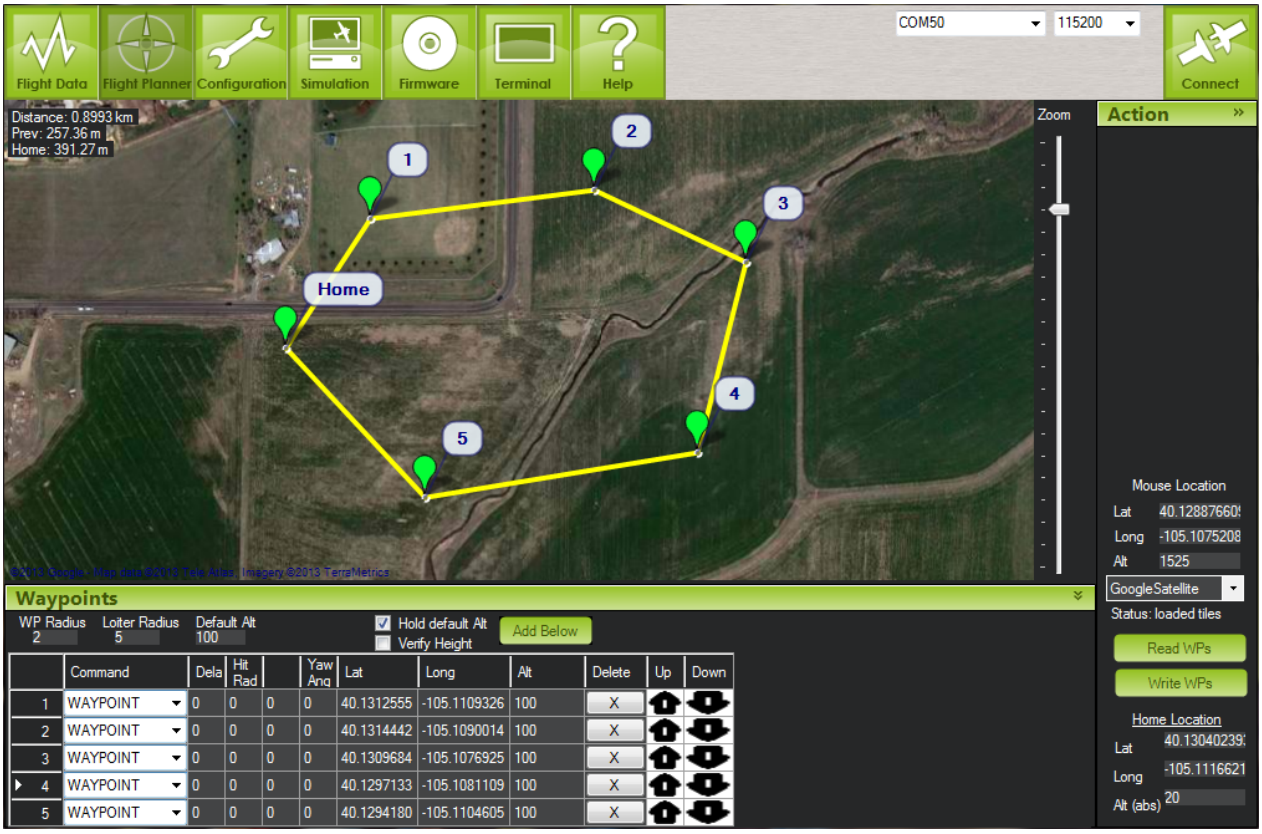

Figure 8.7: User interface for the Mission Planner, created by Michael Oborne. [8]

8.7 Measurement procedure

For a single measurement point, four frequencies are used to examine the soil at four different depths. Per frequency the excitement and relaxation of the soil takes $^1/_{60}$ and $^1/_{40}$ second respectively, which adds up to $^1/_{24}$ second. This is simplified to instant excitement and instant relaxation after $^{10}/_{60}$ second (for four measurements) and is visualised in figure 8.8, where the instant excitement and relaxation have been depicted as arrows.

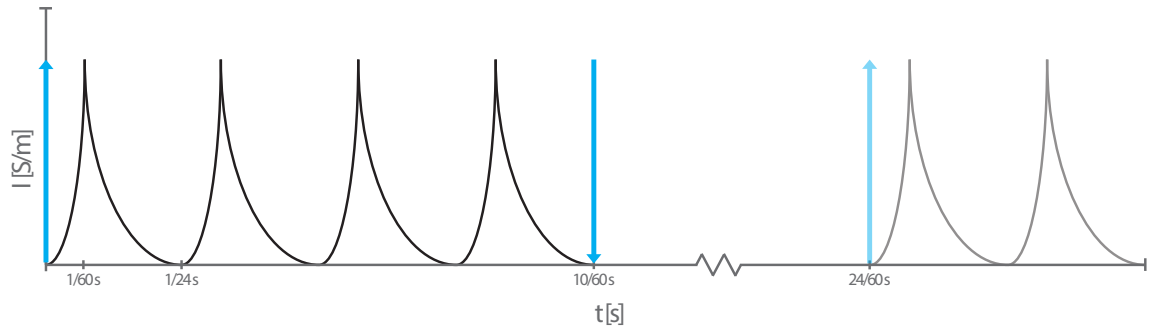

Figure 8.8: Simplification of measurement procedure. Arrows represent instant actions.

While flying at cruise velocity the measurement frequency is set to 2.5 Hz, although it can be increased to a maximum of 6 Hz. This results in a resolution of respectively 10 m and 4.2 m in flight direction, with overlapping ground sample areas, as depicted in figure 8.9. A 3D image is shown in figure 8.10. Even though a smaller resolution is desirable, e.g. in order to find the best place to drill for water, the accuracy of the GPS sensor is limiting to a couple of metres at best [9] and thus a smaller resolution would be superfluous. For more precise measurements the operator can take off the wings and use them as a handheld device, as illustrated in figure 8.11.

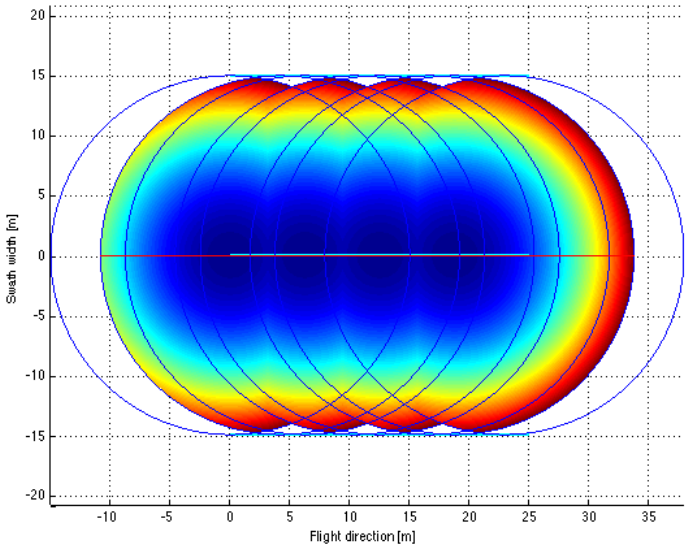

Figure 8.9: Visualisation of 4 measurements on ground for a frequency of 2.5 Hz in 2D. Darker shades correspond to a high overlap during separate measurements.

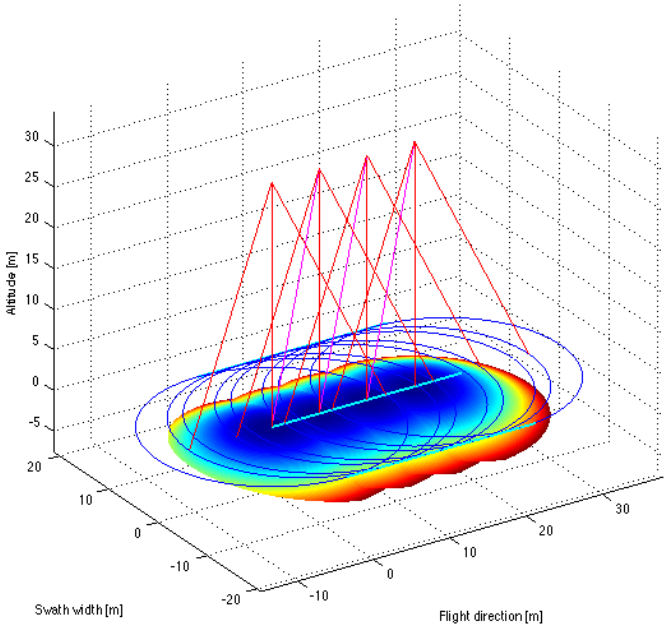

Figure 8.10: Visualisation of 4 measurements on ground for a frequency of 2.5 Hz in 3D. Darker shades correspond to a high overlap during separate measurements.

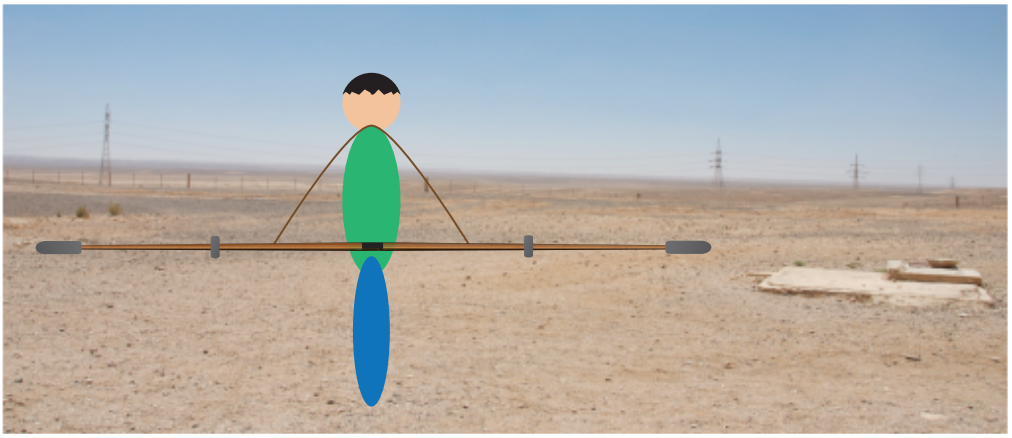

Figure 8.11: Artist impression of the handheld measurement. Rubber padding can be used to protect the equipment from bumping into things.

8.8 Collision avoidance

In order to operate safely and avoid losing vehicles, the SkyDowser is equipped with a collision avoidance system. Different systems have been considered, such as a Laser Range Finder, Radar equipment and stereoscopic cameras. Due to their low cost, low weight and long range, stereoscopic cameras have been implemented in the aircraft. Since these cameras benefit from being placed as far apart as possible, they have been integrated in the wingtips.

The Sunivision AP-IR123BW, that houses a Sony CCD sensor is chosen as base for the stereoscopic collision avoidance system. It has a resolution of 628 by 582 pixels, which is plenty when using a lens with a small view angle. The view angle defines the area which is mapped on the sensor. A wider lens corresponds to a wider area, but less detail. Since the function of this system is to detect object far away, a lens with a small view angle has been chosen. The 25 mm lens that comes with the Sunivision camera has a view angle of 12 degrees. The minimal distance from the vehicle at which an obstacle can be seen is 16.7 m, as illustrated in figure 8.12. Processing 3D images costs a lot of energy and time, although dedicated processors such as the Intel Nuc are available, which reduce the energy necessary. Nevertheless a frame rate of only 5 frames per second has been chosen. This corresponds to a measurement each 5 meter.

In combination with the lens, this sensor can spot objects of only 5 cm at a 150 m distance. The stereoscopic camera can estimate the distance of this obstacle with a 2 m error, which decreases rapidly (for an obstacle 75 m away, the error is only 50 cm). Smaller objects than 5 cm can only be detected from a closer range. This is not considered a problem, since smaller obstacles require smaller evasive manoeuvres.

It is hard to model what kind of obstacles the SkyDowser will be facing. Therefore the vehicle is made such that it can climb 35 m in 150 m in order to evade telephone posts or high trees. In case of larger obstacles, such as cliffs, the SkyDowser can make a 180 degree turn within 50 m from the obstacle as displayed in figure F.3 on page 89. The calculations for this part have been elaborated in section I.4 on page 107.

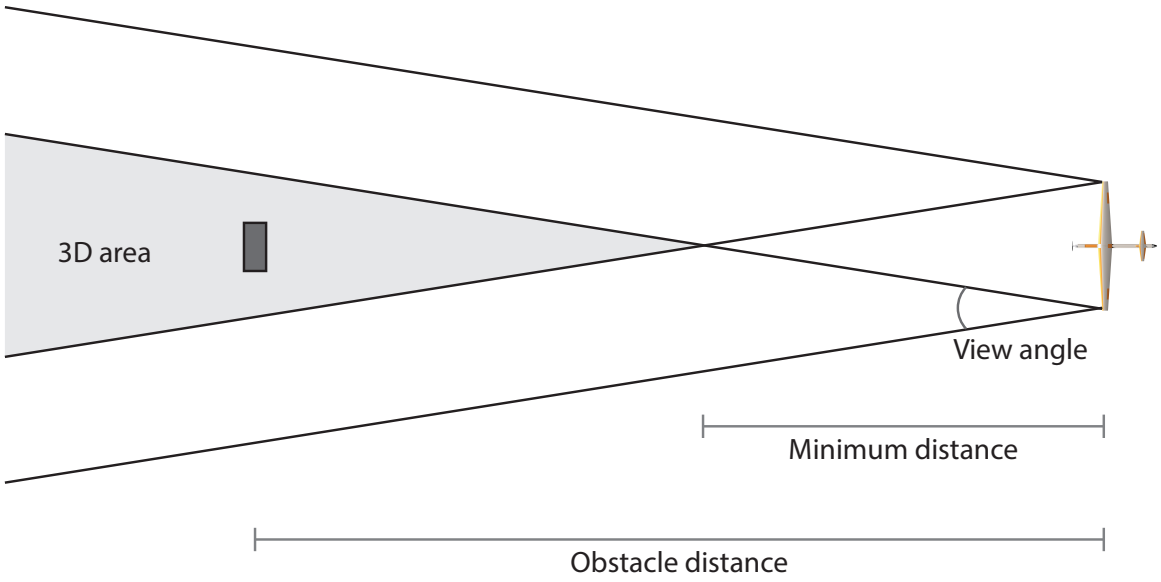

Figure 8.12: The stereoscopic cameras of the SkyDowser and their geometry.

Chapter 9

Resource allocation & budget breakdown

In this chapter the allocated budgets for mass, electrical power, mechanical power and fuel are presented. The presented budgets are based on computed or statistically estimated values and actual values that come from off-the-shelf products that are included in the design.

9.1 Mass budget

The total mass of the SkyDowser is budgeted to be 12.5 kg. The mass budget is one of the most important budgets in this design since it has a huge influence on the other budgets. A lighter UAV is more efficient and therefore the goal is to design as light as possible. A light weight UAV is expected to have smaller structural loads, smaller engines, smaller control surfaces and less fuel that needs to be carried on-board. This reduces the costs, electrical and mechanical power and improves handling of the aircraft by operators. By setting accurate mass budgets for each subsystem, it is ensured that the complete design will not be too heavy and that technical analysis can be performed. The budgeted mass for all sub-components can be found in figure 9.1. Notice that the structural part of the aircraft contributes for almost 50% to the total mass of the SkyDowser. By keeping the design aerodynamically efficient the fuel mass is reduced to only 11% of the total mass. A detailed overview of all masses can be found in appendix J on page 111.

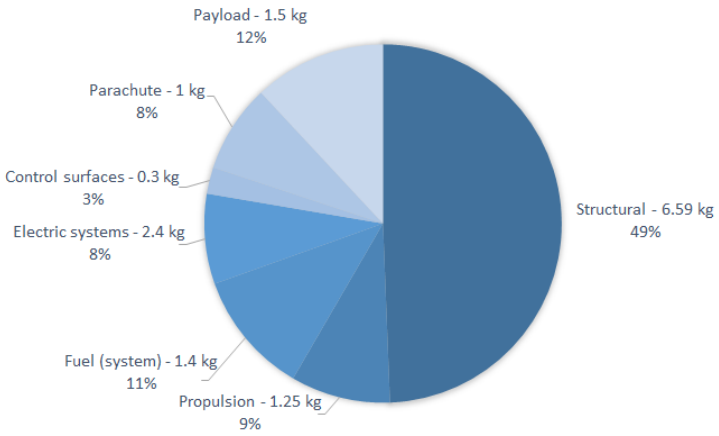

Figure 9.1: Mass budget.

9.2 Electrical power budget

The electrical power budget can be seen in figure 9.2. The detailed overview of the electrical components can be found in figure K.1 in appendix K on page 113. The total power of the electric systems combined equals to 32 Watt. Notice that the collision avoidance system takes up 36% of the total power budget. This comes from the fact that the required processor to create a real time depth map needs to be very powerful. The servos use almost 25%. This is in the most extreme case that the aircraft needs to adjust continuously. All electric systems and systems are chosen such that they have a minimised power consumption in order to lower battery and generator masses.

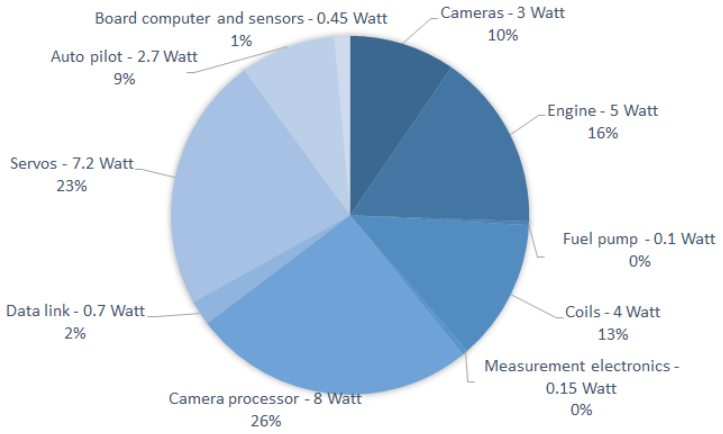

Figure 9.2: Electrical power budget.

9.3 Mechanical power budget

In figure 9.4 the composition of the mechanical power, the so-called shaft power is presented. The engine is able to produce approximately 2000 Watts of shaft power. From this total available power only 16% is used for cruising at different velocities. 50% of the shaft power budget is used for manoeuvres like accelerating, climbing and turning. Finally some reserve power is available which is not expected to be used during normal operation. Keeping the engine out of these high RPM ranges overheating is prevented, engine wear and fuel consumption are reduced.

9.4 Fuel budget

The total fuel budget consists of the minimal mission fuel, an extra fuel block in case of operating in extreme weather conditions and finally a block for reserve fuel. The fuel budget can be seen in figure 9.3. Notice that in ideal weather cases there is still 40% of fuel left in the tank.

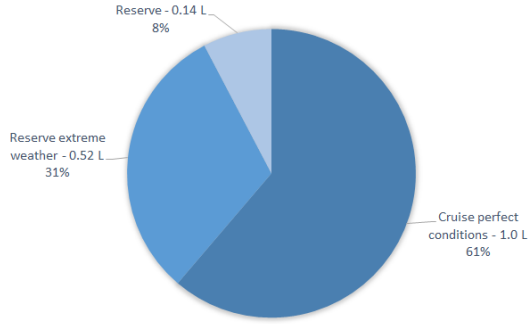

Figure 9.3: Fuel budget.

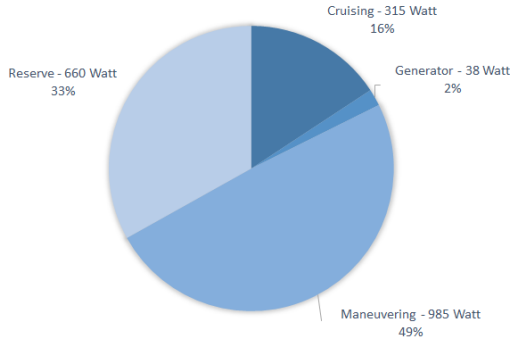

Figure 9.4: Mechanical power budget.

Chapter 10

Technical risk assessment

To ensure a safe operation of the SkyDowser, a risk assessment has been made. In this risk assessment all possible risk during operation of the SkyDowser have been identified, including possible mitigation of the corresponding risks. In this chapter the most important risks and a way to mitigate these are discussed, and shown in a risk map, in figure 10.1. A complete overview of all risks and mitigation can be found in appendix L, on page 114.

- **Collision:** Although there is a collision avoidance system on board, the cameras used might fail. Fortunately, the UAV must always be in line of sight of an operator, who thus serve as a redundancy system. If such a failure occurs, the mission can be aborted by the operator if necessary.
- **Parachute failure:** The parachute may get stuck, cables could break, the hatches might malfunction or the fold could be incorrect. In all cases, it would result in a lost plane. In order for the system to operate properly, the design is such that there are no edges to get stuck on. Since the hatches open because of lift, as long as there is adequate forward velocity, they will open. Lastly, the parachute is slightly over sized and is specifically designed for fixed-wing UAVs. This means it is heavy duty and reinforced with Kevlar-fibres. To prevent wrongful folding or damage, proper instructions and inspection is required for handling the parachute.
- **Launch failure:** The catapult system may fail due to rubber bands that break, or dried out. This can easily be overcome by using more elastic bands. The structure is over designed and can carry twice the maximum load at take-off. Next to that, the lever cannot accidentally be pulled, since a hinge system prevents its movement. This will make sure the UAV will not launch when someone in standing in front of the system for example. Also, when all procedures in the operational manual have been followed, and no technical defects are present, the owner/operator of the particular SkyDowser is responsible for any done damage.
- **Human error:** A risk with significant impact is a possible human error. The probability of this occurring can be minimised by providing proper training and a complete instruction/operation manual. However, in the case the operator does make a mistake, this risk is transferred to the owner of the SkyDowser in question.
- **Structural damage:** Structural damage can occur because of bird strike, possible even damaging it such that flight cannot be sustained. At the positions where impact is most likely, the SkyDowser can be reinforced at those positions. Since both the CAS is used, and an operator is present at all times, the probability of a collision in mid-air is low, minimising possible structural damage. Fortunately, the parachute used for landing can be deployed at any given time. Since an operator is always present, he/she can fire the parachute and instantly abort the mission if such an event occurs.
- **Propulsion failure:** Engine failure can be prevented by proper and regular inspection and maintenance. The chances of the engine overheating are low since the engine is on the outside of the UAV, providing constant cooling. The possible dirt collecting in the engine must be cleaned after every flight. Since the engine is easy accessible, this should not be a problem. A possible fuel leak must be detected by the system status check. If the leak is serious enough the mission can be aborted by using the parachute. The operator can at any moment check the amount of fuel left and if necessary abort the mission manually. If the engine fails the UAV can glide for about 25 to 30 seconds and make a semi-controlled belly landing. The parachute can also be used to abort the flight.
- **Electrical system failure:** If power can no longer be provided, the autopilot will stop working. Here, the parachute can serve as an emergency solution once more. A power failure can be caused by short-circuit, overheating, failure of the generator or even an improper battery. By performing regular checks before each launch and continuous monitoring of all systems during flight, this risk can be minimised.
- **Communication lost:** The used communication link has been tested extensively. Before launch, the vehicle is checked and the communication link is tested once more. In case of malfunctioning, the operator is notified. In worst case scenario, the operator can intervene and a landing can be initiated.

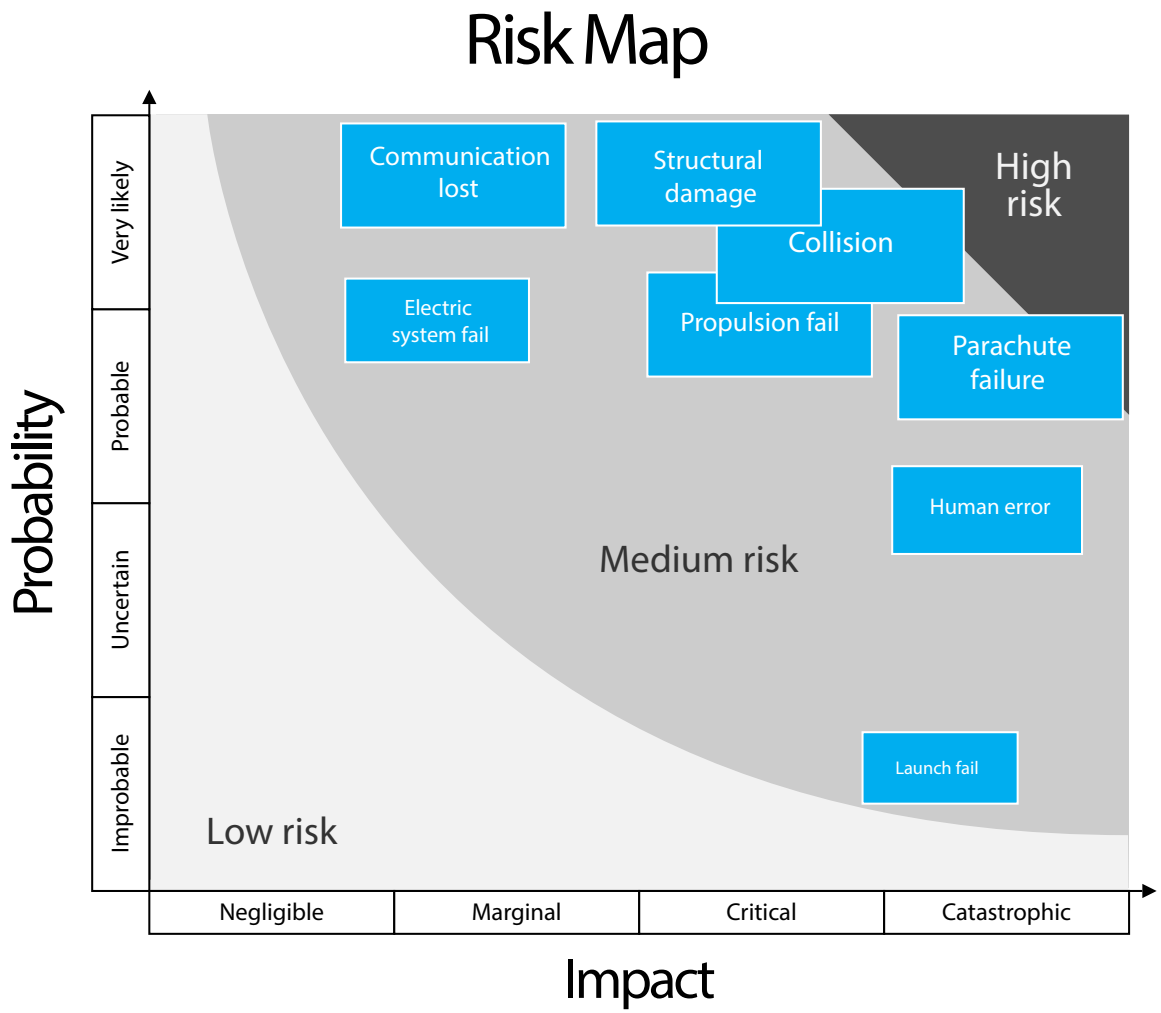

Figure 10.1: Risk map for the most important operational risks. Larger items convey greater threats.

Chapter 11

Sustainable development strategy

In this chapter the ways in which sustainability has been implemented will be shown. This will be done in terms of decisions taken during the design process and in what way the (mission of the) SkyDowser contributes to sustainability.

11.1 Implementing sustainability in the design

Throughout the design of the SkyDowser sustainability was kept in mind, ensuring a sustainably responsible final design. Sustainability is implemented in the design by means of the following protocol:

- **Choosing recyclable and non-toxic materials:** Since the FEM interferes with the presence of metallic materials in the aircraft, the use of aluminium is excluded. Therefore, the majority of the SkyDowser will be made of fibreglass. Fibreglass is cheaper than carbon fibre and provides sufficient structural properties. It also is relatively easily recyclable, in contrast to carbon fibre. Finally, almost no toxic materials are present in the aircraft, except for a small (Li-ion) battery of 11V with 1300 mAh. This battery is used as backup, since normally all power is generated by the on-board generator.
- **Reducing the fuel consumption** With a range of 720 kilometres, the SkyDowser can scan a considerable area per day. Also, the fuel consumption is only 60 grams of fuel per square kilometre scanned, at a cruise velocity of 25 m/s.
- **Exploring the possible usage of bio fuel:** It is possible to use bio fuel as additive to the gasoline and oil mixture if this is locally available. The engine is expected to be able to run on blends of up to 15% bio-ethanol with gasoline. Moreover Bio-gasoline is a good alternative. Bio fuel does however has the implication that the caloric value is less compared that of regular gasoline. Therefore the total required fuel increases in volume. However, since the fuel tank is slightly over-sized this is not a problem. Using bio fuel is part of a sustainable transport strategy since it reduces the dependency on fossil fuels.
- **Expanding the lifetime of the SkyDowser and minimise waste:** The aircraft is designed such that maintenance during operation is easy and thus as cheap as possible. Since most parts are easily replaceable, replacement of that component instead of the entire aircraft is possible. In the extreme case of damaged wings, even these can easily be replaced since they are designed to be dismounted for easy transportation of the aircraft. All this results in the reduction of waste and increases the total lifetime of the aircraft.

11.2 Contributions to sustainability

Sustainability can be divided into three main pillars: social, economic and environmental sustainability [16]. The designed aircraft has a major contribution to the entire project of finding water in remote areas. These contributions are:

- **Social:** Social sustainability depends on different factors; combining to form a condition that enhances life within communities and enables members of these communities to achieve and maintain this condition. A major factor is equity of access to key services [17] such as drinking water. It is therefore clear that access to healthy drinking water and water for irrigation, enhances the social sustainability. Since this aircraft can be an enabling factor in finding water, the contribution to social sustainability is considerable.
  Besides the fact that finding a valuable water source has a large impact on a local community, the final designed system can also contribute a lot to the entire Third World. This is because the SkyDowser is capable of scanning large areas at a time.
- **Economic:** The budgeted unit price of the SkyDowser is approximately €10,000, making the mission of finding underground water reservoirs an economically feasible project according to the client. It

is possible to produce enough units of the SkyDowser to scan a substantial amount of land within a reasonable amount of time, contributing to the economic sustainability of the entire undertaking.

- **Environmental:** Although ground water is in general a good source for water, because of its quality and its abundance compared to fresh surface water[18], the use of ground water may be unsustainable. Since ground water has to be renewed, the rate at which it is pumped to the surface might be a threat to the existence of the underground water basin in the future. For the SkyDowser to contribute to environmental sustainability, it is therefore important to make sure that after underground water is discovered, it is used in a responsible way. Also, the fuel consumption of 60 g/km^2, thus minimising the pollution during the missions to be executed. The fuel consumption at cruise velocity results in a CO_2 exhaust of 0.11 g/km^2.

Chapter 12

Cost breakdown structure

12.1 Cost estimation

During the project a detailed cost estimation was made to investigate how much the project will cost and where the largest costs are located. A detailed cost estimation can be found in appendix M.2 on page 119. In table 12.1 a short version of the cost estimation can be found. Since there are a lot of different costs, relating to another quantity of time or units, the results in this table are normalised. The results in the table represent the total costs for a project of 5 years, the expected lifespan of the UAVs. During this project scans will be made with 100 UAVs for 180 days per year. The price per unit specified in the table therefore holds both the unit price and the costs to operate the unit for five years.

Table 12.1: Cost estimation for the SkyDowswer project case study.

Cost	**Worst case**	**Best case**	**Average**
Man hours	€9,720,000	€7,605,000	€8,662,500
Fixed cost supportive equipment	€140,000	€100,000	€120,000
Car	€1,100,000	€900,000	€1,000,000
Variable cost supportive equipment	€5,400,000	€2,340,900	€3,870,000
Fixed operational cost	€1,500,000	€1,250,000	€1,375,000
Maintenance	€1,750,000	€992,500	€1,371,250
Electrical components	€248,150	€199,400	€223,775
Engines	€58,500	€47,500	€53,000
Materials	€72,000	€60,000	€66,000
Fixed manufacturing costs	€8,420	€6,500	€7,460
Variable manufacturing costs	€210,000	€135,000	€172,500
Development Cost	€1,335,000	€1,059,000	€1,197,000
Total operational cost per UAV	€194,650	€130,834	€162,742
Total investment	€21,524,070	€14,695,800	€18,118,935
Unit price per UAV	€7,287	€5,419	€6,353
Ready to use unit price per UAV	€20,771	€16,124	€18,447
Price per km^2	€8.25	€5.63	€6.94

12.2 Cost breakdown structure

With the cost estimation from section 12.1 the major contributors to the total cost can be distinguished. This overview can be seen in figure 12.1. A more elaborate cost breakdown structure can be found in appendix M on page 119. In this cost breakdown structure the budgeted resources are given in both absolute numbers and as a percentage of the entire budget. The values in the cost breakdown structure are based on the average predicted costs.

It is interesting to see from the cost breakdown structure that for a project of five years almost 90% of the costs are related to operations. The production cost, the costs that are made to produce and develop 100 SkyDowser UAVs are only 10% of the total cost. At this stage the SkyDowser is in a "ready to use state". The ready to use unit price of the SkyDowser, including all equipment to be able to launch it "from your backyard" is estimated to be within a margin of 23% of €18,500. Out of which 66% of the costs are spent on development. Buying the unit and operating it for five years will cost an estimated €162,000 per UAV. The unit price of a single SkyDowser is €6,500. In this case operational cost and development cost are not included.

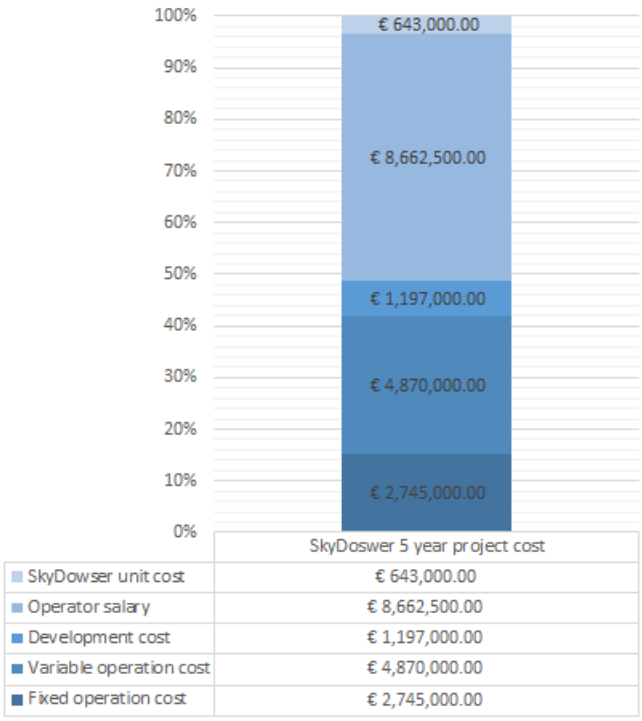

Figure 12.1: Overview of the cost breakdown major branches.

The "ready to use unit price" highly depends on the number of UAVs that will be produced. In figure 12.2 one can see that when taking the development cost into account, the investment price of a single UAV drops below €10,000 when more than 300 SkyDowsers are made. Eventually the ready to use price will converge to the unit price of €6,500 when the number of UAVs produced becomes very large.

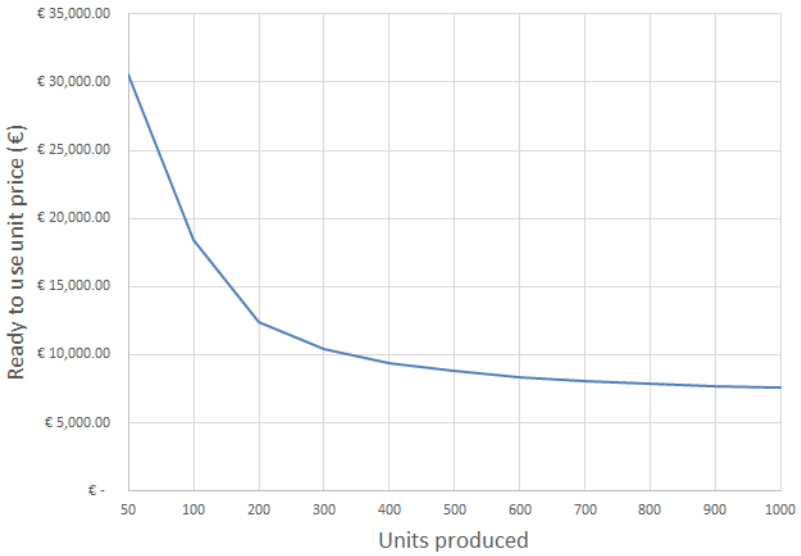

Figure 12.2: Relation between the ready to use price of the SkyDowser and the amount produced, including development cost.

For investigating the profitability of the SkyDowser project it is interesting to see what the total investment price is expressed in a price per square kilometre. The price per km^2 takes into account production cost, development cost and operational cost. The relationship between the price per km^2 and the number of units

produced and operated simultaneously can be seen in figure 12.3. The price per km^2 will eventually approach a price of approximately €6.60 per km^2.

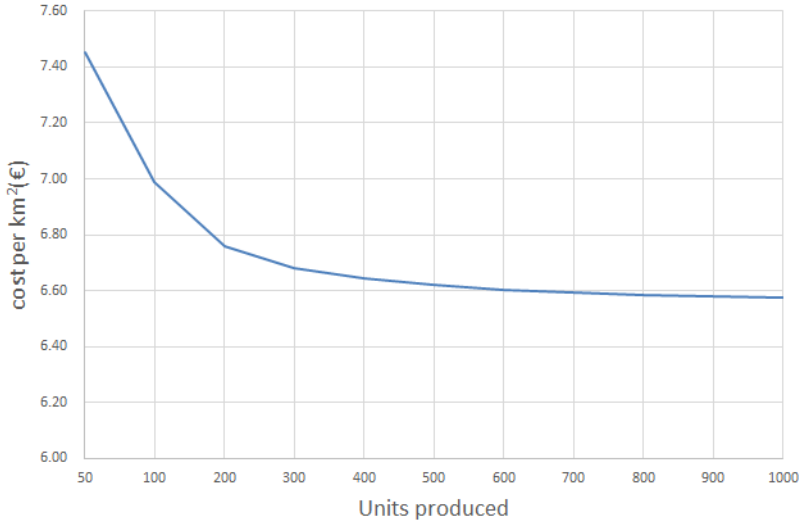

Figure 12.3: Relation between the price per km^2 of the SkyDowser and the amount produced and operated.

Chapter 13

Market analysis

In the Baseline report [2], a market analysis was performed for the market to be entered. This market was defined as: *Searching for groundwater in remote areas.* In this chapter the market analysis that was performed is updated where necessary.

13.1 Current market solutions

As described in the initial market analysis, a few solutions to search for groundwater are currently available. An overview of the solutions that use the same principle (electromagnetics):

- **Ground Electromagnetics (GEM):** The GEM instruments are used as a hand-held instrument which can be carried by a person to scan a desired area [19]. The result is a good image and is a reasonably cheap solution, however the area that can be covered is rather small by a single person, since that is a time intensive process.
- **Helicopter Electromagnetics (HEM) [20]:** The HEM instruments are carried underneath a helicopter and can scan a desired area from the sky. This method has the advantage that it is able to scan large areas at the time. Some downsides to this concept are the high costs and logistics that are involved in using this method.
- **Airborne Electromagnetics (AEM): [21]** AEM measurements are now taken using specially-equipped aircraft. Fixed-wing aircraft give a solution for larger survey areas and for deeper ground penetration. Most AEM surveys are conducted with the aircraft flying at low altitude along straight parallel flight lines with measurements at regular intervals along those flight lines. The aircraft is equipped with a coil running from nose to wingtips to tail. Since this method requires a specially designed full-scale aircraft this method also implies high costs and logistics that are involved.

Currently there are also other methods that are used to find groundwater that use other methods than frequency electromagnetics [22];

- **Finding groundwater by using the topography:** Analysing maps and local vegetation gives a first indication of the presence of water. This can also be used for large-scale investigations. A global analysis can be carried out through the interpretation of satellite images or aerial photos. This method however still implies a lot of resources that are necessary to interpret all possible groundwater locations and still the question remains on how much water can be found. Moreover trapped groundwater deeper underneath the surface might not be detected.
- **Dowsers:** In numerous countries certain people claim to have the ability to investigate and detect the presence of groundwater in the form of veins, faults and aquifers by means of dowsers. This method is not proven to be reliable, moreover findings are imprecise, do not indicate the size of the aquifer and this method does not make it possible to detect small, relatively deep groundwater flows. Although technically this method is of no use for this project, it still is part of the current market segment and thus a distant competitor.
- **Proton Magnetic Resonance (PMR) investigations:** This method consists of sending electric currents into the ground, then measuring the signals emitted by the nuclei of hydrogen atoms in water molecules. This instrument is hand-held and used on site. For scanning large areas it would be very time consuming and labour-intensive. However the quantity of water present can be determined immediately.

13.2 Market size

The market to be entered was described as *Searching for groundwater in remote areas.* As is described in section 13.1 there are only a few existing methods available in this market. Next to this lack of competition,

the potential clients in this market are most likely part of the scientific community and NGOs operating in these remote areas. The number of large NGOs is limited and most, if not all, have limited budgets. Considering this, the market served can be defined as a niche market. An exact figure for the market size cannot be presented, since the required data to do so is simply not available at this moment. However, based on the unit price of the Skydowser one can estimate the possible sale volume and thus revenue. As an example, a Dutch funding programme has been consulted [23]. If a pilot programme would be set up, with the goal to search for groundwater in remote areas, a maximum funding of €600,000 can be received. With this particular funding programme alone, up to 75% of the required development costs could be covered. As can be seen in appendix M on page 119, this would suffice to finish development up to and including the test phase. The total budget available for water management programmes are a multitude of this example, suggesting hundreds of SkyDowsers could be built and used in the desired remote areas. With the large areas that can be covered on this scale, the potential market could be worldwide.

13.3 Market profitability

In order to evaluate the market profitability, Porter's Five Forces Analysis [24] can be used. This analysis consists of a framework providing an organised method to determine the competitiveness within the market, which defines the attractiveness to actually enter the market. Porter defined five forces, which are described in the following list. In this list the according properties for the to be designed system are described.

1. **Threat of substitute products or services:** As is described in section 13.1, three existing (airborne) competitive devices are available; of which one is helicopter-based. Furthermore, the to be designed system must be able to operate in remote areas, most commonly by organisations with little money to spend. This means only cheaper available systems would pose a real threat, which are currently not available. Therefore, one can say that the threat of substitute products and services is negligible.
2. **Threat of new entrants:** The threat of new entrants is certainly not negligible. Because (fresh) water is becoming increasingly scarce, the economical value of this fresh water also increases. This means that it is interesting for new entrants to develop competing measuring devices. If one also assumes the most efficient measuring method is an airborne-based measuring system, the threat of new entrants is even larger. This is mostly because of the rapidly expanding market for UAVs and accompanying decrease in costs of UAVs. Thus, the use of an airborne (UAV-based) measuring system in the search for water is becoming an easier and cheaper option. The threat of new entrants is therefore large.
3. **Threat of established rivals:** The threat of established rivals is nearly non-existent. Since the to be designed UAV is supposed to operate in remote areas. Here, the use of slow, ground-based methods is not a viable option. These devices are simply too inefficient and thus too expensive to scan large, remote areas. Therefore, an airborne solution currently seems to be the most viable option. However, as stated in section 13.1, there are only airborne solutions currently available, which are expensive to operate. Thus, because of the absence of cheap alternatives for the SkyDowser, there is simply no threat of established rivals.
4. **Bargaining power of suppliers:** The bargaining power of suppliers is minimal. In order to minimise the cost of the SkyDowser, as many commercially-off-the-shelf components as possible are used. Furthermore, most materials that can be used for the SkyDowser are commonly available. Besides that, because of the large quantity of UAVs available, most components will be available from multiple suppliers. Thus, the bargaining power of suppliers will be minimal and can be further minimised by using more off-the-shelf components.
5. **Bargaining power of customers:** The bargaining power of customers is small, since there are simply no real alternatives available yet. However, one should keep in mind that customers will have little money to spend. The SkyDowser is a much cheaper alternative than the current products available. However, there is a link between the customer's bargaining power and the threat of new entrants. With more competitors, customers have a choice between several solutions. As the threat of new entrants is large, the bargaining power of customers may increase over time.

To illustrate the possible profitability of this project, an example for scanning all of Somalia for groundwater is given in table 13.1. The unit cost and cost per km^2 are based on the result of the cost estimation in chapter 12. The selling price of €750 per km^2 is the price proposed by the client ($10 per hectare). With 100 SkyDowsers it would take 1.2 years to scan the entire surface of Somalia. If 2% of the area that is scanned where to be sold, that would give a yearly profit of €4,450,000. The break-even point of this example lies at a selling-percentage of 0.93%.

Table 13.1: Example for profitability: scanning Somalia.

Input		**Results**	
# Aircraft produced	100	Years required to scan	1.2
Cost / km^2	€7	Total cost	€4,464,000
Selling price / km^2	€750	Yearly profit	€4,190,000
Area Somalia	637,660 km^2		
Operational days per year	180		
Percentage of scanned area sold	2%		

13.4 Opportunities for new markets

The technology for finding groundwater is based on the conductivity of ground materials. This means that the SkyDowser can also be used in different fields. Next to using the same measurement package, the aircraft could also be used in other markets. Some examples are listed below:

Same measurement package

- **Detecting landmines:** Another possible application is the detection of old weaponry, especially landmines. According to the United Nations around 110 million landmines were still lodged in the ground in 1994 and each year between 2 and 5 million new mines are placed.[25] The United Nations estimates that currently there are 250,000 amputees due to landmines and this number increases with another 800 people per month. Note that this number is just the number of people who survive the explosion and does not include immediate deaths. A dedicated search and removal project would cost at least $33 billion to clear all current mines according to the United Nations. Although, when using FEM technology the search for weaponry can be performed simultaneously with the search for water, as long as the ground is also scanned at a shallow depth.
- **Archaeology:** FEM technology has already been used to map the subsoil in Flanders, Belgium[26] for archaeological purposes. The aircraft can be used to pinpoint the location of an excavation, which reduces the cost archaeological research. This information can be obtained from the same measurements performed for the search for water.

Other roles

- **Surveillance:** As discussed in chapter 6, the aircraft can be fitted with additional fuel tanks to greatly increase the range of the aircraft. Together with (infra-red) camera's this enables the SkyDowser to perform all sorts of aerial surveillance missions, such as border protection or wildlife tracking. It has to be noted that this might not be an option in all countries, due to the requirements of an operator within visual line-of-sight. In this case it is of little use to extend the range of the aircraft.

Chapter 14

Compliance matrix

In this chapter the characteristics of the SkyDowser are compared to the requirements discussed in chapter 2 on page 5. An overview of the requirements is given in 14.1. Where relevant, the values that apply for the SkyDowser are given.

Table 14.1: Compliance matrix.

Top-level requirement	**Sub-requirement**		**SkyDowser**
The UAV must carry a FEM instrumentation package, containing:			
	Three coils	✓	
	A processor	✓	
	A battery	✓	
	Two inclinometers	✓	
	A magnetometer	✓	
	An altimeter	✓	
The UAV must be able to perform measurements at an acceptable level of accuracy			
	Coils two meter apart	✓	
	Cruise velocity below 30 m/s	✓	25 m/s
	Fly at fixed altitude	✓	
	Have coils on same axis	✓	
	Twist between coils below 3°	✓	1.3°
Additional			
	Should be foolproof	✓	
	Operate in all climate circumstances	✓	
	Take-off and land in remote areas	✓	
	Comply with regulations	✓	
	Unit price below €10,000	✗	€18,500
	Scan at least 10 km^2 per day	✓	29.1 km^2
	Fly autonomously	✓	
	Fly for more than two hours	✓	8 hours
	Have a modular design	✓	
Regulations			
	Operate within VLOS of observer	✓	
	Operate within 500 m of observer	✓	
	Cruise velocity below 36 m/s	✓	25 m/s
	Operating mass below 150 kg	✓	12.5 kg

The only requirement that is not met is the requirement of a unit price below €10,000. As discussed in chapter 12 a major portion of the current unit price of €18,500 is the cost for development. The price for the raw components of the aircraft lies between €5,500 and €7,300. However, the unit price is based on the production of 100 SkyDowsers. When more aircraft are produced the unit price reduces, as is shown in figure 12.2 on page 48. The unit price is less than €10,000 when more than 300 SkyDowsers are produced.

Chapter 15

Conclusion

The aim of this project was to design an aircraft that can carry a frequency electromagnetic instrumentation package to map ground water levels. The aircraft should be able to scan at least ten square kilometres per day, whilst providing a stable measurement platform such that accurate measurements can be taken. The designed aircraft will be used in a mission to scan the Earth's land surface in ten years, mapping the ground water. This report discussed the design of the aircraft that can perform this task.

The result is the *SkyDowser*, an autonomous unmanned aerial vehicle with a wingspan of 3.5 metres, weighing 12.5 kilogrammes. Propulsion is provided by a piston engine running on petrol, which is a widely available fuel. It is able to operate in most climate conditions, and take-off and landing is possible from virtually any terrain. Its take-off capabilities are realised by a catapult system that accelerates the SkyDowser over a distance of 3 metres. The aircraft is recovered by a parachute system, which can also be used for emergency landings.

The SkyDowser is capable of fulfilling all set performance requirements, it even exceeds the requirement to scan 10 square kilometres per day. The SkyDowser can cover a maximum of 29 square kilometres per day using only one litre of fuel. Designed with ease of maintenance in mind, a large degree of modularity is achieved. This allows the wing to be dismounted enabling the operator to perform a handheld measurement.

The unit price of the SkyDowser is €18,500, considering a production series of 100 units. This price includes the development costs, which is a large part of the price. The price drops significantly, to a minimum of €6,500, when more units are produced. Given the large coverage area, and unit price of €18,500, the operational costs are €7 per square kilometre. Compared to alternative scanning methods, the SkyDowser delivers great performance for a low cost.

By changing the payload the SkyDowser is able to penetrate a completely different market. Moreover, with an extended fuel tank the range of the SkyDowser can be extended by 24 hours. This makes the SkyDowser highly suitable for various other missions, for instance; aerial surveillance for wildlife preservation or border protection.

With the increasing water shortage, one in three people around the world still do not have access to enough water to meet their daily needs. The SkyDowser can be considered the most suitable solution to look for water close to the communities that most need it.

Chapter 16

Discussion & recommendations

From the conclusion one can see that the current design is a suitable solution which satisfies the requirements. During the short period of ten weeks in which this design was shaped, there are still calculations and design decisions that can be improved further. Moreover, since safety and reliability are of great importance to the client, more risks must be identified and reduced by means of a stronger risk mitigation case. This leads to the following recommendations for further development, which contain the advised procedures on how to optimise and finish the SkyDowser design and operation.

16.1 Improvements on the design

The recommendations to the client are mainly based on further improving the design:

- **Extend market analysis:** A lot of possibilities for other applications of the UAV have been provided in chapter 13. These solutions can be investigated further to add value to the data the SkyDowser gathers. Perhaps adding other measurement equipment can even make the SkyDowser perform multiple tasks in the same flight. This way profitability can be improved.
- **Investigate aesthetics:** Even though technically unimportant, aesthetics may very well improve sales. This might not be of importance if clients seek the cheapest option, but if more options in the same price range exist, this might be decisive. Especially when other applications are investigated, the aesthetics might play a role.
- **Investigate weather effects:** Even though head - and dead wind have been taken into account, effects of gusts, side wind, lightning strikes e.o. are not investigated. Also, consequences of dirt and sand should be analysed.
- **Relate measurements to environment:** To be able to correlate the measurement data of metal objects on the surface with the environment, a photographic camera can be added underneath the aircraft. Peaks in the data can be validated in this way.
- **Add second laser altimeter:** To measure the height of upcoming terrain a second laser altimeter can be placed underneath the aircraft. This laser is slightly pointed forward, with a fixed angle relative to the body axis of the aircraft. Using this device it is possible to change the flight altitude of the aircraft before the actual height change of the terrain takes place. An on-board processor executing an algorithm must decide if the change in terrain height is sufficient to change the aircraft's altitude.
- **Improve the landing system:** With the current design it is possible that the UAV is dragged over the ground after landing. Also, the aircraft could roll during the landing, thus falling on a wingtip. Improvements have to be implemented to diminish these problems, possible improvements include rubber shock absorbers on the bottom of the fuselage and wingtips, landing struts, local reinforcements of the wing structure.
- **Design route optimisation plug-in:** The route planner that comes with the ArduPilot autopilot system is an easy tool for operating the aircraft. At this stage way-points can be inserted by hand. Since the mission is expected to require a lot of way-points, it is preferred that the SkyDowser calculates his own way-points after the operator simply selects an area. A plug-in to realise this needs to be developed.
- **Find a solution to minimise the cost of the supportive vehicle:** The cost that are implied with the required supportive vehicle is relatively large. To minimise operational cost it is good to start with looking at reducing vehicle cost.

16.2 Improvements on technical analyses

There are some aspects of the technical part of the design that have not been investigated, such as aero-elasticity. To make sure the design functions as expected without failure, the analysis needs to be improved further. These steps are listed in the design and development logic, chapter O on page 126. Next to that,

the knowledge acquired in the Bachelor program of Aerospace Engineering is limited, which does not result in the optimal design for each component. For example: creating CFD-models is not within the scope of this project or the Bachelor education, double tapered wings are also not part of the Bachelor program, etc. Below is a list of design parameters that are likely to be changed in the final design:

- **Variable fuselage diameter:** This increases production costs but saves weight, and possibly attachment points for other components do not need reinforcement. This required reinforcement could then be delivered by the fuselage.
- **Placing the coils further towards the wing tips:** The design as it is now has the coils in the wing box. The single coil is placed as far from the fuselage as the wing box dimensions allow. The other coils are not placed as far into in the other wing, to preserve moment equilibrium. However, they can be placed further apart if other systems are placed in the wing as well. Also, the coils can be placed further into the wing box if they can be made more compact. They could even be placed at the wing tips, perhaps in a thickened area, to maximise the distance between the coils. The wing structure will then have to change (and possibly be asymmetrical) to allow for these changes.
- **Redesign load bearing structure of empennage:** The empennage has the same structure as the main wing. A better solution could not be found due to time constraints. Since the loads on the structure are well within limits, a lighter, more efficient structure can possibly be found.
- **Investigate stress-concentrations at cut-outs and mounting points:** The structure around cutouts and mounting points may need reinforcement. However, this analysis is beyond the level of detail of this report.
- **Analyse bonding and connecting elements:** A course analysis has been performed on these elements but this has to be improved upon.
- **Optimise the launching system:** The rail and sled system that was designed is quite large and heavy and can be optimised further.
- **Determine the error of the stereoscopic cameras:** At the moment the error calculation is based on a study of the human eye. It is however uncertain that this can be applied and scaled to the stereoscopic camera system on the SkyDowser.
- **Control surface determination:** A simplified model is used to determined control force and thus surface area. This analysis needs to be extended to get more accurate results.
- **Investigate different aerofoils:** The NACA-2412 aerofoil was chosen because it meets the demands of the aircraft. However to be sure that the best aerofoil has been selected, the analysis should be re-performed for other aerofoils. Only then it can be made sure a most optimal aerofoil is chosen.
- **Investigate propulsion efficiency:** The amount of fuel that is required for the mission is largely dependent on estimated propulsive efficiencies. Since the fuel mass has a lot of influence on the complete design it is advised to obtain better estimated propulsive efficiencies in an early stage with actual tests.

Bibliography

[1] B. Beijer T. Heil J. Vink M. den Brabander V. Verschuure C. Dieleman B. Smeets A. Helmer, B. Nootebos. Dse - looking for water, project plan. 2013.

[2] B. Beijer T. Heil J. Vink M. den Brabander V. Verschuure C. Dieleman B. Smeets A. Helmer, B. Nootebos. Dse - looking for water, baseline report. 2013.

[3] B. Beijer T. Heil J. Vink M. den Brabander V. Verschuure C. Dieleman B. Smeets A. Helmer, B. Nootebos. Dse - looking for water, mid-term report. 2013.

[4] WHO. Fact files, water, 2009.

[5] J.A. ir. Melkert. Project guide design synthesis excercise, issue 2. 2013.

[6] M. Sadraey. *Aircraft Design: A Systems Engineering Approach*. Wiley Publications, 2012.

[7] Saito 4-stroke gasoline engines - instruction manual, 2012.

[8] Apm open source autopilot, 2013. URL `http://ardupilot.com/`.

[9] H. Amar N. Drawil and O. Basir. Gps localization accuracy classification:a context-based approach. 2013.

[10] Linimnco battery 554.32wh, 2013. URL `http://www.batteryspace.com/LiNiMnCo-26650-Battery-50.4V-10.8Ah-544.32Wh-40A-rate-for-e-scooter.aspx`.

[11] Brushless motors, 2013. URL `http://www.rchobbyhelicopter.com/store52/agora.cgi?productBrushless_Motors`.

[12] Fruity Chutes. Iris ultra 96" parachute. URL `http://fruitychutes.com/buyachute/iris-ultra-chutes-36-to-192-c-18/iris-ultra-96-parachute-50lbs-20fps-p-91.html`.

[13] ArduPilot Mega. What do i need for my arduplane fixed wing uav? URL `http://www.ardupilot.co.uk/what-do-i-need.html`.

[14] A. Wagner. International fuel prices, 2013. URL `http://www.giz.de`.

[15] E. van der Putte. Personal Communication.

[16] United Nations General Assembly. Resolution adopted by the general assembly, 60/1. 2005 world summit outcome. 2005. URL `http://data.unaids.org/Topics/UniversalAccess/worldsummitoutcome_resolution_24oct2005_en.pdf`.

[17] Stephen McKenzie. Social sustainability: towards some definitions. 2004. URL `http://w3.unisa.edu.au/hawkeinstitute/publications/downloads/wp27.pdf`.

[18] Wolfgang Kinzelbach; Tobias Siegfried; Philip Brunner; Peter Bauer. Sustainable groundwater management problems and scientific tools. 2003. URL `http://water.columbia.edu/files/2011/11/Siegfried2003Sustainable.pdf`.

[19] Geophex Ltd. Gem-2 principle of operation, 2013. URL `http://www.geophex.com/principal%20of%20operation%20gem_2.html`.

[20] Anders Vest; Auken Esben Siemon, Bernhard ; Christiansen.

[21] Spies; Woodgate. Salinity mapping methods in the australian context, prepared for the natural resource management ministerial ouncil, department of the environment and heritage and department of agriculture, fisheries and forestry, canberra, 2005. URL `http://www.geophex.com/principal%20of%20operation%20gem_2.html`.

[22] Wikiwater. Methods for finding underground water and water tables, 2013. URL http://www.wikiwater.fr/e9-methods-for-finding-underground.html.

[23] Partners voor Wwater. Voor hoeveel subsidie kan ik krijgen, 2013. URL http://wptest.partnersvoorwater.nl/?page_id=188.

[24] Micheal E. Porter. The five competitive forces that shape strategy. 2008. URL http://hbr.org/2008/01/the-five-competitive-forces-that-shape-strategy/ar/1.

[25] Secretary-General. Assistance in mine clearance (a/49/357), 1994.

[26] e.a. De Smedt, Philippe. The 3-d reconstruction of medieval wetland reclamation through electromagnetic induction survey, 2013.

[27] FAA. Order 8130.34b. 2010. URL http://www.faa.gov/documentLibrary/media/Order/8130.34B.pdf.

[28] EASA. Policy statement airworthiness certification of unmanned aircraft systems (uas), e.y013-01. 2009. URL http://www.easa.europa.eu/certification/docs/policy-statements/E.Y013-01_%20UAS_%20Policy.pdf.

[29] Inspectie Leefomgeving en Transport. Remotely piloted aircraft systems (rpas) in the netherlands. 2013. URL http://www.ilent.nl/Images/Informatiebulletin%20lichte%20onbemande%20luchtvaartuigen_tcm334-342963.pdf.

[30] John D. Anderson Jr. *Fundamentals of Aerodynamics*, pages 433–435. McGraw-Hill Series, 2005.

[31] John D. Anderson Jr. *Fundamentals of Aerodynamics*, page 420. McGraw-Hill Series, 2005.

[32] G. La Rocca. Wing design part 3. AE2101 Systems Engineering Elements II Course, TU Delft, .

[33] XFLR5, 2013. URL http://www.xflr5.com/.

[34] H. Abbott. *Theory of Wing Sections*. Dover Publication Inc., 1949.

[35] Propeller calculator by helmut schenk, 2013. URL http://www.drivecalc.de/PropCalc/.

[36] M. Sadraey. *Aircraft Performance Analysis*. Verlag Dr. Muller, 2009.

[37] G. La Rocca. Design for ac longitudinal stability. AE3201 Systems Engineering Course, TU Delft, .

[38] ProAdvice. Aileron sizing. 2013. URL http://www.flightlevelengineering.com/downloads/ProAdvice%203%20-%20AILERON%20SIZING.pdf.

[39] Michael V. Cook. *Flight Dynamics Principles*. Butterworth-Heinemann, 2012.

[40] e.a. J.A. Mulder. *AE3202 Flight Dynamics*. TU Delft, 2013.

[41] Jan Roskam. *Airplane Design Part 6: Preliminary calculation of aerodynamic, thrust and power characteristics*. Roskam Aviation and Engineering, 1990.

[42] UAV factory. Penguin b 3d view, 2010. URL http://www.uavfactory.com/.

[43] ESDU. 88029 - yawing moment coefficient for plain ailerons at subsonic speeds. 2006.

[44] ESDU. 82010 - contribution of fin to sideforce, yawing moment and rolling moment derivatives due to sideslip. 1993.

[45] T.H.G. Megson. *Aircraft Structures for Engineering Students*, pages 558–631. Butterworth-Heinemann, 2007.

[46] B. van Oudheusden L. Veldhuis. Incompressible flow over finite wings. AE2102 Aerodynamics I Course, TU Delft.

[47] Somalia Water and Land Information Management. Climate of somalia, 2007. URL http://www.faoswalim.org/ftp/Water_Reports/Cleared/W-01-Climate%20of%20Somalia.pdf.

[48] Engineering Toolbox. Young modulus for some common materials. URL http://www.engineeringtoolbox.com/young-modulus-d_417.html.

[49] P. Oittinen M. Kyto, M. Nuutinen. Method for measuring stereo camera depth accuracy based on stereoscopic vision. 2011.

[50] S. Dijkstra. The winddrinker, 2014. URL http://www.thewinddrinker.com/#.

[51] Petrol prices around the world, january 2014, 2014. URL http://www.mytravelcost.com/petrol-prices/.

[52] EuroUSC. International - fees, terms and conditions, issue 3.0. 2013. URL http://www.eurousc.com/assets/iftc-issue-3-0.pdf.

Appendix A

System functions

A.1 Functional Flow Diagram

The Functional Flow Diagram (FFD) shows the chronological order of functions the system performs before, during and after mission execution. The FFD is depicted in figures A.1 to A.3. The main functional path, which is shown in the top level of the flowchart, has the following order;

1. Preparation
2. Launch
3. Fly
4. Land
5. Post-Landing
6. Maintenance

In the *Preparation* phase all system and functional checks are included which are required to guaranty a safe flight. Also the payload- and flight plan settings such as scan depth (frequency), flight path and scan height are defined in this phase.

In the *Launch* phase the functions required to get the vehicle from the ground up to cruise altitude are described. Main elements here are the positioning of the catapult, the positioning of the vehicle on the sled and the release of the catapult.

To satisfy the main function the payload must operate at a set altitude and velocity to be able to perform measurements. In the *Fly & Measure* phase the functions required to achieve this are stated. Furthermore the system is continuously monitoring its energy levels and surroundings. There are multiple functional paths that lead to the last sub-function *3.9 - Navigate to landing position* since there are more reasons to abort the flight. These reasons include a low energy level, manual override and reaching the final measurement coordinates.

Next, in the *Land* phase, the functions required to safely land the aircraft are stated. This ranges from turning off the engine and deploying the parachute to the retrieval of the vehicle.

In the *Post-landing* phase, the aircraft is shut down and its measurements are retrieved and processed.

Finally the last functions such as cleaning, checking for structural integrity and performing the actual maintenance are stated in the *Maintenance* phase.

A.2 Functional Breakdown Structure

The Functional Breakdown Structure is a hierarchical representation of all the functions the system performs, including the functions of subsystems. The FBS is presented in the form of an AND-tree, and is based on the FFD. In contrast with the FFD, the functions in the FBS are not necessarily in chronological order. In figure A.4 the FBS can be found.

The primary function of the system as described in the FBS is simply *Perform Mission*, since this is the most abstract objective of the system as a whole. This function is then subdivided into five main functions;

- **Provide power:** In order for all the subsystems to operate, electric power is needed. Furthermore, the power is distributed throughout the system in a controlled fashion.

- **Fly:** In order to be able to fly, lift must be generated. Furthermore, a propulsive system is needed. An autopilot together with control surfaces is responsible for the stability and controllability. Finally, both take-off and landing are performed in a safe manner.
- **Provide navigation and guidance:** For a fully autonomous system, navigation and guidance is of utmost importance. The location is measured, for both the determination of the flight path and mapping of the measurement data. Next, the system is able to generate control commands, determine its flight path and adjust this path according to measurements taken. Finally, the system can detect obstacles in its surroundings and respond by initiating an evasive manoeuvre.
- **Perform measurements:** Measuring the conductivity of the soil is the main driver of this design. During flight, background radiation is present and the system itself generates an electromagnetic field, these disturbances have to be taken into account and corrected for by calibration. Furthermore the measured data has to be stored and encrypted.
- **Allow for maintenance and preparation:** To allow for easy maintenance, modularity of the system has been taken into account during the design. Also, the major parts of the system are off the shelf products. Next to maintenance, the UAV has to be prepared before each flight. In the case of any detected errors by the system, the system is able to inform the user about these errors. This will be done using a downlink with the ground station.

These main functions are further subdivided as can be seen in figure A.4.

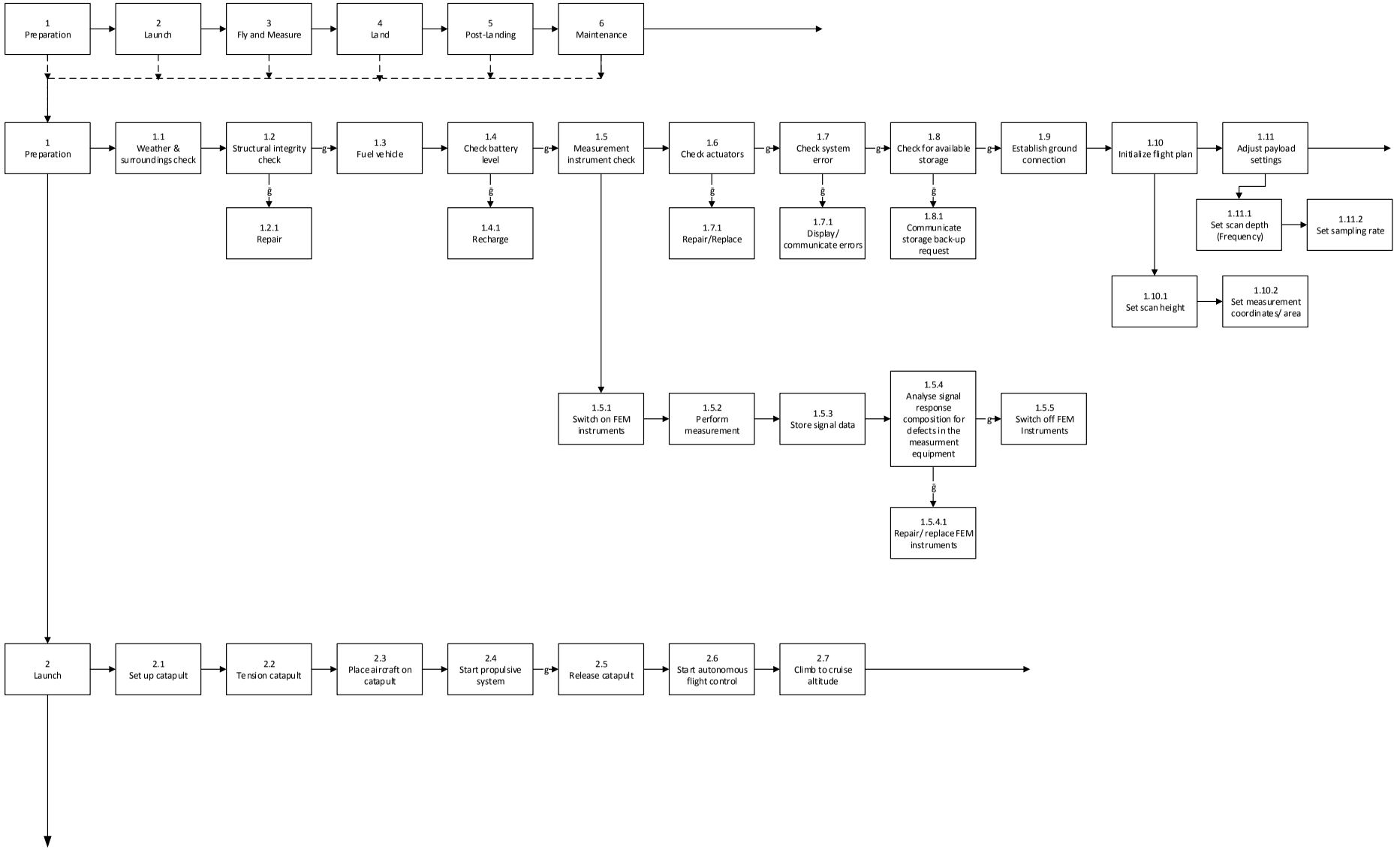

Figure A.1: The part of the FFD describing the preparation and launch phase.

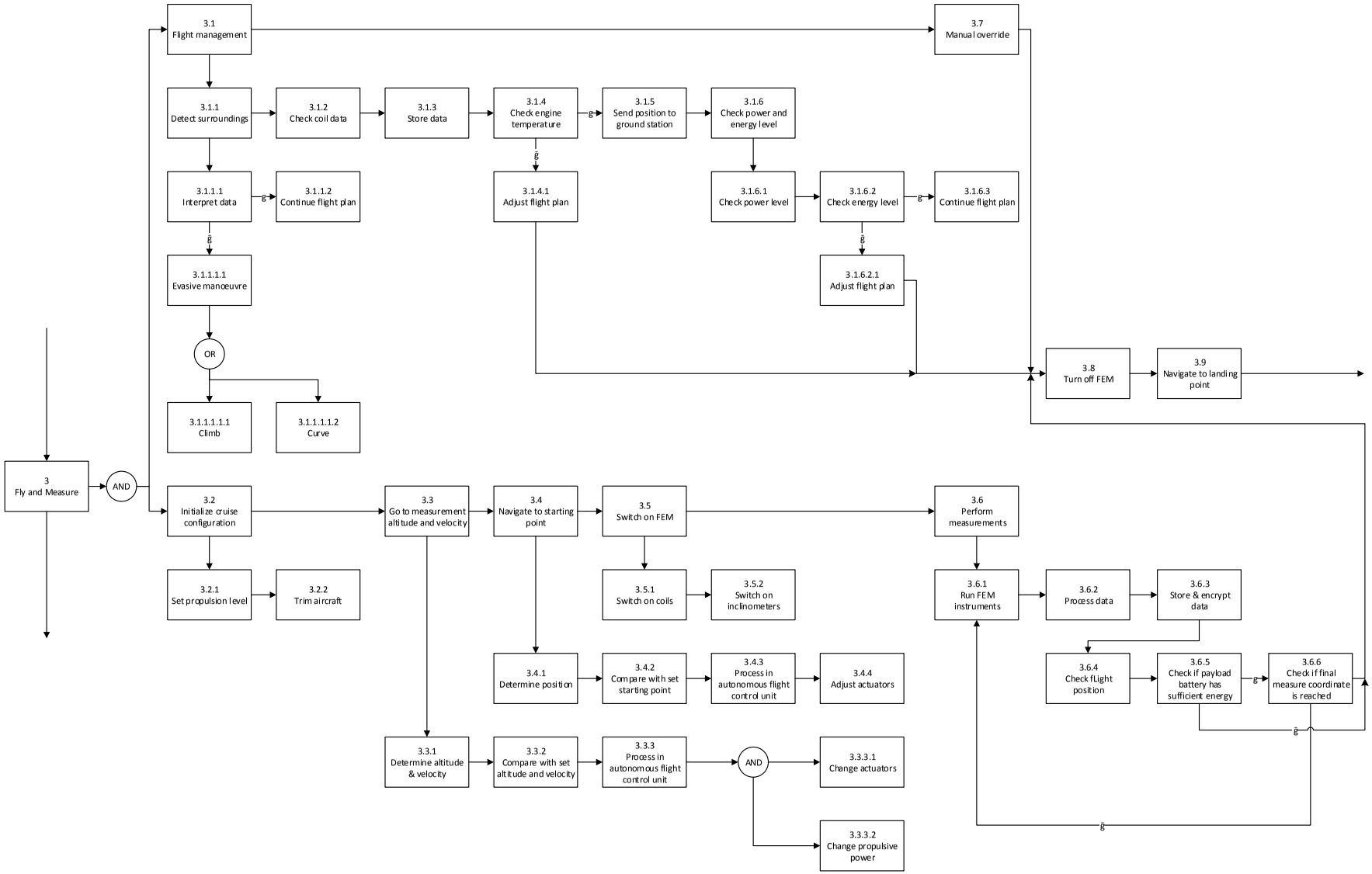

Figure A.2: The part of the FFD describing the fly phase.

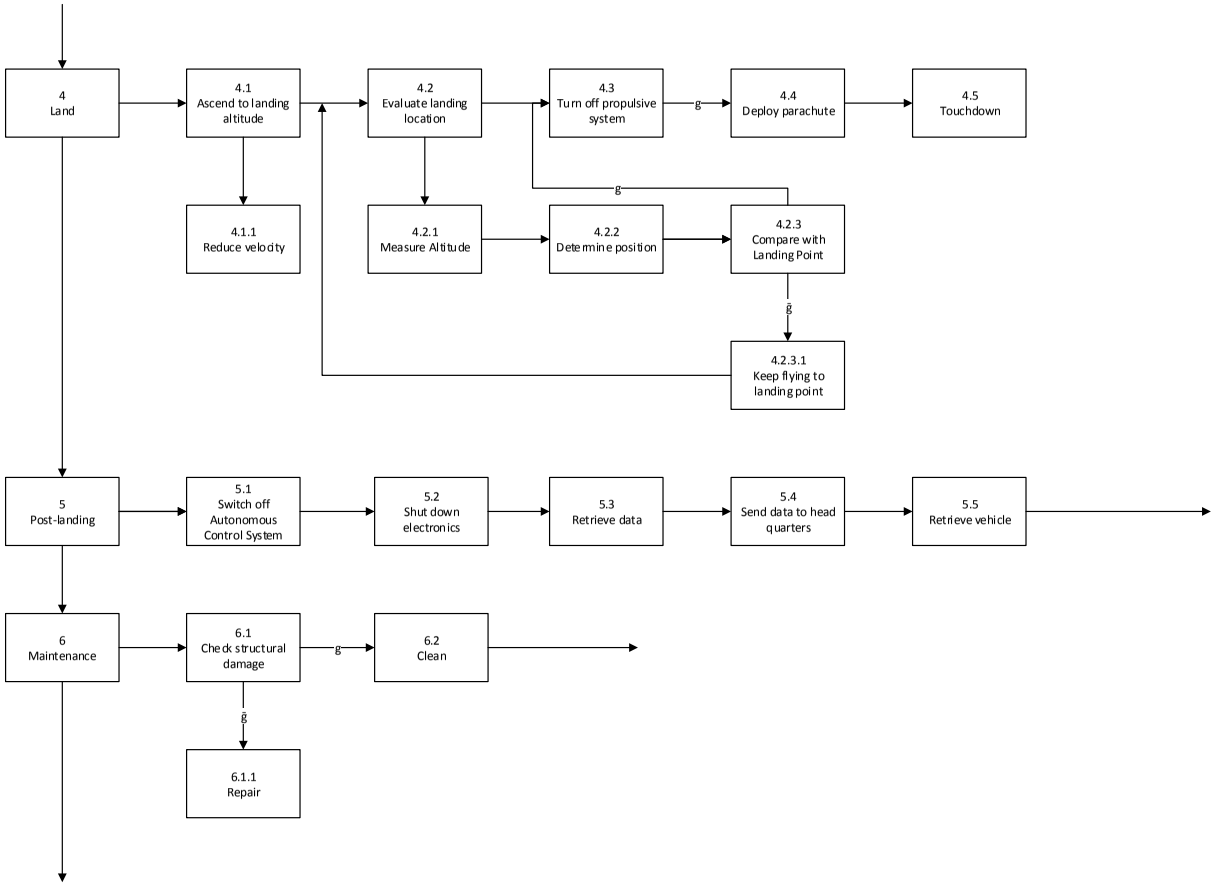

Figure A.3: The part of the FFD describing the landing, post-landing and maintenance.

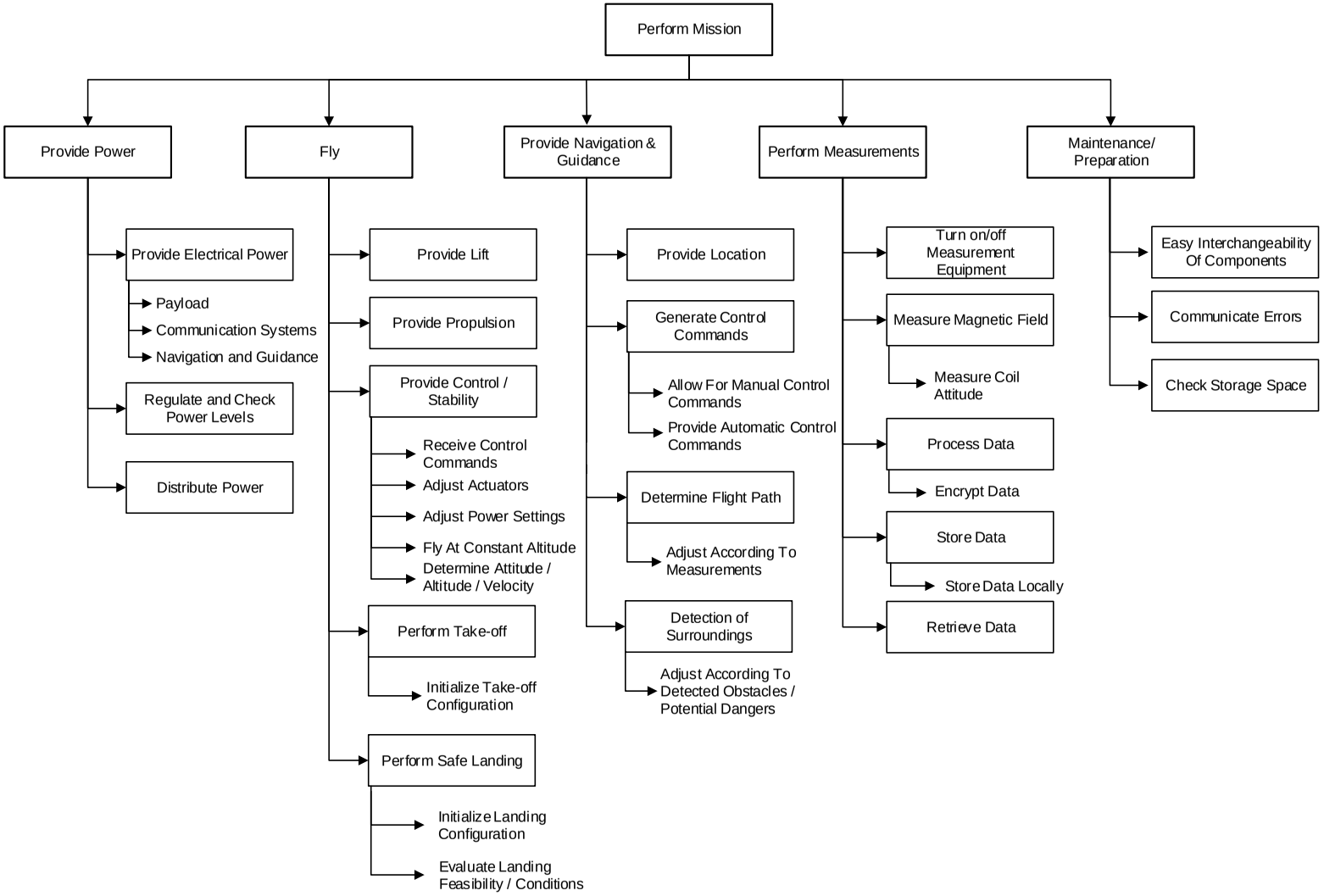

Figure A.4: The Functional Breakdown Structure of the system.

Appendix B

UAV regulations

One of the top level requirements is that a UAV needs to operate within current regulations concerning UAVs. Although these regulations are fairly new and certainly not yet final, the current regulations have been investigated. Since it is assumed that regulations in either the United States of America (USA) or in the European Union (EU) will be the most strict, these regulations have an impact on the mission to be performed. If the final aircraft complies with these regulations, it will most certainly comply with the regulations everywhere around the world.

B.1 United States of America

A complete set of regulations for operating an Unmanned Aircraft System (UAS) in the airspace of the USA, defined as National Airspace System (NAS), are still under development. However some preliminary regulations already apply. To operate an UAS for non-recreational purposes a Special Airworthiness Certificate - Experimental Category (SAC-EC) has to be obtained from the Federal Aviation Authority (FAA). Under this regulation civil-operated UAS can be registered for several purposes: [27]

- Research and development, for development of the UAS
- Crew training
- Market surveys, sales demonstrations

  Currently it is not possible to certify an UAS for commercial purposes, although this might become possible in the future. If a workaround can be found for this issue and the UAS be eligible for certification, the following problematic requirements arise [27]:

  – "The Unmanned aircraft (UA) Pilot in Command (PIC) must hold and be in possession of, at a minimum, an FAA private pilot certificate, with either an airplane, rotorcraft, or powered-lift category; and single- or multi-engine class ratings, or the military equivalent, appropriate to the type of UA being operated."
  – "Observers must be able to see the aircraft and the surrounding airspace throughout the entire flight. Observers must be able to determine the UAs altitude, flight path, and proximity to all aviation activities and other hazards (e.g., terrain, weather, structures) sufficiently (...), and prevent the UA from creating a collision hazard."
  – "All observers must either hold, at a minimum, an FAA private pilot license or military equivalent, or must have successfully completed specific observer training acceptable to the FAA. An observer does not require currency as a pilot. All observers must have in their possession a valid second-class (or higher) airman medical certificate."

B.2 European Union

The European Aviation Safety Agency (EASA) is responsible for all aviation regulations in the EU. EASA has several regulations for UAVs [28], yet these do not apply for UAVs that have an operating mass of less than 150 kg. For these UAVs, member states have to develop their own regulations. The SkyDowser weighs less than 150 kg, and therefore has to comply with the different regulations of the European countries.

The Netherlands has one of the most strict legislation, and therefore those regulations concerning lightweight UAVs were investigated. According to those regulations [29], the most important limitations are the maximum altitude (120 m), the distance from the observer (500 m), and the maximum velocity (36 m/s). Furthermore it is not allowed to fly near (150 m) buildings and humans. The distance from the observer can limit the range of a UAV. One can however apply for a permit if it can be proven that a UAV is able to fly autonomously at large distance from the observer.

B.2.1 Impact on design

From the regulations in the USA, EU and The Netherlands, a few common limitations on the design can be found.

- A UAV has to be within visual line-of-sight (VLOS) of an observer.
- A UAV has to be in a maximum distance from the observer of 500 m.
- A observer needs to have the ability to manually control the UAV, in case of emergencies.
- A observer has to be certified to fly a UAV.
- A UAV velocity should not exceed 36 m/s.
- A UAV operating mass should not exceed 150 kg.

The SkyDowser will comply with the limitations listed above in order to assure that the mission can be performed anywhere around the world. Yet the regulations are all under development, so within a few years it might be possible to fly without an observer if one can prove that the SkyDowser's navigation and guidance system is able to operate completely autonomously, without posing a threat to its environment.

Appendix C

Data exchange methodology

In this chapter the data exchange methodology is explained. Several different analyses were performed in the design of the SkyDowser. In order to effectively exchange design parameters and design characteristics, the following method was implemented.

Creating a centralised model where the entire design is accessible for all analysis teams is the most suitable solution. The data exchange consists of a data sheet of all verified design parameters. Figure C.1 visualises the implemented data exchange methodology. The data exchange data sheet is protected from unverified changes and is read-only for the analysis teams. To update a set of parameters the set has to be approved by the head of engineering and the specific analysis specialist. Approval is only given when: firstly, the new parameters have been verified with the already existing data. Secondly, the response of the design corresponds to the expectations based on the sensitivity analysis results. Lastly, the feasibility of the proposed set of parameters has been proven. After approval the new set is implemented in the design and published for all other analysis teams.

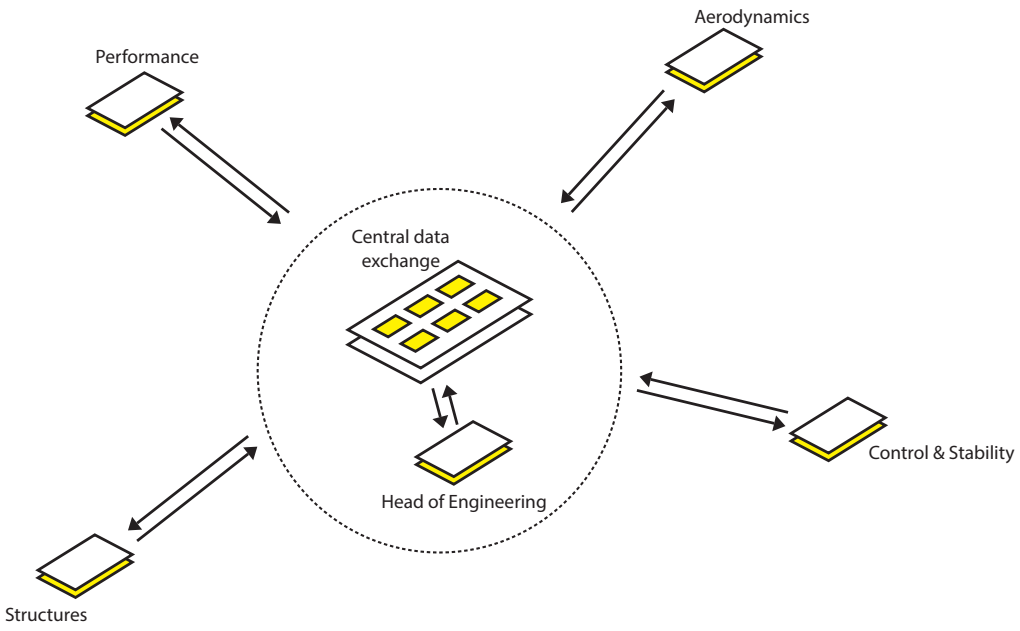

Figure C.1: Visualisation of the model used for concurrent engineering and quality control.

Appendix D

Aerodynamics

In this appendix the used methods and the calculations that were used during the aerodynamic analysis of the SkyDowser are presented. These calculations led to the results as shown in part 3 of the report; the design analysis. First the sizing of the wing is discussed, after which the aerofoil characteristics are analysed. Finally, with the use of lifting line theory, the main wing and horizontal stabiliser are aerodynamically evaluated.

In this section a distinction is made between the proposed methodology and the implemented methodology. This is because of an unfortunate and still unknown fault in the analysis based on the lifting line theory. Therefore, another (simplified) method is implemented, to ensure approximate aerodynamic properties were available in time for the analysis of the rest of the aircraft. This simplified method, including results, is presented in the final part of this appendix.

D.1 Wing sizing

The first and most important step of the aerodynamic analysis is the sizing of the main wing and the horizontal stabiliser. Next, the actual aerodynamic properties of these surfaces can be calculated, as described in this appendix.

D.1.1 Main wing

During cruise, the lift generated by the wing should compensate for the weight and the negative lift of the tail. The ratio of main wing surface area and horizontal tail surface area, $\frac{S_h}{S}$, is 0.12, following from the longitudinal stability analysis (see section 5.3).

$$L_w = W + L_h \tag{D.1}$$

$$= W + \frac{S_h}{S} L_w \tag{D.2}$$

$$L_w = \frac{W}{\left(1 - \frac{S_h}{S}\right)} \tag{D.3}$$

$$\tag{D.4}$$

The lift that has to be generated can now be calculated with equation D.5.

$$L = qSC_L = \frac{1}{2}\rho V^2 S C_L \tag{D.5}$$

Since the lift force is determined and the cruise velocity is set at $V_{cruise} = 25$ m/s, the two design factors are the wing surface area and the lift coefficient C_L. Using a set $C_{L,design}$ in equation D.5, the wing surface follows from:

$$S = \frac{L}{qC_{L,\text{design}}} \tag{D.6}$$

Now that the necessary wing surface area is known, the aspect ratio AR can be determined, since the wingspan b is fixed for practical reasons. The relation between wing surface area and aspect ratio is given in equation D.7

$$AR = \frac{b^2}{S} \tag{D.7}$$

The final shape of the wing is finally determined by the taper ratio λ, also set at a fixed value. Then the chord length at the wing tip follows from:

$$c_{\text{tip}} = \frac{2\lambda}{1+\lambda}\frac{S}{b} \tag{D.8}$$

The chord length at the root can also be calculated:

$$\lambda = \frac{c_{\text{tip}}}{c_{\text{root}}} \tag{D.9}$$

$$c_{\text{root}} = \frac{c_{\text{tip}}}{\lambda} \tag{D.10}$$

D.1.2 Horizontal stabiliser

For the horizontal stabiliser a slightly different method was used. First, the surface area was determined by $\frac{S_h}{S}$. Since usability is not a limiting factor, the aspect ratio of the horizontal stabiliser is used as input, instead of a maximum span-width. The aspect ratio was chosen from structural perspective and to ensure enough space is available within the horizontal tailplane, for placement of servos for controlling surfaces. All this resulted in a chosen aspect ratio of 4.11, resulting in a surface area of 0.115 m^2. This lower aspect ratio is also beneficial for stall behaviour, since a decrease in aspect ratio results in an increase of the angle of attack at which stall occurs. Using equations D.7 to D.10 the other sizes of the wing can be found.

D.2 Aerodynamic properties

When calculating the aerofoil characteristics; one can either calculate the lift and moment characteristics analytically or obtain these values from readily available measurement data or simulated data. In order to determine the aerodynamic properties of the aircraft analytically, a combination of lifting line theory and thin aerofoil theory has been used. Starting with a chosen aerofoil, the lift properties of the main and tail wings are calculated. Since lifting line theory is used, these characteristics are calculated using thin aerofoil theory.

D.2.1 The aerofoil

Since the cruise velocity is only 25 m/s, the corresponding Reynolds number is low, and can be calculated using equation D.11.

$$Re = \frac{\rho V c}{\mu} = 1.0 \cdot 10^6 \tag{D.11}$$

From this, an aerofoil for the main wing is chosen; the NACA-2412. See figure D.1. This cambered aerofoil is often used for low-velocity wings, has a high $C_{L_{max}}$ and is relatively easy to manufacture. Compared to similar NACA profiles designed for low velocity this aerofoil is not very susceptible to roughness, caused by insects and sand on the wing, making it a very suitable aerofoil for this mission.

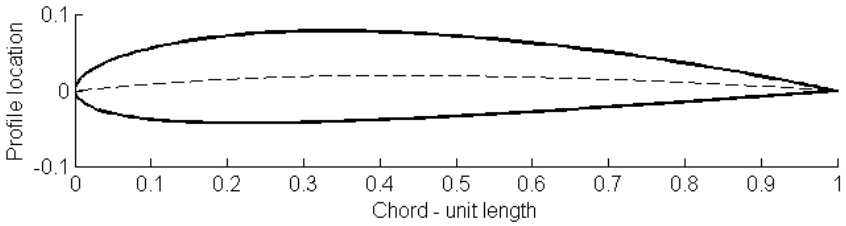

Figure D.1: The chosen NACA-2412 aerofoil geometry (as fraction of local chord length).

For the horizontal stabiliser a different aerofoil is chosen; a symmetric profile is most suitable since negative lift has to be generated. A NACA-0012 profile has been chosen (shown in figure D.2), providing sufficient lift at cruise angle of attack.

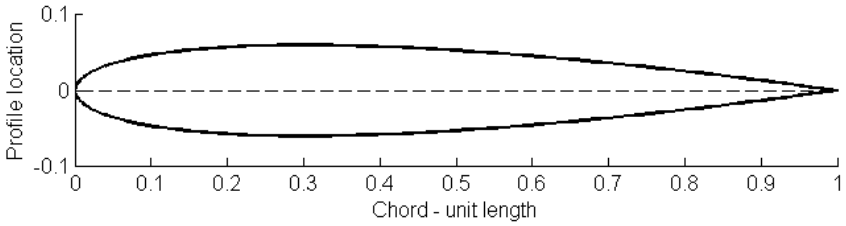

Figure D.2: The chosen NACA-0012 aerofoil geometry (as fraction of local chord length).

When using thin aerofoil theory, vortexes are placed on the camber line $z = z(x)$. The slope of the camber line has to be determined by the following equations:

$$\left(\frac{dz}{dx}\right)_1 = \frac{2M}{P^2}\left(P - \frac{x}{c}\right) \text{ for } \frac{x}{c} < P \tag{D.12}$$

$$\left(\frac{dz}{dx}\right)_2 = \frac{2M}{(1-P)^2}\left(P - \frac{x}{c}\right) \text{ for } \frac{x}{c} \geq P \tag{D.13}$$

Where M and P are follow from the NACA code: NACA(MPxx) and $\frac{x}{c}$ is the x-location as fraction of the chord length c. From the slope of the camber line and using a coordinate transformation, $x = \frac{c}{2}(1 - \cos\theta)$, aerofoil coefficients can be calculated:

$$A_0 = \alpha - \frac{1}{\pi}\left[\int_0^{\theta_1}\left(\tfrac{dz}{dx}\right)_1 d\theta + \int_{\theta_1}^{\pi}\left(\tfrac{dz}{dx}\right)_2 d\theta\right] \tag{D.14}$$

$$A_n = \frac{2}{\pi}\left[\int_0^{\theta_1}\left(\tfrac{dz}{dx}\right)_1 \cos(n\theta)d\theta + \int_{\theta_1}^{\pi}\left(\tfrac{dz}{dx}\right)_2 \cos(n\theta)d\theta\right] \tag{D.15}$$

Where α is the angle of attack and θ follows from the coordinate transformation stated above. With these coefficients, the circulation over the aerofoil can be calculated using:

$$\Gamma = cV(\pi A_0 + \frac{\pi}{2}A_1) \tag{D.16}$$

Plugging in equation D.16 into D.17 results in the lift per unit span of the aerofoil.

$$L' = \rho_\infty V_\infty \Gamma \tag{D.17}$$

With these coefficients various aerofoil characteristics can be calculated, as shown in equations D.18 to D.23.

$$c_l = \pi(2A_0 + A_1) \tag{D.18}$$

$$\frac{dc_l}{d\alpha} = 2\pi \tag{D.19}$$

$$\alpha_{L=0} = A_0 - \frac{1}{2}A_1 \tag{D.20}$$

$$c_{m_{LE}} = -\frac{\pi}{2}(A_0 + A_1 - \frac{1}{2}A_2) \tag{D.21}$$

$$c_{m_{0.25}} = -\frac{\pi}{4}(A_2 - A_1) \tag{D.22}$$

$$\frac{x_{xp}}{c} = \frac{1}{4}\left(1 - \frac{A_2 - A_1}{2A_0 + A_1}\right) \tag{D.23}$$

D.2.2 Proposed methodology - Lifting line theory

After this, it is important to calculate the lift distribution over the span of the wing. The lift distribution depends on the variation of chord length with wingspan, but also on the fact that for a finite wing, tip vortices will occur. These tip vortices reduce the local angle of attack, α by an induced angle of attack α_i to an effective angle of attack: $\alpha_{eff} = \alpha - \alpha_i$. This will result in a lower lift coefficient than expected from aerofoil theory. The lift distribution will have a rounded shape towards the tips, since the vortexes are strong there and the resulting lift will be zero.

Numerical method

A numerical method based on classic lifting line theory is used in this analysis, as explained in Anderson [30]. Please note this theory is only valid for the linear part of the lift curve, and can not be used for high taper ratios.

1. First, the wing is divided in a number of sections k in y-direction. In this case $k = 1000$.
2. Second, a circulation over the wing in every section is assumed. This is assumed to be the elliptical lift distribution:

$$\Gamma(y) = \Gamma_0 \sqrt{1 - \left(\frac{y}{\frac{b}{2}}\right)^2} \tag{D.24}$$

   Where $\Gamma(y)$ is the local circulation per location, Γ_0 is the maximum circulation, taken to be the maximum circulation calculated in the 2D case, y is the y-location on the wing and $\frac{b}{2}$ is half the wing span.
3. Now the induced angle of attack at every span wise location can be calculated with:

$$\alpha_i(y_n) = \frac{1}{4\pi V_\infty} \int_{-\frac{b}{2}}^{\frac{b}{2}} \frac{\frac{d\Gamma}{dy}}{y_n - y} dy \tag{D.25}$$

   Where V_∞ is the velocity of the aircraft in m/s, $\frac{d\Gamma}{dy}$ is the derivative of circulation, y_n is the local position in y-direction and y is the entire y.
4. Now that α_i is known, the effective angle of attack can be calculated:

$$\alpha_{eff}(y_n) = \alpha(y_n) - \alpha_i \tag{D.26}$$

5. The next step is to determine the lift coefficient based on the effective angle of attack $c_l(\alpha_{eff})$. This lift coefficient is different from c_{l_α}. The information comes from the c_{l_α}-curve of the aerofoil.
6. With this local lift coefficient a new circulation can be calculated with

$$\Gamma(y_n) = \frac{1}{2} V_\infty c_n c_{l(y_n)} = \Gamma_{new} \tag{D.27}$$

   Where c_n is the local chord length.
7. Finally this new Γ_{new} must be compared with the old circulation. A new input is created by

$$\Gamma_{input} = \Gamma_{old} + D(\Gamma_{new} - \Gamma_{old}) \tag{D.28}$$

   Where D is a damping factor, which should be $D = 0.05$ as described in the literature. All these steps are evaluated in an iterative process converging to a final lift distribution. Literature states that the converging is finished if, for 5 consecutive iterations, the values of the circulation are within 0.1% of each other.

Of course, the lift can be calculated by equation D.5

$$L = \frac{1}{2} \rho_\infty V_\infty^2 C_L S \tag{D.29}$$

From the circulation over the wing, the lift distribution and the total lift follow from:

$$L'(y) = \rho_\infty V_\infty \Gamma(y) \tag{D.30}$$

$$L = \rho_\infty V_\infty \int_{-b/2}^{b/2} \Gamma(y) dy \tag{D.31}$$

Therefore, from the lift equation, equation D.29, and equation D.31, the lift coefficient can be determined:

$$C_L = \frac{L}{\frac{1}{2}\rho_\infty V_\infty S} = \frac{2}{V_\infty S} \int_{-b/2}^{b/2} \Gamma(y) dy \tag{D.32}$$

Also, the induced drag coefficient C_{D_i} can now be calculated from C_L with:

$$C_{D_i} = \frac{C_L^2}{\pi A R e} \tag{D.33}$$

Where, AR is the aspect ratio and e is the span efficiency factor, which is taken to be 0.98 for the current design. This is a value based on theory for a wing with a taper ratio around 0.4 [31]. By iterating this process for a range of angles of attack (within the linear part of the 2D lift curve, a C_{L_α}-curve and a C_{D_α}-curve can be generated.

Since thin-aerofoil theory does not account for the non-linear part of the C_{L_α}-curve, the value for $C_{L,max}$ is given by an equation given in the lectures of Systems Engineering on wing design [32]: $C_{L,max} = 0.9C_{l,max}\cos\Lambda_{0.25c}$. Since the sweep is 0, $C_{L,max} = 0.9C_{l,max}$.

Results

The simulation program that was set up proved to be not fully functional. The program does not iterate correctly and does not stop at the right iteration. Therefore, it cannot be guaranteed the results from simulation are valid, and during verification of the results this proved to be the case.

When evaluating a rectangular wing, the results are as expected, and the simulation programs seems to be accurate. For completeness, the resulting circulation of a rectangular wing is shown in figure D.4. In figure D.3 the lift curve of a wing with taper ratio of 0.4 is shown, where the C_L and C_l clearly overlap.

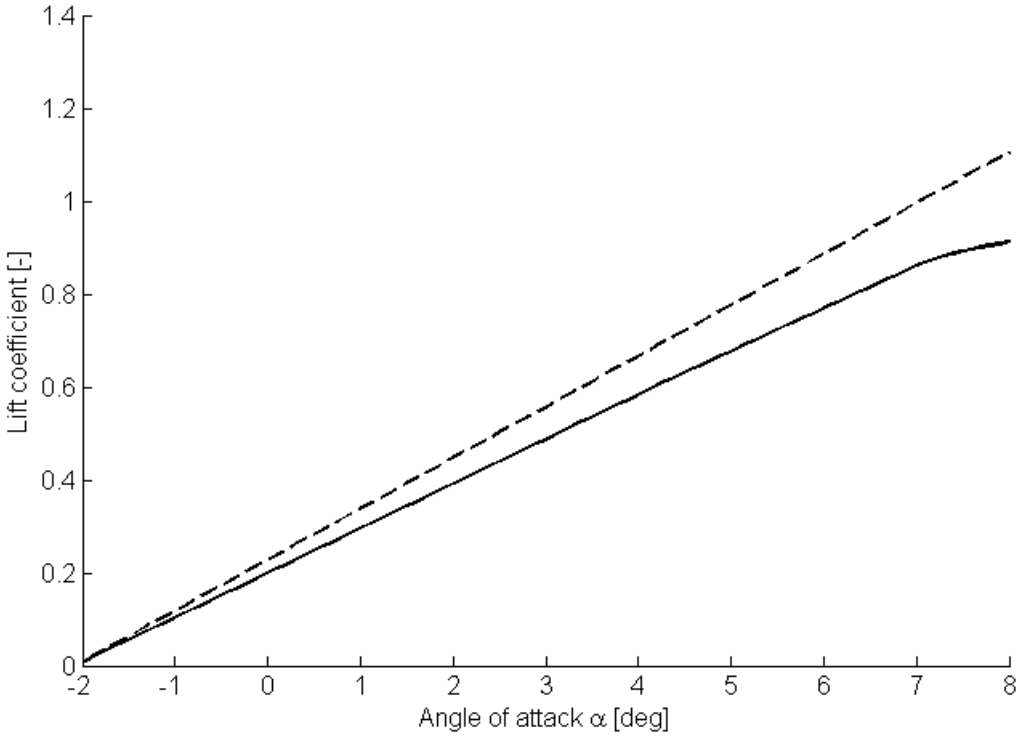

Figure D.3: $C_L - \alpha$ (solid line) and $C_l - \alpha$ (dashed line) of an untapered wing, V = 25 m/s, Re = $10 \cdot 10^6$.

However, when the lift distribution over a tapered wing is simulated, the software does not deliver the desired results. When $\lambda \leq 0.7$, the calculated $C_L \geq C_l$, which is obviously invalid. Also, the 'shape' of the circulation, and thus the lift distribution over the wing is incorrect. This is because of an non-converging iteration process; for unknown reasons the consecutive determined circulations do not converge as desired. Thus, the plots provided here are the result after a manual stop; a maximum of ten iterations is performed.

D.2.3 Implemented methodology

Since the proposed methodology could not be properly implemented, and aerodynamic properties had to be determined within the set time constraints, a simplified model has been used. This methodology described below is implemented, using aerofoil data from XFLR5 [33] [34].

For a general aerofoil, equation (D.34) is used to determine the lift slope, where α is in the linear range of the lift curve. The same relation holds for the lift slope of an elliptical wing, also described in equation D.34.

$$C_{l_\alpha} = \frac{C_l}{\alpha - \alpha_{l=0}} -> C_{L_\alpha} = \frac{C_L}{\alpha - \alpha_{L=0}} \tag{D.34}$$

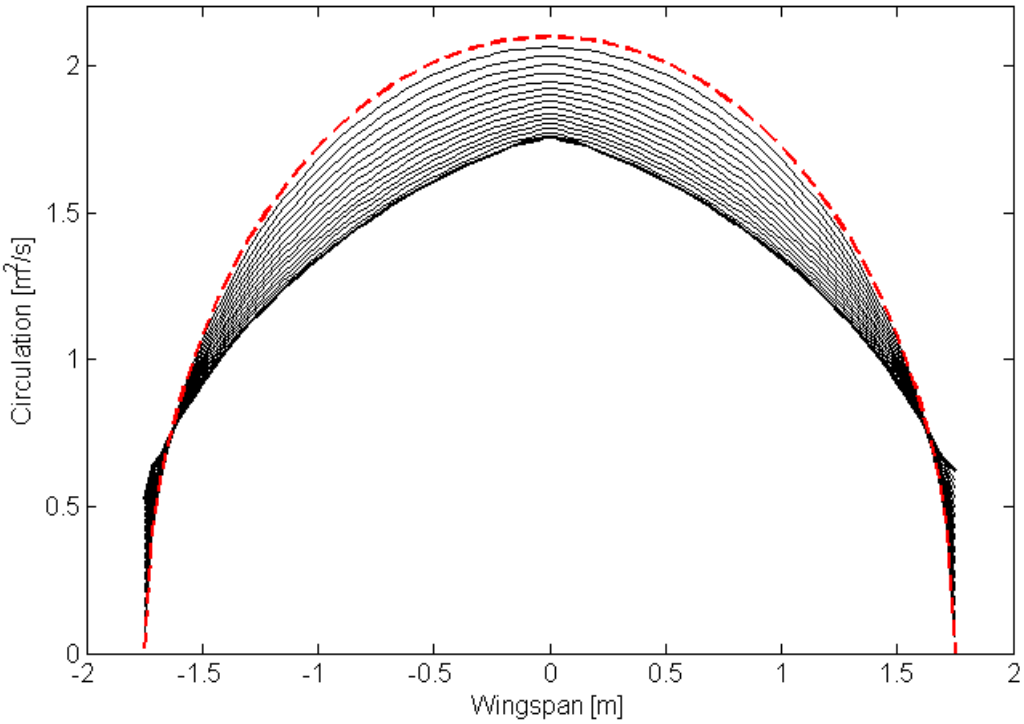

Figure D.4: Circulation vs. wingspan of an untapered wing, angle of attack of 2° , V = 25 m/s, Re = $10 \cdot 10^6$.

In this equation, C_L is calculated using the effective angle of attack, with the use of equation D.35.

$$C_L = c_{l_\alpha}(\alpha - \frac{180/\pi C_L}{\pi AR} - \alpha_{L=0}) \tag{D.35}$$

Then, to obtain the actual lift slope, the relation between the lift slope of a three-dimensional (general) wing and that of the two-dimensional wing is used (equation D.36).

$$C_{L_\alpha} = \frac{C_L}{\alpha - \alpha_{L=0}} = \frac{C_{l_\alpha}}{1 + \frac{180/\pi c_{l_\alpha}}{\pi eAR}} \tag{D.36}$$

Now, from this C_L the drag coefficient of the wing is calculated using equation D.37, combining the profile drag of the aerofoil and the induced drag of the wing.

$$C_D = C_d + \frac{C_L^2}{\pi eAR} \tag{D.37}$$

Finally, both the total drag and total lift of the wing can be calculated using the found lift coefficients. For this equations D.38 and D.39 are used.

$$L = C_L \frac{1}{2} \rho V_\infty S \tag{D.38}$$

$$D = C_D \frac{1}{2} \rho V_\infty S \tag{D.39}$$

These relations can be used for both the main wing and tail; when using the corresponding wing areas and appropriate two-dimensional aerofoil data for the NACA-2412 and NACA-0012 respectively.

Results

Here a short overview of the implemented aerodynamic analysis is presented. In figure D.5 the C_L vs C_D graph for the complete aircraft is shown.

Next, in figure D.6 the $C_L - \alpha$ graph of the complete aircraft is presented. Note that this is again only for a limited range of angle of attack, since the theory used is only suitable for the linear part of the lift curve.

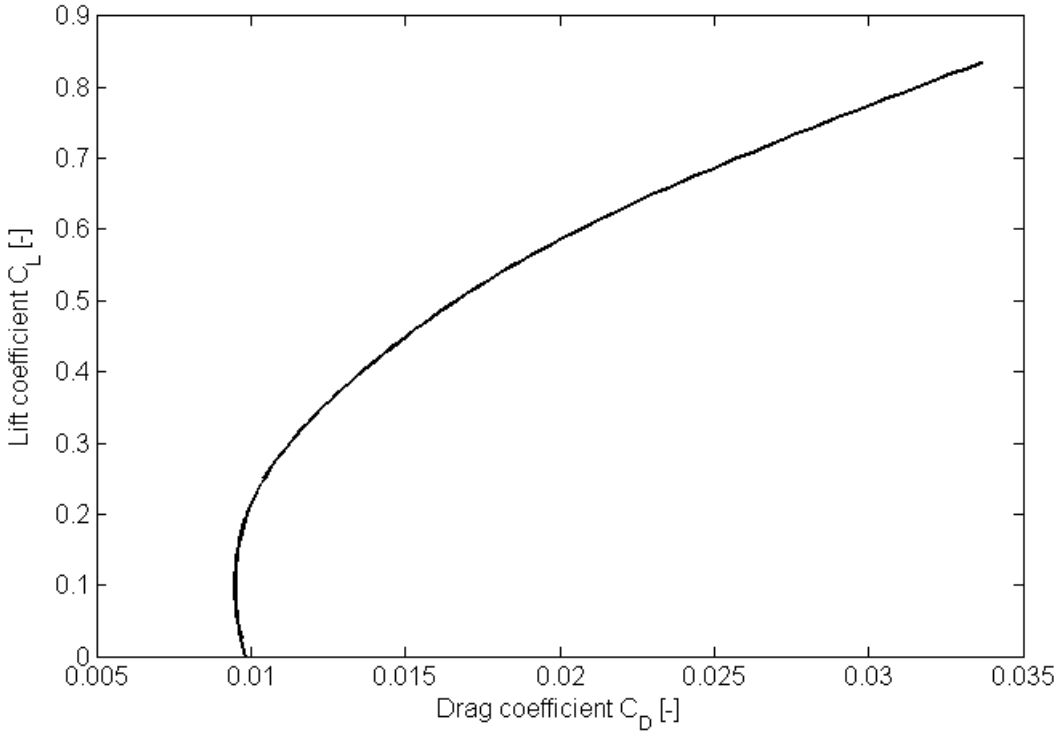

Figure D.5: C_L - C_D polar of the complete aircraft, V = 25 m/s, Re = $10 \cdot 10^6$.

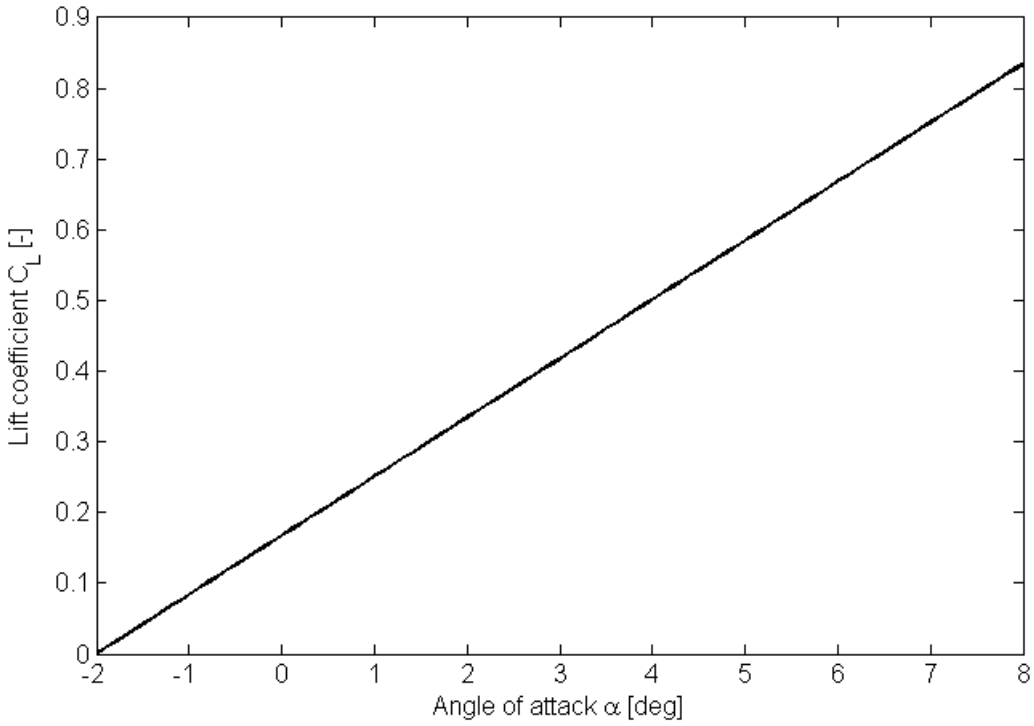

Figure D.6: Lift coefficient of the complete aircraft versus angle of attack, V = 25 m/s, Re = $10 \cdot 10^6$.

Finally, in tables D.1 and D.2 a summary of the found values is presented, as they have been used for the various analyses done. In the first table the characteristics of the separate aerodynamic surfaces are presented, in the second the characteristics of the aircraft as a whole are shown.

Table D.1: Aerodynamic characteristics of the main wing and horizontal stabiliser.

Property	**Main wing**	**Horizontal stabiliser**	**Unit**
Aerofoil	NACA-2412	NACA-0012	[-]
Wing area	0.92	0.115	$[m^2]$
Wingspan	3.5	0.82	[m]
Root chord length	0.375	0.2	[m]
Tip chord length	0.15	0.08	[m]
Aspect Ratio	13.31	4.1	[-]
Cruise angle of attack	2.0	-2.0	[°]

Table D.2: Aerodynamic characteristics of the complete aircraft.

Property	**Complete aircraft**	**Unit**
Cruise velocity	25	[m/s]
Cruise lift coefficient	0.35	[-]
Cruise drag coefficient	0.014	[-]
Maximum lift coefficient	1.348	[-]
Lift over drag ratio	0.08	[-]

Appendix E

Performance analysis

This appendix provides the method and the calculations that were performed for the performance analysis of the SkyDowser aircraft. The calculations presented form the basis of the results of chapter 5.

E.1 Power versus velocity diagram

Figure E.1 shows a typical power versus velocity curve for a propeller aircraft. Curve P_r is the power required plot showing the required power to overcome the drag at a certain velocity. The power required is calculated using equation E.1. The drag in this equation follows from aerodynamic calculations. The power available line (P_a) shows the amount of power the aircraft can deliver. The power available depends on the shaft brake power of the engine, given as P_{br}, and the propulsive efficiency of the propeller. Equation E.2 shows the relation between power available and shaft brake power.

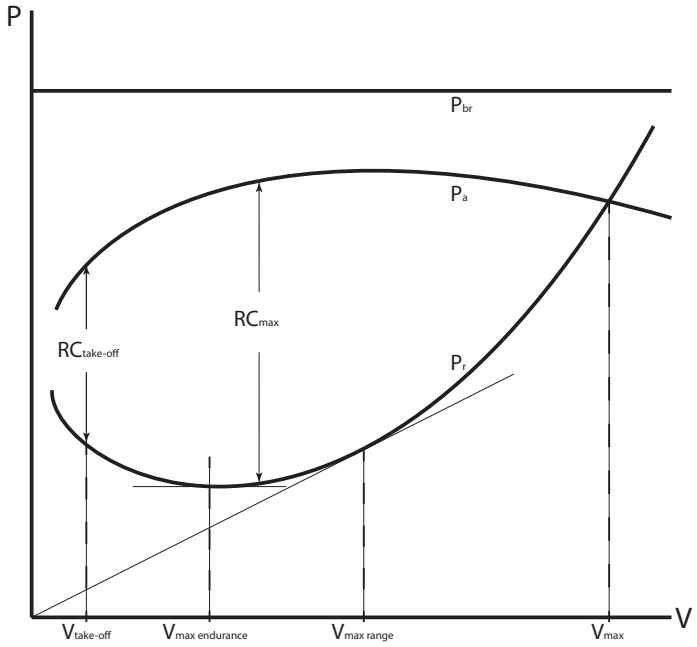

Figure E.1: Power versus velocity for a propeller aircraft.

$$P_r = D \cdot V \tag{E.1}$$

$$P_a = T \cdot V = \eta_j \cdot P_{br} \tag{E.2}$$

The difference between the power available curve and power required curve at $V_{\text{take-off}}$, shown in figure E.1, determines the rate of climb an aircraft can perform at take-off. For the design of the SkyDowser the take-off phase of its mission is stated crucial. The aircraft needs to be able to clear an obstacle of 30 m in a distance of 110 m, resulting in a take of angle of 15°. With an initial velocity given by the launch system of 16 m/s, the rate of climb at take-off can be sized using equation E.3.

In general equation E.4 can be used to determine the rate-off climb if the difference between P_a and P_r is known. This difference is the excess power that can be used to perform a quasi-steady climb during flight.

$$RC_{\text{take-off}} = V_{\text{take-off}} \cdot \sin \gamma_{\text{take-off}} \tag{E.3}$$

$$RC = \frac{P_a - P_r}{W} \tag{E.4}$$

$$\gamma_{climb_{max}} = \arcsin \frac{RC}{V} \tag{E.5}$$

The next interesting point in figure E.1 is where the excessive power is the largest. At this velocity the rate of climb is largest and the aircraft can climb fastest. The steepest climb angle for a certain velocity can be calculated by using equation E.5. Furthermore, at minimum power required the velocity for maximum endurance can be found. The line from the origin, tangent to the power required curve, defines the velocity for maximum range. To fly as efficient as possible, the cruise velocity must be equal to this velocity. Finally the maximum velocity can be found where the power required equals the power available. At this point the available thrust of the SkyDowser is equal to its drag. There is no excess power to accelerate or climb.

E.2 Power analysis

The starting point of the determination of the power available curve, is the rate of climb at take-off. At an initial take-off velocity of 16 m/s (delivered by the catapult system), a rate of climb rate of 4.5 m/s is required to clear an obstacle of 30 m tall. Since the drag is known at the take-off velocity by aerodynamic calculations, the required power is known. Equation E.6 can now be used to calculate the power available by the engine to climb.

$$P_{a_{\text{take-off}}} = P_{r_{\text{take-off}}} + RC_{\text{take-off}} \cdot W \tag{E.6}$$

The power a propeller can deliver depends on its propulsive efficiency. To size and determine the profile of the propeller, the simulation tool PropCalc [35] is used. This tool simulates the performance of propellers based on wind tunnel test data. PropCalc calculates the thrust, power and propulsive efficiency for a range of velocities for a typical propeller. The RPM its operating at can be adjusted.

A propeller with a diameter that is as large as possible is beneficial for the efficiency. However at the tips of too large propellers the sound barrier can be reached. For the flight velocity of the SkyDowser this will not be the case. A propeller that meets the requirements is a RASA propeller with 384 mm diameter and 203 mm pitch. Its efficiency is around 0.80 when thrust for cruise velocity needs to be delivered. This propeller has been analysed further in PropCalc.

The power available is the maximum power that the aircraft can deliver per flight velocity. For maximum power the engine will operate at a high engine setting between $8,400$ and $9,200$ RPM. Figure E.2a shows propulsive efficiency curves at these RPM ranges per flight velocity. It can be seen from this figure that maximum power at low velocities has the consequence that the efficiency decreases significantly. For the take-off velocity the propulsive efficiency factor is 0.51.

Using equation E.2 the shaft brake power of the engine is calculated using the propeller efficiency of 0.51. The shaft brake power that the engine must deliver is 1.3 kW. Knowing this value an engine can be sized for the SkyDowser. Taking the power over weight ratio of all engines options into account, the Saito FG-30B is chosen as a suitable [7]. The specifications of this engine can be found in table E.1.The 2.1 kW power of this engine is more than the needed shaft power. Since it is desired to have some excess power in case the engine power output would be less then expected. Furthermore flying at the engine limits will increase wear and thus would imply more maintenance.

Table E.1: Specifications of the Saito FG-30B engine [7].

Specification	Value
Power	2.1 kW
Specific power	2.0 kW/kg
Weight	1.1 kg
Fuel type	Petrol + 5 % oil
RPM range	$2,000$ - $10,000$

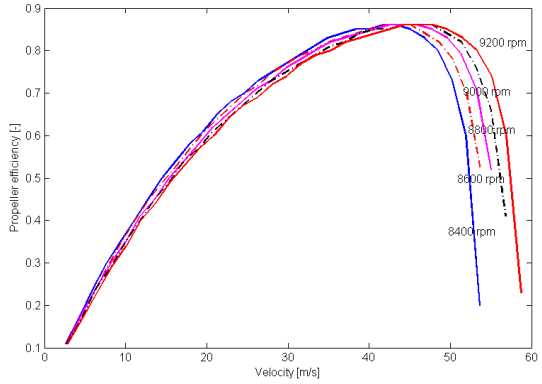

(a) Propeller efficiency for different rpm whilst providing maximum thrust.

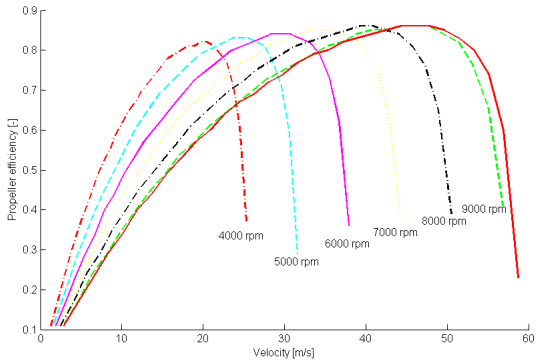

(b) Propeller efficiency for different rpm during cruise phase.

Figure E.2: Propulsive efficiencies.

Since for high RPM rates the efficiencies are in the same range, see figure E.2a, one general efficiency curve can be generated for high maximum power settings of the engine. If the engine does not need to operate near maximum power, the RPM setting is lowered. This is done for steady horizontal flight. The efficiencies for the total range of RPM rates can be seen in figure E.2b. Also from these curves a general efficiency curve can be generated by taking the maximum points of all curves. The results of both general curves can be seen in figure E.3a. The $\eta_{\text{prop}_{\text{Pa}}}$ curve is used to generate the power available curve of the aircraft. The $\eta_{\text{prop}_{\text{steady}}}$ curve is used to calculate the amount of power needed during steady flight where no maximum power available is needed. This efficiency and the efficiency of the engine is used to calculate the energy consumption in section E.6. The engine efficiency is assumed to be constant and estimated to be 0.15 based on the statistical data of several engines. Knowing the energy consumption the amount of fuel required for the mission can be calculated.

Finally a power versus velocity diagram as been described in section E.1 can be created for the SkyDowser, see figure E.3b.

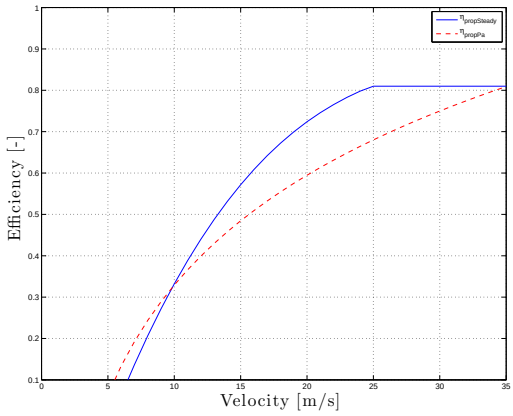

(a) General propulsive efficiencies.

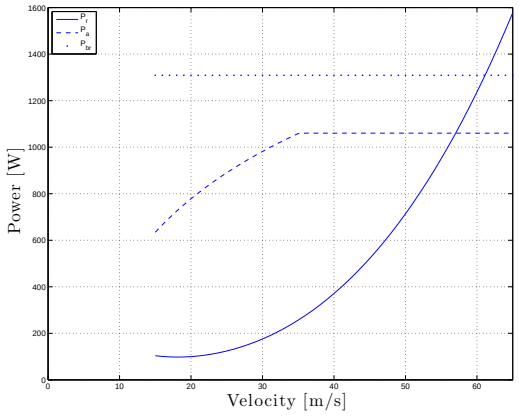

(b) Power versus velocity diagram for the SkyDowser.

Figure E.3: Propulsive efficiencies resulting in power curves.

E.3 Climbing

Results of climbing performance are shown in figures E.4a and E.4b. The maximum climb angle from figure E.4a defines the steepest climb that can be performed. The fastest climb is the maximum climb rate in figure

E.4b.

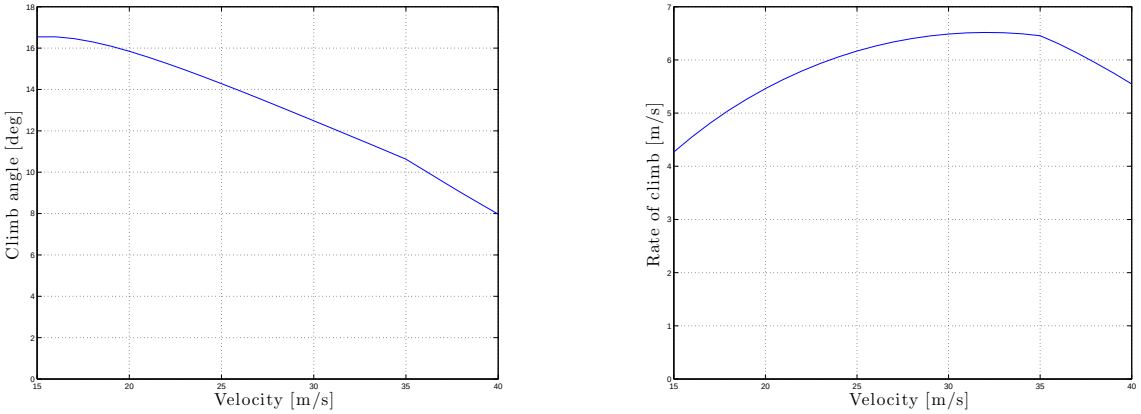

(a) Climb angle versus velocity.

(b) Rate of climb versus velocity.

Figure E.4: Climb characteristics.

E.4 Turning performance

It is beneficial to remain at constant altitude during the complete scan mission, so the SkyDowser must be able to make coordinated turns. Using equation E.7 the turn radius can be calculated. Substituting equation E.8 and rewriting C_L to $\frac{\rho V^2 S}{2L}$ gives equation E.9, the turn radius in terms of load factor and velocity.

$$R = \frac{W}{S}\frac{2}{\rho}\frac{1}{g}\frac{1}{C_L}\frac{1}{\sin\Phi} \tag{E.7}$$

$$n = \frac{L}{W} = \frac{1}{\cos\Phi} \tag{E.8}$$

$$R = \frac{V^2}{g\sqrt{n^2-1}} \tag{E.9}$$

The load factor during a turn is directly dependent on the lift coefficient. It is important that the maximum lift coefficient is not exceeded. If this happens a dangerous stall at low flying altitude can be disastrous. Therefore $C_{L_{\text{turn,max}}}$ is set 10% lower then $C_{L_{\text{max}}}$. This has the result that the load factor will be slightly lower and the turn radii larger for certain velocities. The results of the calculations can be seen in figure E.5. The operating range of the SkyDowser is defined in the figure.

With a $C_{L_{\text{turn,max}}}$ of 1.22 and performing a turn with cruise velocity of 25 m/s gives a load factor of 3 for a 22 m turn radius. The power required during a turn can be calculated using equation E.10. For the turn described the total power needed equals 0.67 kW.

$$P_r = nW\sqrt{\frac{nW}{S}\frac{2}{\rho}\frac{C_D^2}{C_L^3}} \tag{E.10}$$

E.5 Loading diagrams

To set load requirements for the structural analysis of the aircraft load diagrams are determined. The manoeuvring load range (figure E.6a) is calculated using equation E.11 for positive and negative $C_{L_{max}}$. The negative $C_{L_{max}}$ is based on the 2D NACA-2412 aerofoil and is -0.49 from literature[34]. The positive limit load factor is determined by taking a velocity 10% above the cruise velocity. Knowing the maximum lift coefficient for this velocity (27.5 m/s), the maximum load factor becomes 4.7. At velocities exceeding 27.5 m/s the aircraft must be limited to lower angles of attack in order to never exceed load factor 4.7. The

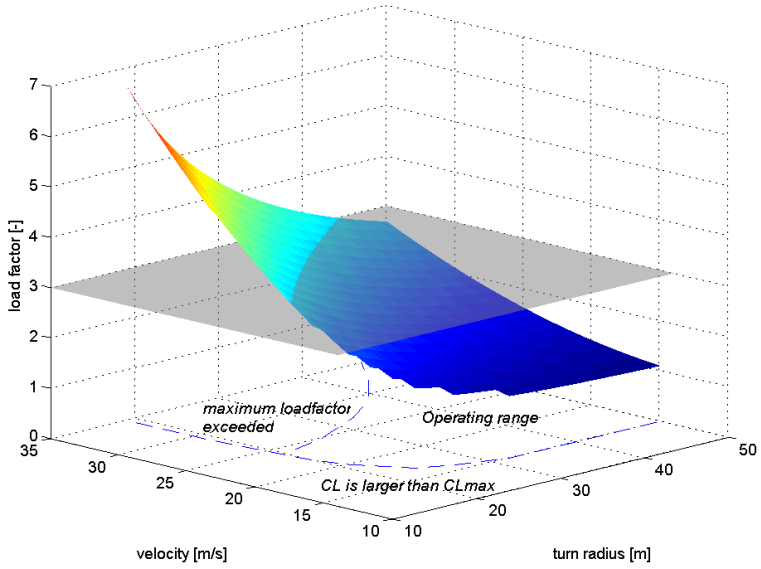

Figure E.5: Load factor during a steady horizontal turn as a function of the radius and velocity.

minimum load factor is set -1.5 by reference data[36]. Figure E.6b shows the gust loading diagram of the SkyDowser. The gust loading is relatively small compared to the manoeuvring loads, since the aircraft has a low weight its not very sensitive for gusts. Equation E.12 is used to determine the gust loads.

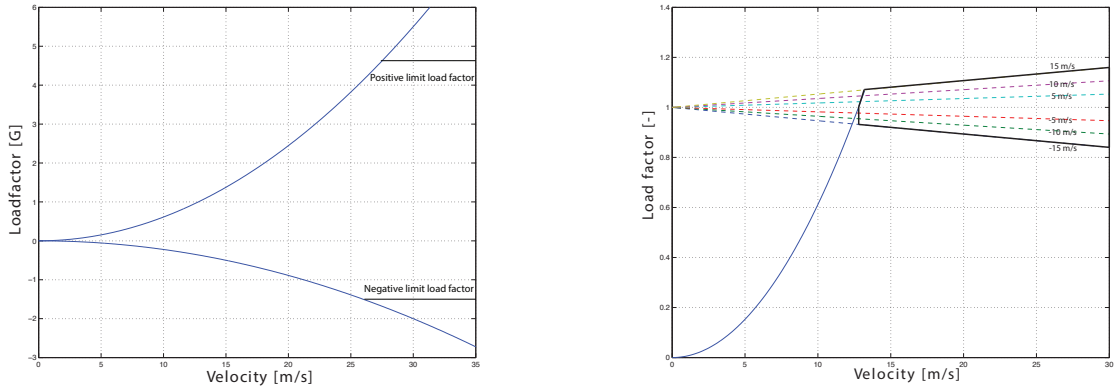

(a) Manoeuvring loads.

(b) Gust loads.

Figure E.6: Loading diagrams for the SkyDowser.

$$n_{max} = \frac{S\rho V^2 C_{L_{max}}}{2W} \tag{E.11}$$

$$n = 1 \pm \frac{dC_L}{d\alpha} \frac{\frac{1}{2}\rho_0 U_e V_e}{W/S} \tag{E.12}$$

E.6 Fuel consumption

The flight range is calculated by integrating the ground velocity over the total flight time. The velocity with respect to the ground is kept constant during the measurement phase to allow for consistent measurements. The scanned area is determined by multiplying the effective range with the scan width plus separation width of the measurement system. In this case the turns are not taken into account. The total energy consumed by the aircraft can be found by using equation E.13.

$$E = \int P dt \tag{E.13}$$

In the case of head wind or wind from behind the effective free stream airspeed changes. With this change in free stream air velocity the UAV flies at a different angle of attack. In the case the wind has a power of 5 Bft and comes from an angle of 0°. from the the flight path the fuel consumption is increased with 50%. Since the aircraft flies in lanes that go in both directions, both headwind and wind from behind is simulated. In the latter case it is dangerous that the free stream velocity will not come close to the stall velocities. In this case the UAV is able to accelerate to a more safe velocity, however the ideal measurement velocity with respect to the ground can not be met. Moreover the velocity may not surpass a velocity of 36 m/s due to regulations. It can be concluded that for safe operation the aircraft can not fly with wind velocities higher than a power of 5 Bft. The ground operator must monitor the weather before and during flight.

An overview of the performance can be seen in table E.2.

Table E.2: Performance overview.

Cruise velocity	25 m/s
Range at V_{cruise}	720 km
Scanned area	29.1 km^2
Used fuel	$0.79 - 1.19$ kg

Steepest climb	4.5 m/s at $\gamma = 16.5°$ at $v = 15$ m/s
Fastest climb	6.4 m/s at $\gamma = 11.6°$ at $v = 32$ m/s

Appendix F

Control and Stability

In this section the calculations of the control and stability characteristics of the SkyDowser are described. The control part covers the sizing of the control surfaces (elevators, ailerons, rudder) based on the most extreme manoeuvres the aircraft is expected to encounter. Using the information about the control surfaces the stability is checked to ensure a stable aircraft.

F.1 Sizing of horizontal stabiliser

For the sizing of the horizontal stabiliser the scissor-plot method has been used.[37] This method relates the position of the centre of gravity with the ratio of the surface of the horizontal stabiliser with the surface of the wing. The plot is shown in figure F.1.

The equations used for this plot are:

$$\bar{x}_{cg} = \bar{x}_{ac} + \frac{C_{L_{\alpha_h}}}{C_{L_\alpha}}\left(1 - \frac{d\epsilon}{d\alpha}\right)\frac{S_h l_h}{S\bar{c}}\left(\frac{V_h}{V}\right)^2 - \text{SM}, \tag{F.1}$$

for stability, where SM is the stability margin of 0.05 and

$$\bar{x}_{cg} = \bar{x}_{ac} - \frac{C_{m_{ac}}}{C_{L_{A-h}}} + \frac{C_{L_h}}{C_{L_{A-h}}}\frac{S_h l_h}{S\bar{c}}\left(\frac{V_h}{V}\right)^2, \tag{F.2}$$

for control. Due to the T-tail configuration, in both equations $\frac{d\epsilon}{d\alpha}$ can be considered 0 and $\frac{V_h}{V}$ is approximately 1. Using this graph a S_h/S of 0.12 has been chosen, which places the design point fairly close to the controllability line and far from the stability. With respect to the static stability, the design will be very stable, but hard to control.

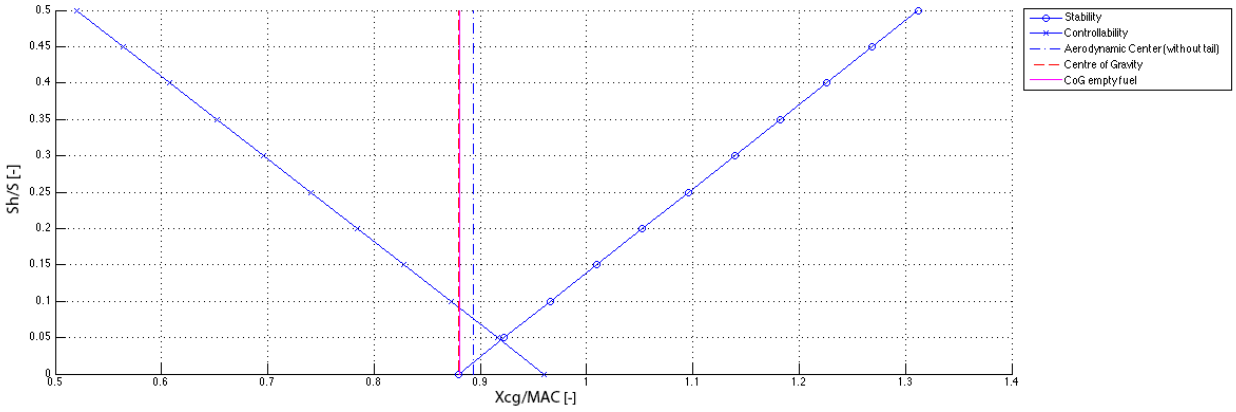

Figure F.1: Scissor-plot for final configuration.

F.2 Sizing of control surfaces

The vehicle is controlled using three types of control surfaces; a single rudder for yaw control, two ailerons for roll control and two elevators for pitch control. In this section the sizing of these surfaces is discussed.

F.2.1 Elevators

For many aircraft the critical flight condition for sizing the elevators is the rotation at take-off. Since the SkyDowser is launched by a catapult, the climb directly after the launch is considered the most critical condition that the elevators will encounter. As discussed in section 8.8 the vehicle needs to be able to climb 35 m in 150 m horizontal distance. In order to fulfil this requirement, the vehicle needs a pitch acceleration, $\ddot{\theta}$ of 16 deg/s^2 , as can be seen in figure F.2, where paths for different pitch accelerations have been simulated. Since the rotational inertia is known over the Y-axis, the necessary moment to achieve this acceleration can be calculated:

$$M = I_{yy}\ddot{\theta} \tag{F.3}$$

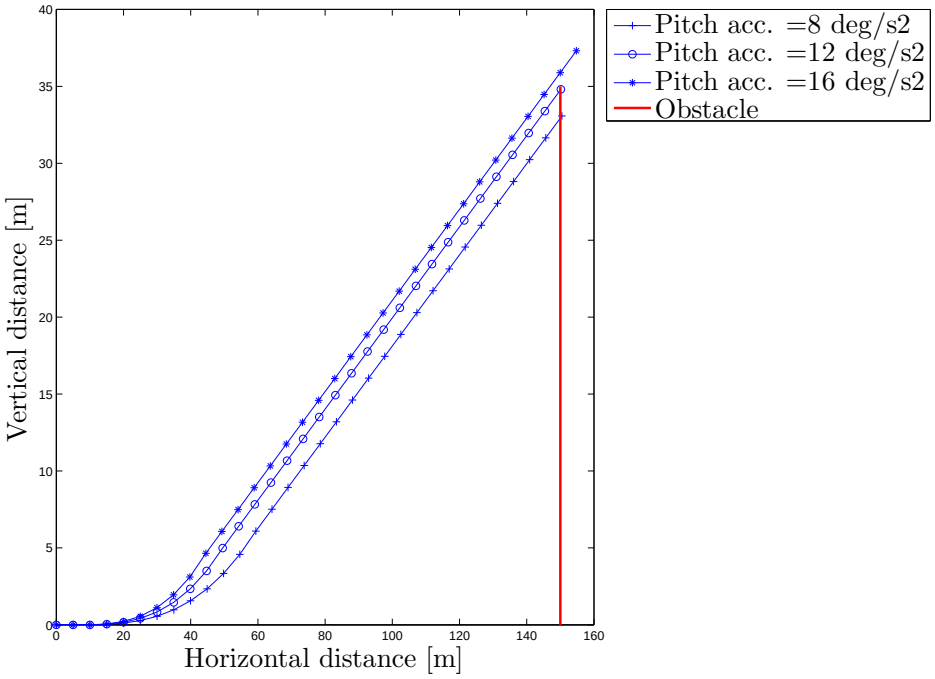

Figure F.2: Object clearance for different pitch accelerations.

Here it has been assumed that only the deflection of the elevators has an effect on the pitch moment M. From this moment, the necessary change in lift δL_h can be determined. The elevator surface that corresponds with this change in lift can be estimated using the lift equation, as such

$$S_e = \frac{\Delta L_h}{\frac{1}{2}\rho V_{\text{cruise}}^2 C_{L_e}}, \tag{F.4}$$

where C_{L_e} is estimated by dividing the hinge moment coefficient C_{L_e} by the quarter chord of the elevator, assuming it is attached at $0.7c_h$. This simplifies the system that attaches the elevator to the horizontal tail surface. A elevator surface of 0.05 m^2 has been computed and the corresponding geometry is shown in figure 4.5.

F.2.2 Ailerons

Once the autopilot decides to roll the vehicle, there will be a transient radial acceleration until the so called steady state roll rate ($\frac{pb}{2V}$) is reached. The turn radius is heavily dependent on this steady state roll rate. The roll rate is affected by the size of the ailerons through $C_{l_{\delta_a}}$. The roll rate is given by equation F.5.

$$\frac{pb}{2V} = -\frac{C_{l_{\delta_a}}}{C_{l_p}}\delta_a \tag{F.5}$$

The relation between steady state roll rate and the turn radius has been simulated in figure F.3. In order to make the turn with radius 22 m, as described in section 5.3, the SkyDowser needs a steady state roll rate of 0.18, which is high when compared to example fighter aircraft that usually have 0.09 [38].

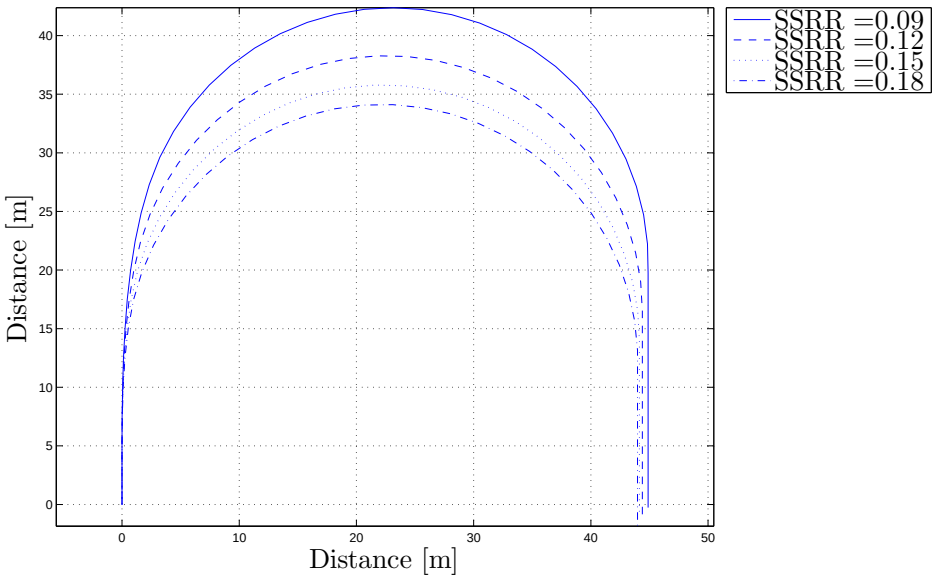

Figure F.3: 180-degree turn simulations for different steady state roll rates.

The relation between the steady state roll rate and $C_{l_{\delta_a}}$ is as follows [38].

$$C_{l_{\delta_a}} = \frac{pb}{2V}\frac{C_{l_p}}{\delta_a} \tag{F.6}$$

According to [39], the $C_{l_{\delta_a}}$ can be approximated by the following equation, where definitions are given in figure F.4.

$$C_{l_{\delta_a}} = -\frac{1}{S\frac{b}{2}} C_{L_\alpha}\left(\frac{(c_{t_w} - c_{r_w})}{\frac{b}{2}}\left(\frac{\eta_i^3 + \eta_o^3}{3}\right) - c_{r_w}\left(\frac{\eta_i^2 + \eta_o^2}{2}\right)\right). \tag{F.7}$$

Equating equations F.6 and F.7, and assuming an aileron effectiveness of 50% an aileron deflection of 6 degrees is found to achieve a turn with 22 m radius for ailerons of the dimensions illustrated in figure 4.5. This can further be optimised, since an effective aileron deflection of 10-15 degrees is normal.

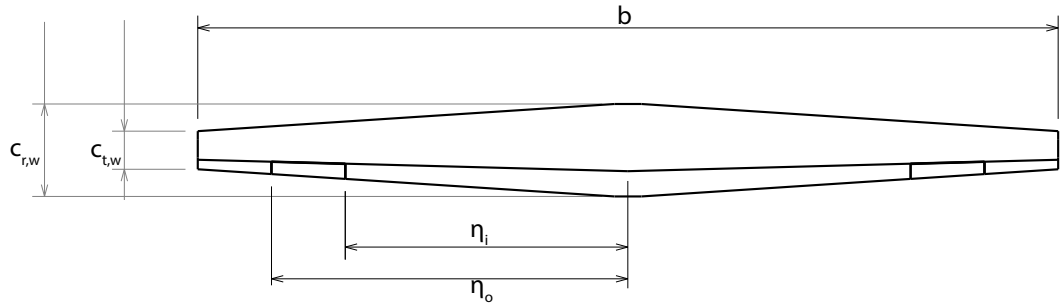

Figure F.4: Ailerons dimensions for sizing.

F.2.3 Rudder

The rudder can be sized for different requirements. Examples are asymmetric thrust (multi-engine aircraft), crosswind landing, spin recovery and coordinated turn. For remote controlled and model aircraft the most critical flight condition usually is the coordinated turn.[6] Therefore, the rudder of the SkyDowser has been sized for this flight condition.

The coordinated turn has a couple of advantages, such as no slipping, constant turn radius and constant turn rate. It is achieved by using a simultaneous deflection of the rudder and the ailerons. The governing equations for the flight condition are based on Newton's second law and are taken from[6].

$$F_{A_{Y_t}} = F_C - W \sin\phi L_{A_t} = R_1 Q_1 (I_{zz} - I_{yy}) N_{A_t} = I_{xz} R_1 Q_1, \tag{F.8}$$

where

$$F_C = m\frac{V^2}{R_t} Q_1 = g\frac{\sin^2\phi}{V\cos\phi} R_1 = \frac{g\sin\phi}{V}. \tag{F.9}$$

Using the equations for $F_{A_{Y_t}}$, L_{A_t} and N_{A_t} a linear system can be deduced with variables β, δ_a and δ_r. The dimensions of the rudder are hidden in the control derivatives with respect to the rudder deflection δ_r (see Section F.3.2). This linear system (equation F.10) can thus be used to see whether the deflections of the rudder and ailerons are acceptable for a certain rudder size.

$$\begin{bmatrix} F_{a_{yt}} - \frac{R_1 b}{2V} C_{Y_{\delta r}} \\ L_{a_t} - \frac{R_1 b}{2V} C_{Y_{\delta r}} \\ N_{a_{yt}} - \frac{R_1 b}{2V} C_{Y_{\delta r}} \end{bmatrix} = \begin{bmatrix} C_{y_\beta} & C_{y_{\delta a}} & C_{y_{\delta r}} \\ C_{l_\beta} & C_{l_{\delta a}} & C_{l_{\delta r}} \\ C_{n_\beta} & C_{n_{\delta a}} & C_{n_{\delta r}} \end{bmatrix} \cdot \begin{bmatrix} \beta \frac{1}{2}\rho V^2 S \\ \delta_a \frac{1}{2}\rho V^2 S b \\ \delta_r \frac{1}{2}\rho V^2 S b \end{bmatrix} \tag{F.10}$$

For the tightest turn which the vehicle can handle (22 m radius, with 25 m/s) corresponds with $\beta = -10.82$deg, $\delta_a = 14.4$deg and $\delta_r = 10.64$deg for a rudder of $S_r = 0.04 m^2$. For manufacturing reasons it is easy to attach the rudder on the last spar in the vertical tail, which is located at 0.7 chord.

F.2.4 Control forces

Deflecting the control surfaces results in an aerodynamic force. The actuator deflecting the control surface will have to able to exert a sufficient moment to deflect the control surface. The maximum control force occurs at maximum deflection, this maximum force is an input for the structural analysis of the aircraft.

Equations F.11 to F.13 can be used to calculate the control forces for a control surface without a trim tab.[40].

$$F_e = -\frac{d\delta_e}{ds_e}\frac{1}{2}\rho V^2 S_e \bar{c}_e \left(C_{h_\alpha}\alpha_h + C_{h_\delta}\delta_e\right) \tag{F.11}$$

$$F_a = -\frac{d\delta_a}{ds_a}\frac{1}{2}\rho V^2 S_a \bar{c}_a \left(C_{h_\alpha}\Delta\alpha_a + C_{h_\delta}\frac{\delta_a}{2}\right) \tag{F.12}$$

$$F_r = -\frac{d\delta_r}{ds_r}\frac{1}{2}\rho V^2 S_r \bar{c}_r \left(C_{h_\alpha}\alpha_v + C_{h_\delta}\delta_r\right) \tag{F.13}$$

In these equations C_{h_α} is the hingemoment derivative due to angle of attack and C_{h_δ} is the hingemoment derivative due to control surface deflection. An estimation of these hingemoment derivatives has been made based on[41], section 10.4. Given the sizes of the control surfaces, and a maximum deflection of 20 degrees, the following control forces are found:

- **Aileron:** 0.022 N
- **Elevator:** 0.004 N
- **Rudder:** 0.069 N

It has to be noted that the forces found are quite low. It has not been possible to validate this data. Therefore the control surfaces of reference aircraft have been investigated. The control surfaces of the Penguin B[42] are comparable to those of the SkyDowser, and therefore it is expected that the size of the control surfaces will suffice for the aircraft. However, further research has to be done on the control forces, especially for the sizing of the actuators.

F.3 Stability

Both types of stability, static and dynamic, have been considered during the design. Static stability comprises the equilibrium during flight and the reaction to small disturbances. Manoeuvres and the recovery to equilibrium are part of the dynamic stability.

F.3.1 Static stability

Lateral static stability follows from the symmetry of the vehicle.

Longitudinal static stability is achieved by complying with two requirements. [37]

1. The vehicle should experience an equilibrium of moments in steady flight. This is the so-called *Trim Condition*.
2. After a disturbance the aircraft should return to its equilibrium position. There should be stability around the trim condition.

Since the vehicle is unmanned, it is unnecessary to include trim tabs. This means that the first requirement should met by using elevators to trim the aircraft. For each airspeed, which the vehicle may be exposed to, this trim condition should be checked. The relation between the airspeed and the elevator deflection that ensures trim stability [40] is

$$\delta_e = -\frac{1}{C_{m_{d_e}}}\left(C_{m_0} + \frac{C_{m_\alpha}}{C_{N_\alpha}}\frac{W}{\frac{1}{2}\rho V^2 S}\right) \tag{F.14}$$

The second requirement is met when the neutral point of the aircraft lies aft of the centre of gravity of the aircraft. The aircraft design is checked on this condition for four different situations: full fuel tank, empty fuel tank, all fuel in front of fuel tank and all fuel in the rear of the fuel tank. The situations in which all the fuel is in the front or rear of the fuel tank represents the centre of gravity location in the event of steep climbs and descents. Equations F.15 and F.16 are used to calculate the location of the neutral point.

$$\frac{X_{c.g} - X_{n_{free}}}{\bar{c}} = \frac{C_{m_{\alpha free}}}{C_{N_\alpha}} \tag{F.15}$$

$$\frac{X_{c.g} - X_{n_{fixed}}}{\bar{c}} = \frac{C_{m_\alpha}}{C_{N_\alpha}} \tag{F.16}$$

F.3.2 Dynamic stability

To evaluate the dynamic stability of the aircraft the equations of motion for both the longitudinal and lateral motion have been evaluated. The equations of motion [40] are:

Longitudinal:

$$\begin{bmatrix} C_{X_u} - 2\mu_c D_c & C_{X_\alpha} & C_{Z_0} & C_{X_q} \\ C_{Z_u} & C_{Z_\alpha} + (C_{Z_{\dot{\alpha}}} - 2\mu_c)D_c & -C_{X_0} & C_{Z_q} + 2\mu_c \\ 0 & 0 & -D_c & 1 \\ C_{m_u} & C_{m_\alpha} + C_{m_{\dot{\alpha}}} D_c & 0 & C_{m_q} - 2\mu_c K_Y^2 D_c \end{bmatrix} \begin{bmatrix} \hat{u} \\ \alpha \\ \theta \\ \frac{qc}{V} \end{bmatrix} = \begin{bmatrix} -C_{X_{\delta_e}} \\ -C_{Z_{\delta_e}} \\ 0 \\ -C_{m_{\delta_e}} \end{bmatrix} \delta_e \tag{F.17}$$

Lateral:

$$\begin{bmatrix} C_{Y_\beta} + (C_{Y_{\dot{\beta}}} - 2\mu_b)D_b & C_L & C_{Y_p} & C_{Y_r} - 4\mu_b \\ 0 & -\frac{1}{2}D_b & 1 & 0 \\ C_{l_\beta} & 0 & C_{l_p} - 4\mu_b K_X^2 D_b & C_{l_r} - 4\mu_b K_{XZ}^2 D_b \\ C_{n_\beta} + C_{n_{\dot{\beta}}} D_b & 0 & C_{n_p} + 4\mu_b K_{XZ}^2 D_b & C_{n_r} + 4\mu_b K_Z^2 D_b \end{bmatrix} \begin{bmatrix} \beta \\ \phi \\ \frac{pb}{2V} \\ \frac{rb}{2V} \end{bmatrix} = \begin{bmatrix} -C_{Y_{\delta_\alpha}} & -C_{Y_{\delta_r}} \\ 0 & 0 \\ -C_{l_{\delta_\alpha}} & -C_{l_{\delta_r}} \\ -C_{n_{\delta_\alpha}} & -C_{n_{\delta_r}} \end{bmatrix} \begin{bmatrix} \delta_\alpha \\ \delta_r \end{bmatrix} \tag{F.18}$$

The equations of motion are rewritten to a state-space form, which is used to simulate the aircraft's response to a certain input. This conversion is done according to the description in section 4-4 and 4-5 of [40].

In order to simulate the motions, the stability and control derivatives listed in equations F.17 and F.18 have to be known. Most of these derivatives have to be determined from flight-data. Since no flight-data is available for the UAV to be designed, they have to be estimated using literature. Table F.1 lists the equations required to calculate the derivatives, and the literature this equation has been based on. It has to be noted that these calculations provide a first estimate for the aircraft's stability and control derivatives. Test flights have to be performed for an accurate determination of the derivatives.

Some of the derivatives are based on parameters obtained from literature. For C_{Y_β}, the values of J_b, J_t and J_w have been found in ESDU file 88029 [43]. For $C_{n_{\delta_a}}$ the values of G and H have been found in ESDU file 82010 [44].

Table F.1: Control and Stability derivatives

Derivative	Equation	Value	Source
C_{X_0}	$\frac{W \sin\theta_0}{\frac{1}{2}\rho V^2 S}$	0	[40]
C_{Z_0}	$\frac{-W \cos\theta_0}{\frac{1}{2}\rho V^2 S}$	-0.3493	[40]
C_{X_u}	$-2C_D$	-0.0280	[40]
C_{Z_u}	$-2C_L$	-0.8000	[40]
C_{M_u}	neglected	0	[40]
C_{X_α}	$C_L\left(1 - \frac{2C_{L_\alpha}}{\pi A e}\right)$	0.2956	[40]
C_{Z_α}	$-C_{N_\alpha} - C_{Nh_\alpha}\left(1 - \frac{d\epsilon}{d\alpha}\right)\left(\frac{V_h}{V}\right)^2 \frac{S_h}{S}$	-6.0131	[40]
$C_{Z_{\dot\alpha}}$	$-C_{N_{h_\alpha}}\left(\frac{V}{V^2}\right)^2 \frac{d\epsilon}{d\alpha}\frac{S_h l_h}{s\bar{c}}$	0	[40]
C_{m_α}	$C_{N_\alpha}\frac{x_{c.g.}-x_w}{\bar{c}} - C_{Nh_\alpha}\left(1 - \frac{d\epsilon}{d\alpha}\right)\left(\frac{V_h}{V}\right)^2 \frac{S_h l_h}{S\bar{c}}$	-2.3994	[40]
$C_{m_{\dot\alpha}}$	$-C_{N_{h_\alpha}}\left(\frac{V}{V^2}\right)^2 \frac{d\epsilon}{d\alpha}\frac{S_h l_h^2}{s\bar{c}^2}$	0	[40]
C_{X_q}	neglected	0	[40]
C_{Z_q}	$-2C_{Nh_\alpha}\left(\frac{V_h}{V}\right)^2 \frac{S_h l_h}{S\bar{c}}$	-4.9278	[40]
C_{m_q}	$-(1.1)C_{Nh_\alpha}\left(\frac{V_h}{V}\right)^2 \frac{S_h l_h^2}{S\bar{c}^2}$	-19.965	[40]
$C_{X_{\delta_e}}$	neglected	0	[40]
$C_{Z_{\delta_e}}$	$C_{L_{\alpha_e}}\frac{S_h}{S}$	-0.5506	[39]
$C_{m_{\delta_e}}$	$C_{L_{\alpha_e}}\frac{S_v l_t}{S\bar{c}}$	-2.20278	[39]
C_{Y_β}	$-J_b J_t J_w C_{Y_{v_\alpha}}\frac{S_v}{S}$	-0.1457	[44]
$C_{Y_{\dot\beta}}$	neglected	0	[40]
C_{l_β}	$C_{Y_\beta}\frac{CP_{v_{\bar{z}}}\cos\alpha_0 - CP_{v_{\bar{x}}}\sin\alpha_0}{b}$	-0.0033	[44]
C_{n_β}	$-C_{Y_\beta}\frac{CP_{v_{\bar{z}}}\cos\alpha_0 + CP_{v_{\bar{x}}}\sin\alpha_0}{b}$	0.0071	[44]
$C_{n_{\dot\beta}}$	neglected	0	[40]
C_{Y_p}	neglected	0	[40]
C_{l_p}	$-\frac{(C_{L_\alpha}+C_D)\frac{b}{2}}{2S}\left(\frac{c_{t_w}}{4} + \frac{c_{r_w}}{12}\right)$	-0.3509	[39]
C_{n_p}	$-\frac{C_{L_\alpha}-C_{D_\alpha}\frac{b}{2}}{S}\left(\frac{c_{t_w}}{4} + \frac{c_{r_w}}{12}\right)$	-0.0262	[39]
C_{Y_r}	$2C_{Y_{v_\alpha}}\left(\frac{V_v}{V}\right)^2 \frac{S_v l_v}{Sb}$	0	[40]
C_{l_r}	$C_{Y_r}\left(\frac{z_v - z_{c.g.}}{b} cos\alpha_0 - \frac{x_v - x_{c.g.}}{b}\sin\alpha_0\right)$	0.1196	[40]
C_{n_r}	$C_{Y_r}\frac{l_v}{b}$	-0.0351	[40]
$C_{Y_{\delta_a}}$	neglected	0	[40]
$C_{l_{\delta_a}}$	$-\frac{1}{S\frac{b}{2}}C_{L_\alpha}\left(\frac{(c_{t_w}-c_{r_w})}{\frac{b}{2}}\left(\frac{\eta_i^3+\eta_o^3}{3}\right) - c_{r_w}\left(\frac{\eta_i^2+\eta_o^2}{2}\right)\right)$	0.5791	[39]
$C_{n_{\delta_a}}$	$(G-H)\frac{l_v}{b}$	0.0225	[43]
$C_{Y_{\delta_r}}$	$C_{L_{\alpha_r}}\frac{S_v}{S}$	0.2987	[39]
$C_{l_{\delta_r}}$	$C_{Y_{\delta_r}}\left(\frac{z_v - z_{c.g.}}{b} cos\alpha_0 - \frac{x_v - x_{c.g.}}{b}\sin\alpha_0\right)$	0.0056	[40]
$C_{n_{\delta_r}}$	$-C_{Y_{\delta_r}}\frac{l_v}{b}$	-0.0877	[40]

With an estimate for all stability and control derivatives the aircraft's response to a disturbance can be simulated. Figures F.5 to F.7 illustrate these responses.

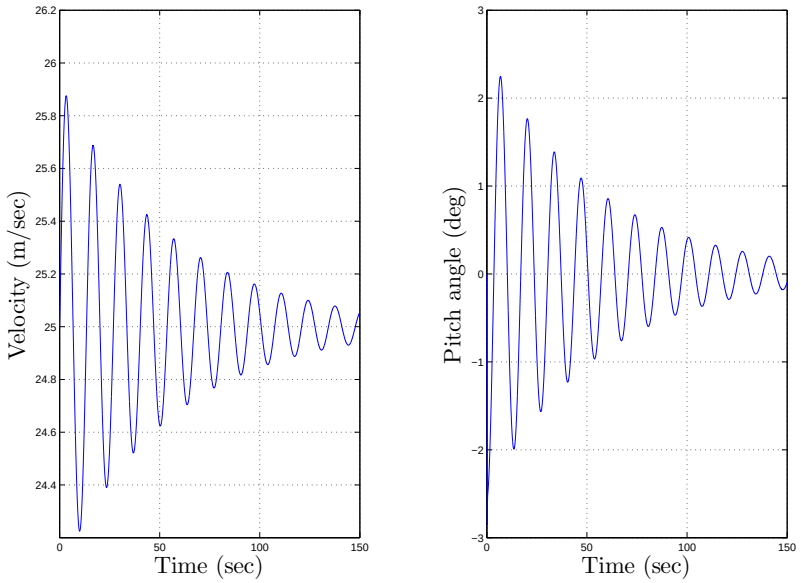

Figure F.5: Aircraft's longitudinal response to an elevator deflection of 2 degrees for 3 seconds.

Figure F.5 shows the response of the aircraft to an elevator deflection. This deflection results in a *phugoid* motion, in which the aircraft continuously exchanges altitude for velocity and vice versa. This is a slowly damped motion with a time to half-amplitude of about 40 seconds. Since it is a damped motion, the aircraft is dynamically stable in terms of response to an elevator deflection.

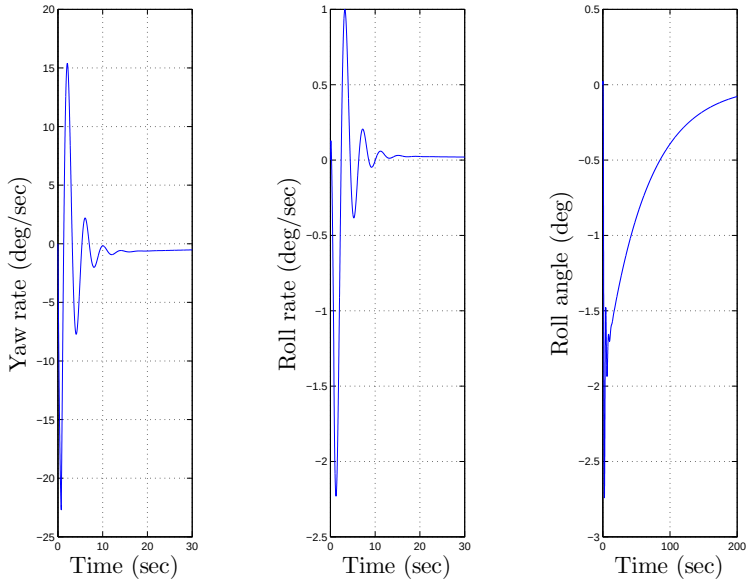

Figure F.6: Aircraft's lateral response to a rudder deflection of 2 degrees for 3 seconds.

Figure F.6 shows the response of the aircraft to a rudder deflection. This deflection results in a motion in which the aircraft will start to roll and yaw. As can be seen in the figure, the rate at which the aircraft rolls and yaws decreases over time. After 4 minutes the aircraft has returned to its original orientation. The time to half-amplitude of the roll angle is about 42 seconds. As a result the aircraft is dynamically stable in terms of response to a rudder deflection. A more accurate simulation will have to be performed in the final

phase of the design of this aircraft to evaluate the aircraft's response to a rudder deflection. Also, the time it takes for the aircraft to return to its original state can be decreased by increasing the size of the vertical tail.

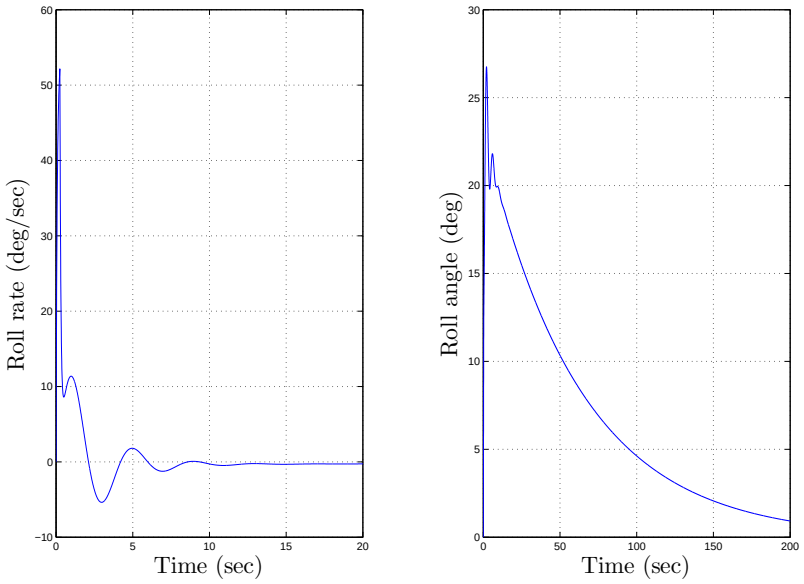

Figure F.7: Aircraft's lateral response to an aileron deflection of 2 degrees for 1 seconds.

Figure F.7 shows the response of the aircraft to an aileron deflection. This deflection will manoeuvre the aircraft to a roll angle of about 45 degrees. As can be seen in the figure the aircraft returns to its original orientation in 4 minutes, with a time to half-amplitude of about 42 seconds. From this response it can be concluded that the aircraft is dynamically stable in terms of response to an aileron deflection. Also in this case, the time required to return to the original state can be decreased by increasing the size of the vertical tail.

The simulated motions show that the aircraft is dynamically stable for both longitudinal and lateral motions. However, this is based on on a first estimation for the stability and control derivatives. These derivatives will have to investigated in more detail in the final design phase of the aircraft, and validated with test-flight data.

Appendix G

Structural analysis

This section provides the method and the calculations that were performed for the structural analysis. The method will be explained first, after which the results are presented.

MATLAB was used to perform the analysis. A complete overview of the MATLAB layout can be found in figure G.1. The equations and methodology are based on what is taught in Megson [45]. The assumptions used in the calculations can be found below:

- The cross-sections used are thin-walled
- The cross-section remains in plane, perpendicular to the length of the wing.
- All loads are applied perpendicular the plane in which they act.
- At the tip of the wing, all loads are zero, unless loads are applied there.
- All material used is homogeneous and is linearly elastic.
- The direct stress is directly proportional to the bending moment.
- There is no warping in the structure.

The sign convention is as follows:

- internal normal: tension positive
- internal shear: up and towards trailing edge positive
- internal moments: bottom and leading edge in tension positive
- internal torque: clockwise possible

A safety factor of 1.5 is applied on all loads, on top of the load factor of 4.7.

G.1 Fuselage

First, all input parameters are defined. A lot of input parameters are the result of calculations of other disciplines. These are imported from a main file in which output of all the programs is stored. Internal parameters are then defined. The loads taken into account for the calculations of the fuselage are:

- Weight of all components (e.g. engine weight, wing weight, etc.) as point loads.
- Lift and Drag of the aerodynamic surfaces as point loads.
- Propulsion as a point load.
- Weight of the fuselage as a distributed load.

All loads in z-direction cause moments, it is assumed that all other loads cause no torques or moments. The fuselage is assumed to be a cylinder of which the moment of inertia is given by:

$$I_{yy} = I_{zz} = \pi({R_o}^4 - {R_i}^4) \tag{G.1}$$

Here, R_o is the outer radius of the cylinder, R_i is the inner radius, defined as $R_i = R_o - t$. I_{yz} is zero due to symmetry. The fuselage is then split into a number of cross-sections, for each of these cross-sections the local loads are calculated, and multiplied by a safety factor of 1.5 times the maximum aerodynamic load factor. The stresses corresponding to these loads are calculated next, using the following equation to relate the local moment to normal stress:

$$\sigma_x = \frac{M_y z}{I_{yy}} \tag{G.2}$$

Where z is the distance from the centre of gravity to the z-location on which the moment is calculated. After adding the stress caused by the local normal force the maximum stress is found at either the top or bottom of the fuselage. Starting at the minimum thickness required for manufacturing the stresses are calculated for increasing thicknesses until the fuselage is strong enough to not fail under the applied loads.

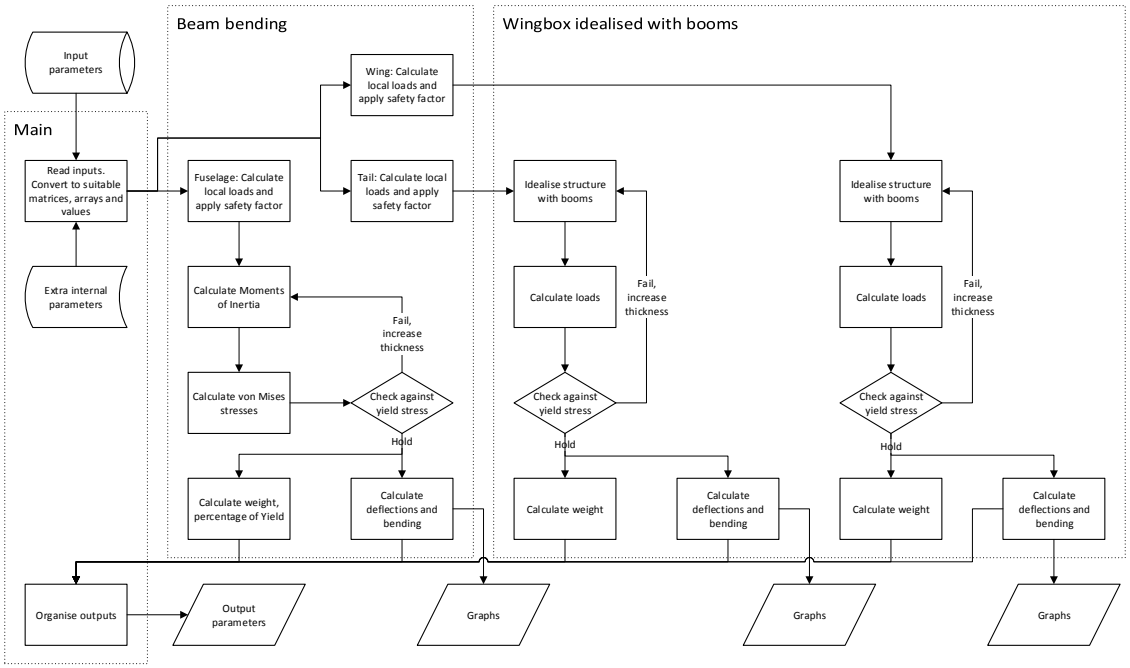

Figure G.1: Layout of the structural analysis MATLAB program.

G.2 Wing and tail

The input for the wing box is defined similar to the way it is for the fuselage. A wing box is used for both wing, horizontal tail and vertical tail. The wing box follows the aerodynamic contour of the aerofoil so may have an asymmetrical cross-section. The wing box is tapered in both directions.

G.2.1 Idealisation

First, the wing box cross-section is idealised with booms. The provided script calculates coordinates of the NACA2412 aerofoil using an uneven spacing. This data is interpolated, such that boom positions can be defined to have an even spacing with respect to each other. All coordinates are given as percentage of the local chord length. The centre of gravity and moments of inertia are then calculated from the skin section in between each of the booms. Here, the thickness is kept out of the equation, such that multiplying the outcome by the chord length cubed and thickness will provide the actual moment of inertia. This way, the moments of inertia and the centre of gravity location only have to be calculated once per aerofoil type.

G.2.2 Wing box normal stress

Similarly to the fuselage, the loads are calculated at cross-sections along the length of the wing box. First of all, the boom angles due to the taper are defined. This means that normal forces in booms are not normal to the cross-section, this causes extra components that need to be taken into account in the calculations. For each cross-section, the normal forces, shear and moments in all directions are calculated. The point loads add up to a resultant force in z-direction and x-direction. The normal stresses caused by local moments are calculated using the following equation:

$$\sigma_y = \frac{M_z I_{xx} - M_x I_{xz}}{I_{xx} I_{zz} - {I_{xz}}^2} x + \frac{M_x I_{zz} - M_z I_{xz}}{I_{xx} I_{zz} - {I_{xz}}^2} z \tag{G.3}$$

Here, x is the horizontal distance to the boom location from the centre of gravity of the cross-section, z is the vertical location. The stress due to the applied normal force is added, and the effect of taper is added.

From this total normal stress distribution, the boom area can be determined.

G.2.3 Wing box shear stress

Now, the shear stresses must be determined. The shear is determined in the xz-plane. The local force in z-direction and x-direction are used (S_z and S_x respectively). First, a cut is made between the lower-left boom and the boom above. This will allow for the calculation of the basic shear flow. The following equation is used:

$$q_b = \frac{S_x I_{xx} - S_z I_{yy}}{I_{xx} I_{zz} - {I_{xz}}^2} B_r x_r + \frac{S_z I_{zz} - S_x I_{xz}}{I_{xx} I_{zz} - {I_{xz}}^2} B_r z_r \tag{G.4}$$

The result is the basic shear flow per boom, which is assumed constant over the skin in between booms. Because this means that peaks in shear flow are averaged out this might result in an under-designed structure. Therefore it is important that the result has a proper safety margin. Now, the structure is closed and moment is taken around the centre of gravity to adjust the basic shear flow. the constant shear flow that performs this (q_{s_0}) can be determined using:

$$S_x \eta_0 - S_z \xi_0 = \oint q_b p ds + 2A q_{s_0} - \sum_{r=1}^{m} P_{x_r} \eta_r + \sum_{r=1}^{m} P_{z_r} \xi_r \tag{G.5}$$

Where P_x and P_y are the in-plane components of the boom force and η and ξ are the arms to the moment centre, around which the calculation is performed. Now, by dividing the total shear flow by the thickness of the skin, the shear stress in the skin (τ) is found.

After these calculations have been performed for all cross-sections a check is performed to see if the wing box fails under the applied loads, also considering buckling, if it does the thickness is increased and the calculations are repeated until a suitable thickness is found. Using this thickness the deflection, deflection angle and twist angle along the wing are also calculated.

G.2.4 Weight calculation

After the minimum thicknesses are calculated the mass of the parts is calculated. For the wing and tail, the aerodynamic parts have the minimum material thickness. A margin is added to the masses of the parts to take into account the extra masses associated with mounting points and reinforcements at cutouts. These margins are tabulated in table G.1.

Table G.1: Mass margins for structural parts.

Part	Mass margin
Fuselage	33%
Wing	8%
Horizontal tail	5%
Vertical tail	5%

G.3 Results

The results will now be presented for each different part: Fuselage, wing, and tail.

G.3.1 Fuselage

The fuselage is 11 cm in diameter, and minimum thickness is 0.8 mm for manufacturing reasons. Under the applied loads the maximum stress that occurs in the fuselage is around 8% of yield stress, at minimum thickness. However, the fuselage has many cutouts for access to components, and for mounting of the wings and tail. This will generate many stress concentrations and thus increase the local stress. In some places reinforcements may be necessary but this will have to be evaluated per case. The mass of the fuselage, after adding the mass margin, is 1.53 kg. In the current design the fuselage is over-designed and thus may be too heavy. The mass can be reduced by decreasing the diameter of the tube. The section under, and in front of the wing can not be reduced in size because of the components that have to fit inside. The diameter of the

part behind the wing could be reduced since hardly any components are fitted inside. This might however create problems when landing since, as will be explained in Appendix I.2, the loads are already at 23% of buckling load. This means that the diameter can only be reduced by 4 cm before the buckling load will be exceeded. This could result in a mass reduction of 0.25 kg so this is definitely an option which can be investigated in future development.

G.3.2 Wing

Under the applied loads, and at minimum thickness of 0.8 mm, the structure in the wings will reach 13% of its yield loads, the stress in the booms is shown in figure G.2. The maximum shear stress that occurs is at 3% of failure.

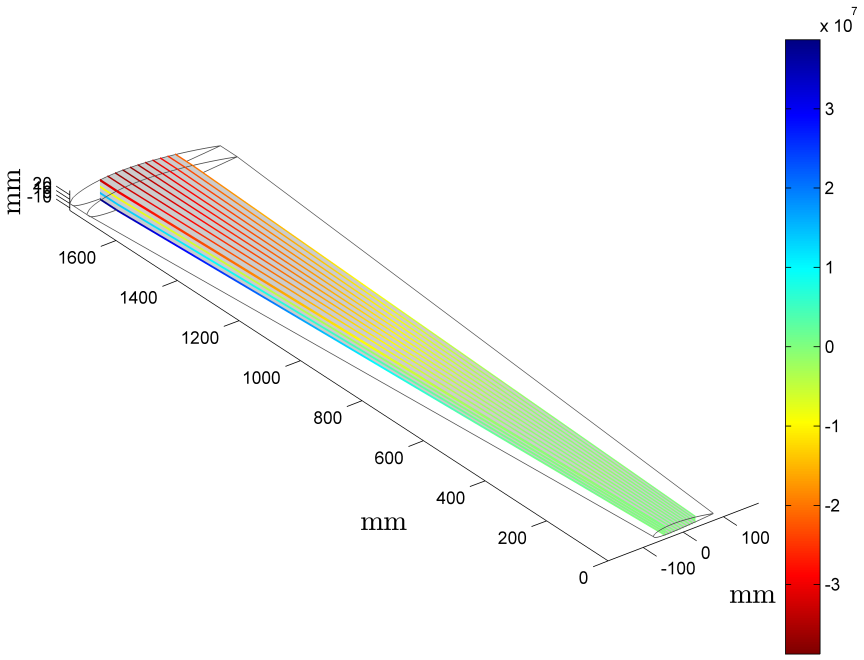

Figure G.2: Stresses in the booms, in Pa.

Although it may seem that the structure is over-designed, it is not. Buckling due to compression occurs in the top skin, this is obviously undesirable. To prevent this buckling the thickness can be increased, longitudinal stiffeners can be added, or a combination of both. Trying different solutions to this problem showed that only adding stiffeners and not increasing the thickness gave the lightest structure. The buckling loads after optimisation of the number and location of stiffeners is shown in figure G.3. In this figure, the wingtip is on the left. Starting from the root of the wing the first section has four stiffeners, the second section has two, the third has one, and the final part requires no stiffeners. As can be seen, this reduces the maximum buckling load to 90%. Since the loads on the wings are asymmetric, the same analysis has been performed on the other wing. This yielded similar results, the difference being the lengths of the stiffeners that have to be used. The total mass of the wing, after adding the margin, is 3.73 kg.

Under the applied loads the wingtip has an upwards deflection of 58 mm, at an angle of 2.6°. It must be noted that this deflection angle is beyond the limit of 1.5°, which is required for performing the measurements, but during regular flight the angle is well below this limit. The wing twists 1° at the tip, this is within limits. The wing deflection and deflection angle are shown in figures G.4 and G.5.

G.3.3 Tail

The analysis performed on the tail is similar to that performed for the main wings. Again, normal stress and shear are not critical, but the buckling load is exceeded. The negative value indicates buckling in the lower skin. A single stiffener is used for a small part of the tail to limit the buckling load to 75%. The buckling loads are shown in figure G.3.

Additional to the regular loads, the vertical tail section also has to carry the loads generated by the horizontal tail. Yet again, normal and shear stresses are not critical. The stress increases to 26% of the buckling load so no stiffeners have to be used. It seems the structure is over-designed, it is recommended that options to reduce the weight of the structure be explored in further design. With the current design, the total mass of the tail, after adding the margin, is 0.63 kg.

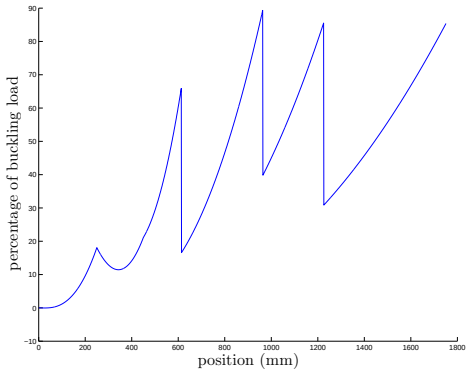

Figure G.3: Loads related to buckling in the wing.

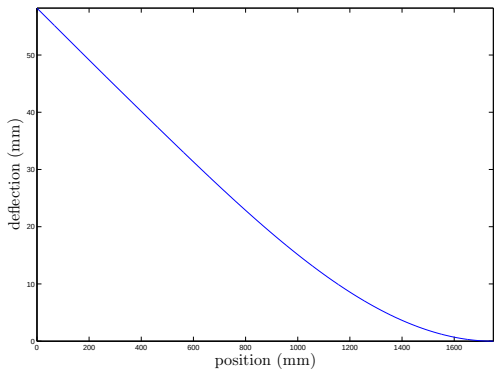

Figure G.4: Wing deflection, upwards positive.

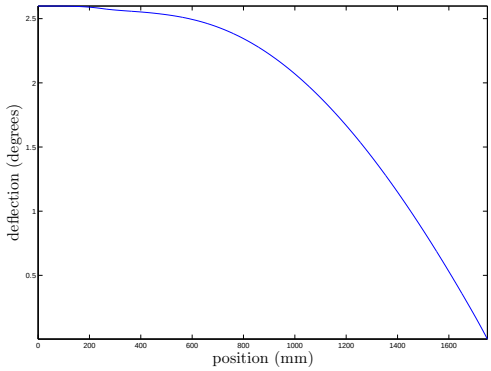

Figure G.5: Wing deflection angle, upwards positive.

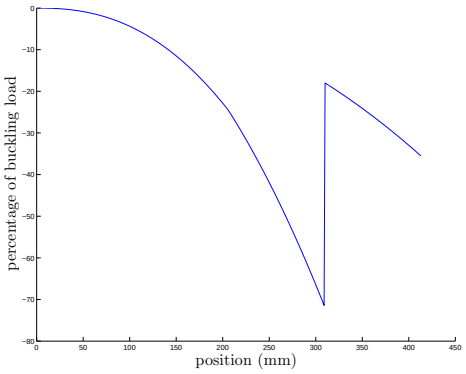

Figure G.6: Loads related to buckling in the horizontal tail.

Appendix H

Verification and validation

In this chapter the verification procedures results of the technical analysis are presented.

H.1 Aerodynamics

The calculations performed to determine the size of the wings are calculated by hand. Since these values are fairly easy to calculate and are based on simple equations that can be performed on the back of a coaster. Values for lift- and drag coefficients for the 2D-case, where the aerofoil is considered as an infinite wing, can be verified by experimental data from literature, like Abbott [34]. The real life values for lift- and drag coefficients are harder to verify, since they depend on the shape of the wing and no literature exactly meeting the same conditions as in the design exists. Also, since the calculation of lifting line theory involves an iterative process that can take between the 50 and 100 iterations, this is very time consuming to perform by hand. However, some simplified methods exist that can approximate the values for C_L and C_D. These methods can be checked by hand to correspond with simulated values. The results of this verification can be found in table H.1.

The validation of the aerodynamic properties is difficult since in real life this should be done with experiments and wind tunnel testing. The simulation method itself follows from different literature sources [30] [46] and can therefore be assumed to be a valid procedure.

Table H.1: Results of the verification procedures of the aerodynamics analysis.

Variable	Simulation result	Manual calculation result	Error
AR_{wing}	13.31	13.31	0%
$c_{\text{root}_{\text{wing}}}$	0.38	0.38	0%
$c_{\text{tip}_{\text{wing}}}$	0.15	0.15	0%
S_{wing}	0.92	0.92	0%
MAC_{wing}	0.28	0.28	0%
b_{tail}	0.82	0.82	0%
$c_{\text{root}_{\text{tail}}}$	0.20	0.20	0%
$c_{\text{tip}_{\text{tail}}}$	0.08	0.08	0%
S_{tail}	0.12	0.12	0%
MAC_{tail}	0.15	0.15	0%
C_{L_α}	5.344	6.303	18%

H.2 Performance

To verify the calculations and results of the performance analysis several variables have been calculated by hand and compared to the simulated values. In order to easily calculate these values manually, the input design parameters have been changed to easy integer values where possible. The input values for the verification procedures can be found in appendix section H.2. When the errors are within 5% it is verified that the simulation provides reasonable results.

Validating the performance analysis is done by looking at the expected slope and shape of resulting plots and figures. Assumptions must be validated with comparing them to existing solutions. The methods that are used can be validated by choosing a theoretic applicable approach.

The verification results that can be seen in table H.3. The results are based on the input variables found in table H.2.

The validation of the performance tool can not be done in much detail in this stage of the development stage. In order to validate some major design decisions and performance drivers the following steps must be taken:

- Perform wind tunnel tests to find actual lift and drag coefficients
- Test the chosen engine for actual engine efficiencies
- Test the propeller for different velocities and thrust settings for actual efficiencies
- Test the engine and propeller combination in a wind tunnel for actual power required and available plots
- Test fuel consumption of the engine in cruise thrust settings
- Test the compliance of the electrical system
- Run more advanced simulator tests to validate actual loading
- Perform a test flight with an actual model to simulate real-life performance

Table H.2: Input variables verification procedures performance analysis.

Input Variables	**Value**
Total mass	10
Wing surface area	1
Turn radius at cruise velocity	25
Cruise velocity	25
$C_{L_{\text{cruise}}}$	0.2563
$C_{D_{\text{cruise}}}$	0.015
$C_{L_{\text{max}}}$	1

Table H.3: Results of the verification procedures performance analysis.

Variable name	**Simulation result**	**Manual calculation result**	**Error**
V_{stall}	12.6556	12.6556	0%
N_{max}	4.7217	4.7217	0%
n_{cruise}	2.7376	2.7376	0%
ϕ_{cruise}	68.575	68.575	0%
$Pr_{\text{turn,cruise}}$	285.181	285.22	0%
Pr_{cruise}	143.5547	143.555	0%
RC_{max}	6.4577	6.4577	0%
$RC_{\gamma,\text{max}}$	16.541	16.541	0%
RC_{takeoff}	4.2705	4.27	0%
$S_{\text{tot,cruise}}$	720	720	0%
$C_{L_{\text{req,cruise}}}$	0.2563	0.2562	0%

H.3 Control & stability

The calculations performed to determine the controllability and stability of the aircraft are also calculated by hand to determine the correctness of the simulated values. Since most calculations are based on the

control and stability derivatives, these are calculated by hand to verify the simulation's outcome. Next to the derivatives, the centre of gravity and moments of inertia of the aircraft have a large influence on the calculations, therefore these are also calculated by hand. The results of this verification can be found in table H.4.

The validation of the control and stability derivatives is difficult since these can only be accurately determined based on in-flight data. However, the procedure applied to determine the aircraft's dynamic stability can be validated. Since the derivatives of the Cessna Citation 550 are known, the procedure applied can be validated. As a result one can say that the outcome of the dynamic stability analysis is accurate since the input values have been verified by hand-calculations, and the applied procedure has been validated with aircraft data.

Note: the verification of the derivatives has been performed on *a* configuration of the aircraft, therefore the values of the derivatives presented here can be different than the values given in table F.1. Also the derivatives that are neglected are not verified.

Table H.4: Results of the verification procedures of the control and stability analysis.

Variable	**Simulation result**	**Manual calculation result**	**Error**
C_{X_0}	0.0000	0.0000	0%
C_{Z_0}	-0.3453	-0.3453	0%
C_{X_u}	-0.0280	-0.0280	0%
C_{Z_u}	-0.8000	-0.8000	0%
C_{X_α}	-16.5180	-16.5180	0%
C_{Z_α}	-5.9515	-5.9515	0%
$C_{Z_{\dot{\alpha}}}$	0.0000	0.0000	0%
C_{m_α}	-2.1939	-2.1939	0%
$C_{m_{\dot{\alpha}}}$	0.000	0.000	0%
C_{Z_q}	-4.5666	-4.5666	0%
C_{m_q}	-17.9918	-17.9918	0%
$C_{Z_{\delta_e}}$	-0.5276	-0.5276	0%
$C_{m_{\delta_e}}$	-1.8898	-1.8898	0%
C_{Y_β}	-0.5751	-0.5751	0%
C_{l_β}	-0.0288	-0.0286	0%
C_{n_β}	0.0437	0.0437	0%
C_{l_p}	-0.3489	-0.3489	0%
C_{n_p}	-0.0262	-0.0262	0%
C_{Y_r}	0.4780	0.4780	0%
C_{l_r}	0.0232	0.0232	0%
C_{n_r}	-0.1421	-0.1421	0%
$C_{l_{\delta_a}}$	0.5791	0.5971	0%
$C_{n_{\delta_a}}$	0.0223	0.0223	0%
$C_{Y_{\delta_r}}$	0.8244	0.8244	0%
$C_{l_{\delta_r}}$	0.0399	0.0399	0%
$C_{n_{\delta_r}}$	-0.2450	-0.2450	0%

H.4 Structural analysis

The verification of the structural analysis is performed by simplifying the wing box. It is modelled such that it has an asymmetric cross-section, with four booms on each of the two vertical sections (webs). No extra booms have been placed along the flanges. The model can be found in figure H.1, where an axis system is also defined. The loads with which the verification has been performed have the following magnitude and direction, they all act on the tip of the structure:

- 10 N along the y-axis, at the centre of gravity thus resulting in a compressive load only.
- 50 N along the x-axis, at the centroid of the cross-section, causing shear, bending, and torque.
- 100 N along the z-axis, at 125 mm from the leading edge,causing shear, bending, and torque.
- 60 Nm over the y-axis, a pure torsion load.

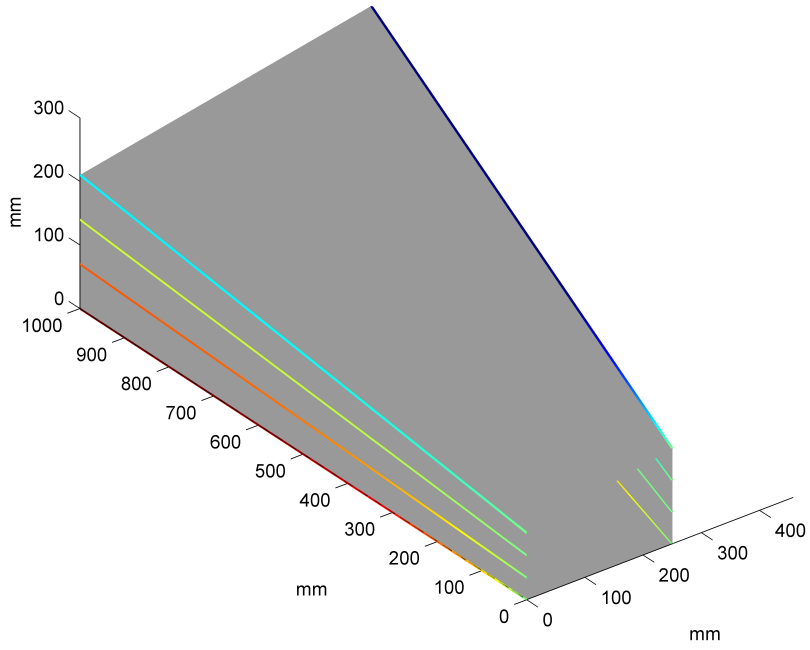

Figure H.1: Wing box used for verification of structural analysis.

In order to verify if the calculations done in MATLAB are correct, the calculations will be performed by hand on this simplified model. If the margin of error is within acceptable limits, the program will be considered as correct and verified. The results of the verification are listed in table H.5. Only the final results are listed since all intermediate steps are in line with the final results. Similarly, results for a part of the booms and skins have been omitted since they have similar results. Next to that, during programming, unit test have been performed. This was done by substituting values of '1', '0' or boundary values. This method quickly shows if equations provide the desired result.

The minute errors in boom stresses and boom areas can be related to rounding of values during the calculations. In the shear calculations there is an error which can not be ignored. This error is caused by the method used in the MATLAB script, which assumes that boom area does not vary over the length of a section. However, Because of the taper the boom area does change. Another method can be used which does not produce this error, but due to time constraints this has not been implemented. Due to the nature of the loads applied to the wing box, shear is not expected to be the failure mode. Nevertheless, a significant safety margin has to be used when considering shear.

To see if the script places the booms correctly on the aerofoil a visual inspection is performed. Figure H.2 shows that this is correct.

Validation of the calculations is possible in two general ways. The first being comparing the results to already proven concepts. However, this does require for such data to be available. In this case, the loads and shape

Table H.5: Results of the verification procedures of the structural analysis.

Variable	Simulation result	Manual calculation result	Error
stress in boom 6	-1.322 N/mm^2	-1.314 N/mm^2	1%
7	0.748 N/mm^2	0.754 N/mm^2	1%
8	2.809 N/mm^2	2.812 N/mm^2	0%
area of boom 6	588.5 mm^2	590.7 mm^2	0%
7	69.9 mm^2	69.9 mm^2	0%
8	70.0 mm^2	70.0 mm^2	0%
shear in skin 6	-2.47 N/mm	-2.72 N/mm	9%
7	-2.37 N/mm	-2.62 N/mm	9%
8	-2.06 N/mm	-2.30 N/mm	11%

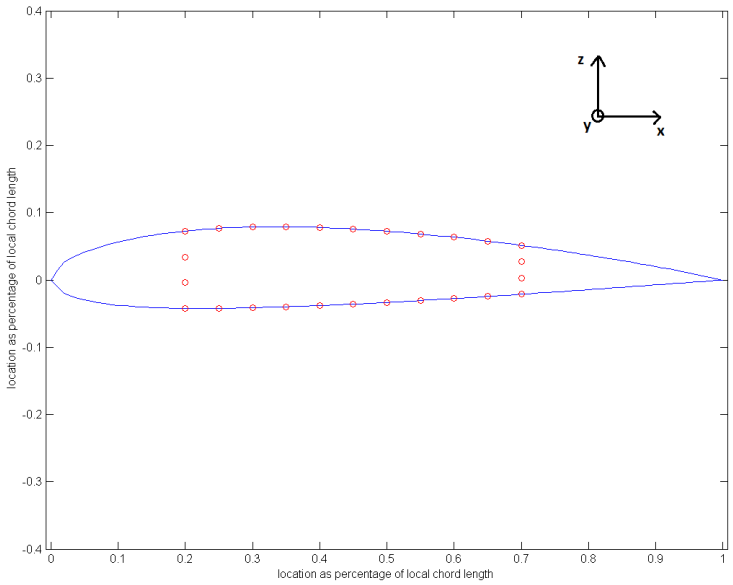

Figure H.2: Verification of placement of booms.

of the wing are rather specific and even though the structure is quite common, test results for fibreglass wing boxes of similar size could not be found. This is why it is advised to validate the design trough testing. Tests can be performed on a comparable (cheaper) fibreglass construction. By placing a few point loads on this structure, a close representation of the actual wing loads can be achieved. By checking the results in stresses and deformations, a comparison can be made with the results from MATLAB. If these results are in the same order of magnitude and lay within expectation, the program can be considered validated. Of course such tests need to be performed on the actual structure as well, to confirm the expected behaviour.

A second way of validating the analysis is to validate the equations used. Fortunately, the methodology applied is very common and is taught in various aerospace engineering books such as Megson [45].

Appendix I

Operations

In this section the calculations for the operations are elaborated. This includes the take-off and landing, the optimal routing and the collision avoidance system.

I.1 Take-off

The take-off sequence is also modelled in MATLAB. The spring constant of an elastic band is found to be 30 N/m. To determine the acceleration of the SkyDowser, the spring force is determined. By dividing the force by the mass of the SkyDowser, the acceleration is found. However, if the SkyDowser moves, the tension in the elastic bands decreases. A loop in MATLAB iterates this process over time, as long as the force is larger than zero. Some assumptions made are:

- There is no friction between the sledge and the rails.
- The rubber bands and the sledge are massless.
- The SkyDowser itself does not deliver thrust.
- There is no wind.

Even though friction, mass of the bands and sledge and wind are not taken into account, the analysis should be valid. This is due to the fact that the engine will also deliver thrust. Next to that, the launch is most effective with head wind and should not be performed with tail wind. The spring force is given by:

$$F_s = ks \tag{I.1}$$

Where k is the spring constant and s is the elongation of the bands. The spring constant used is 30 N/m, which is the spring constant for common rubber bands. This is chosen such that the bands can be tensioned by hand. To deliver the force required, the number of elastic bands used was adjusted. This resulted in 14 bands that are required, to accelerate the SkyDowser to 16 m/s over a distance of 3 metres at 15 deg angle from the ground. To determine the acceleration, the following relation was used:

$$a = \frac{F_s - W \sin 15}{m} \tag{I.2}$$

The maximum force during take-off was found to be 1.3 kN. By checking this force against buckling (I.3) and compression yield ($\frac{F}{A}$), an aluminium rail was designed. To be able to accelerate over 3 m and accommodate the SkyDowser in rest, the rails had to be 4.5 m in length. For guidance and strength, the rails is designed as a square beam of 30 cm by 10 cm, with a wall thickness of 1 mm. The rails can be split into four parts, to allow for transportation. Further explanation on the system is found in 4.3.1.

$$P_{crit} = \frac{\pi^2 EI}{L^2} \tag{I.3}$$

I.2 Landing

The first part of the calculation encompasses the deploying of the parachute and the trajectory of the SkyDowser after deployment. The second part will deal with the landing impact.

The landing is performed at 30 m altitude, assuming a dead wind velocity of 8 m/s. At higher wind speeds, the stability of the aircraft becomes an issue, which is why this is a valid speed for this analysis. Next to that the average wind speed in for example Somalia is known to be 4-6 m/s[47]. It is estimated that a descent

speed of 4 m/s is acceptable and will result in an impact that the SkyDowser can sustain. This will be verified in the impact analysis. To size the parachute, the following relation can be deduced from the drag formula:

$$A_p = \frac{2gm}{\rho c_{D_p} {V_i}^2} \tag{I.4}$$

Where the drag coefficient of the chosen parachute is found to be 2.2 [12]. The area found from this equation is: 4.7 m^2. Next, the drag and lift force caused by the parachute and SkyDowser are split into horizontal and vertical components. The lift and drag equations are used to determine their magnitude, assuming the parachute is deployed at 16 m/s airspeed. The results at this velocity form the initial conditions of this problem. Since the mass is known, the acceleration in both horizontal and vertical direction can be found from the sum of forces in that direction. Multiplied by the time, the speed at any given moment can be calculated, if the equations are performed for a given time span. Increments of 0.01 seconds were used to get an accurate representation.
This data and the equations were scripted in MATLAB. A while loop was used that calculated all the above, until the altitude reached zero metres. All that is left is to determine the maximum force of the parachute. This is done by taken the maximum value calculated for the acceleration during the descent and multiplying it with the mass of the system. This force equals 1.8 kN. It can easily be carried by aluminium beams.

The second part of the analysis deals with the impact force. To dampen the impact, a small strain rubber cone is used. The Young's modulus for this sort of material is found to be $0.01 * 10^9$ Pa [48]. It is assumed the ground is infinitely stiff and strong. Therefore the calculated force is the maximum force the SkyDowser will have to endure. The length of the cone is fixed at 15 cm, for practical reasons. It has a bent elliptical shape, which will make sure a large surface area hits the ground on impact. The cone will be not be solid. For this analysis however, the cone is simplified to a solid cylinder, with a radius of half that of the actual cone. It is known that the SkyDowser will slow down from 4 m/s to 0 m/s ($dV = 4$ m/s). Hence, the average speed during impact is 2 m/s. The deformation of the rubber cone is assumed to be linear.
In order to determine the force on the fibreglass fuselage, the deformation of the rubber cone (s_c) must be calculated first, according to:

$$s_c = \frac{F_c L_c}{E_r A_c} \tag{I.5}$$

Where F_c is the force required to dissipate the momentum (F_i) plus the gravity force (F_g), L_c is the length of the cone, A_c is the area of the simplified cone and E_r is the modulus of elasticity of rubber. Here, F_i can be written as:

$$F_i = \frac{mdV}{dt} \tag{I.6}$$

Substituting this in equation I.5 gives:

$$s_c = \frac{mdV L_c}{E_r A_c dt} + \frac{mgL_c}{E_r A_c} \tag{I.7}$$

If we set $dt = s_c/V$, with V being the average velocity of 2 m/s, we can solve the equation for s_c. Substituting s_c back into equation I.5, the total force F_c is found. This is the force that the fuselage will have to endure, therefore it is checked against the critical buckling load and maximum compressive stress of the fibreglass tube. The maximum impact force on the fuselage equals 5200 N. This means 23% of the critical buckling load is reached and only 6% of the compression yield. Therefore landing with the parachute is of no risk to the SkyDowser.

I.3 Optimal routing

To determine the optimal routing, a couple of assumptions have been made:

- The operator can drive the car up to 35 km/h.
- The car can never be closer than 100 m from the SkyDowser, to avoid distortions in the measurements.
- The longer the lanes are, the more efficient SkyDowser flies.
- Break time should be more than 3 minutes, in order to make the break worth while.
- The SkyDowser flies with a constant velocity of 25 m/s.
- The SkyDowser may never be further away than 500 m from the operator.

A simulation has been performed according to these assumptions. The lateral distance between the vehicle and the operator (as described in section 8.4) was varied between 100 m and 400 m. The relations with the break time of the operator and the lane length have been displayed in figure I.1

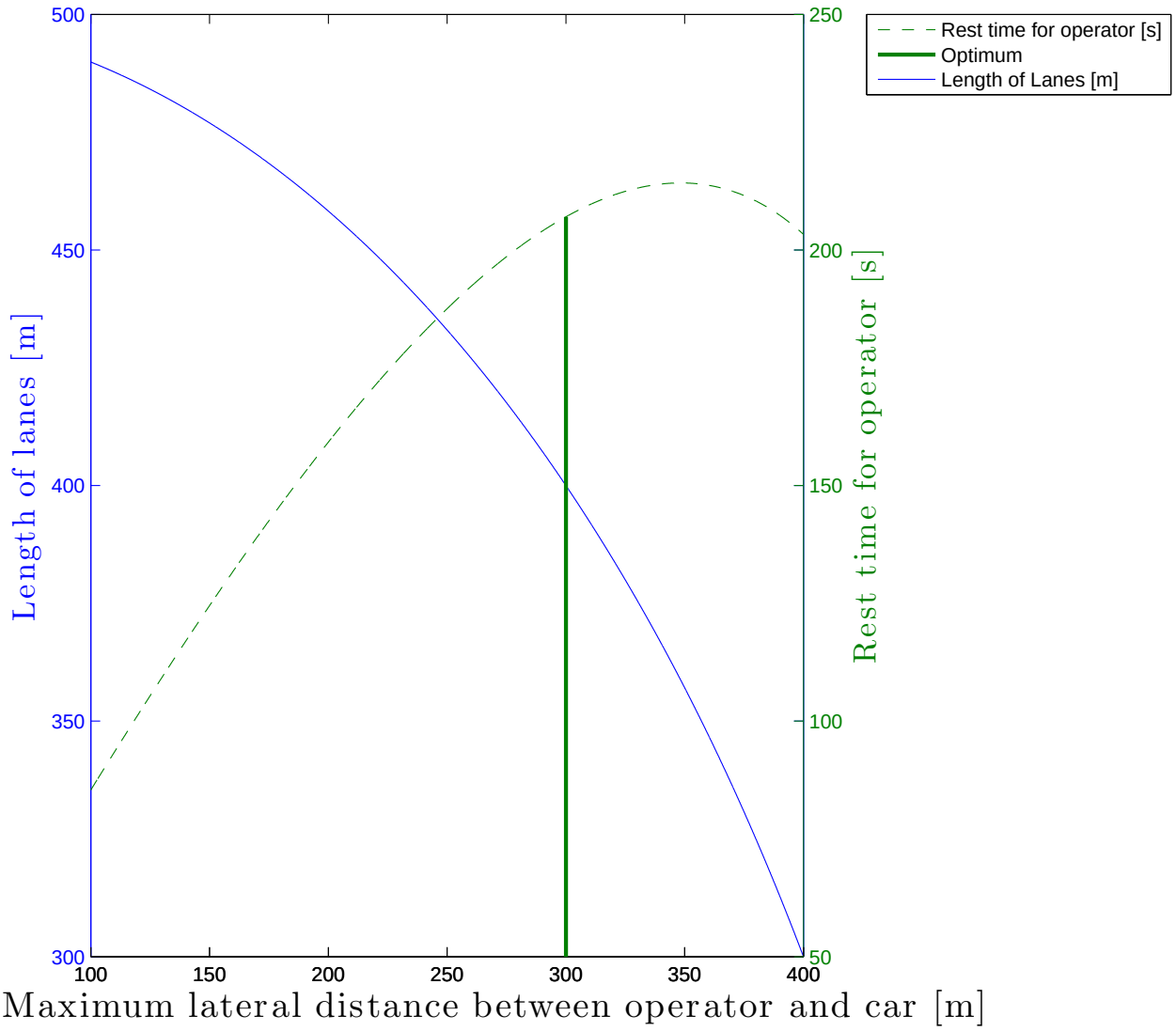

Figure I.1: Relation between lateral distance to the vehicle, the break time and lane length.

The optimal route has been chosen to be the bold line in the plot. This corresponds to a lane length of $2 \cdot 400$ m $= 800$ m and a break time of 207 seconds. This means that the operator has 207 seconds of rest before he/she needs to drive for 30 seconds. It is a hectic schedule, but is unavoidable due to the 500 m line of sight requirement.

I.4 Collision avoidance

Stereoscopic cameras have been placed in the wingtips as to benefit from the maximum distance in between them. Three particular specifications are important when picking a camera for collision avoidance; the resolution, the view angle and the frame rate.

I.4.1 Resolution

The resolution is an important characteristic, because it relates the amount of pixels of an object with the distance from the lens. Too low resolution would hinder the camera in seeing objects that are smaller than the view angle per pixel, as illustrated in figure I.2.

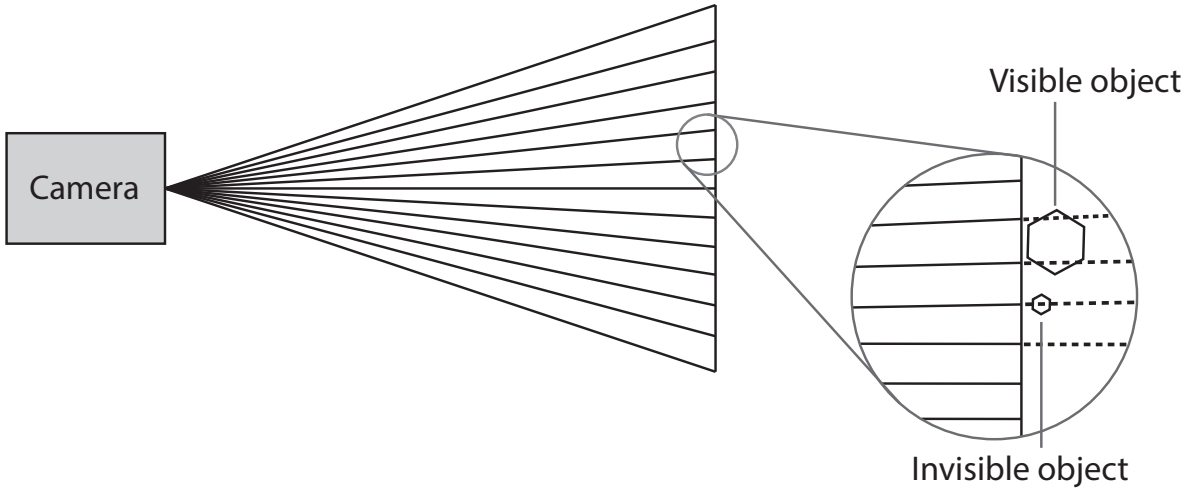

Figure I.2: Resolution of a sensor. Objects smaller than a pixel will be invisible on the picture.

Since too high resolution would require a fast and power consuming processor, a camera with a fairly low resolution has been chosen: the Sunivision AP-IR123BW. This camera houses a Sony sensor with 628 by 582 pixels. The chosen sensor, together with a 12 degree view angle, produces the relation between object distance and pixel size that is displayed in figure I.3. Using this particular sensor and lens, objects of 5 cm can be distinguished at 150 m.

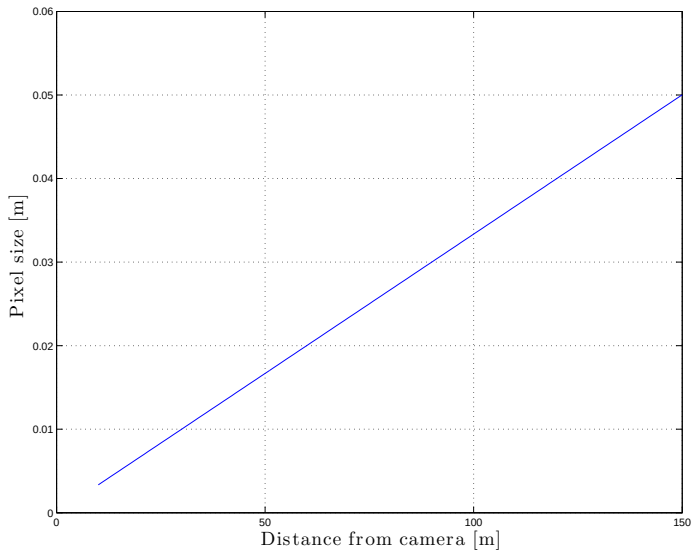

Figure I.3: The relation between the pixel size and distance from the sensor. Any object under the line is not seen by the camera.

I.4.2 View angle and 3D effects

The view angle defines the area which is mapped on the sensor. A wider lens corresponds to a wider area, but less detail. Since the function of this system is to detect object far away, a lens with a small view angle has been chosen. The 25 mm lens that comes with the Sunivision camera has a view angle of 12 degrees. From this view angle and the span of the cameras, the minimum distance, where objects can be seen in 3D, can be determined. This distance is also visualised in figure 8.12. For the current setup this distance (in metre) is:

$$d_{\min} = \frac{b}{2\tan\frac{\psi}{2}} \tag{I.8}$$

$$= \frac{3.5}{2\cdot\tan 6} = 16.7, \tag{I.9}$$

which is acceptable considering the cruise speed of 25 m/s. In this equation ψ is the view angle.

In figure I.4 an example is given of an obstacle at three different distances. This distance is estimated based on the pixel offset d between the position on the image of a camera (either left or right), and the centre position, as indicated in figure I.4. The maximum offset is half of the horizontal resolution of 628 pixels and the minimum is 1. If no offset exists, the system assumes the obstacle is infinitely far away.

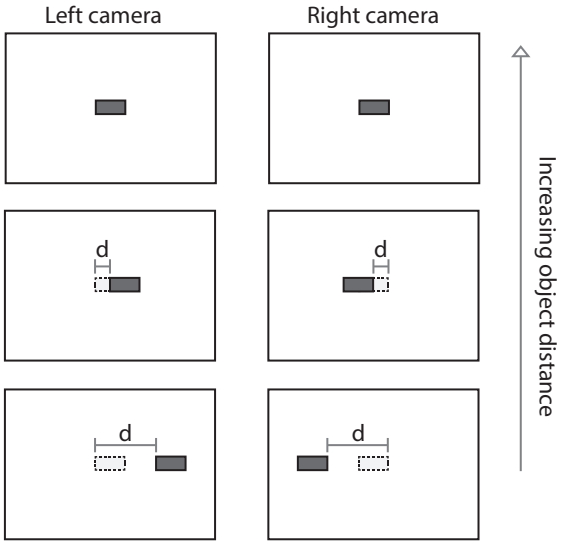

Figure I.4: Visualisation of an obstacle seen by the left and right camera. The further the object is from the centre line, the closer it is.

In figure I.5 the relation between obstacle distance and pixel offset is given. The estimation for the error (dashed lines) is based on the human depth resolution as explained in [49]. The corresponding equation is equation I.10, where r is the distance of the obstacle, ξ is the angular resolution and b is the distance between the cameras.

$$\epsilon = \frac{r^2\xi}{b} \tag{I.10}$$

In theory, the system should be able to determine an obstacle, which covers only one pixel. This is however, heavily dependent on the algorithm and is considered beyond the scope of this project. It is recommended to research this further in the future. For now it is assumed that at a distance of 150 m an object larger than 1 m poses a threat and needs to be detected at a 150 m distance. This is no problem for this system. Smaller objects are harder to see, but are also more easily evaded.

I.4.3 Frame rate

The desired frame rate is mostly dependent on the velocity and processing power. For a cruise velocity of 25 m/s, a frame rate of 5 frames per second would correspond to a photo each 5 meters. Considering the

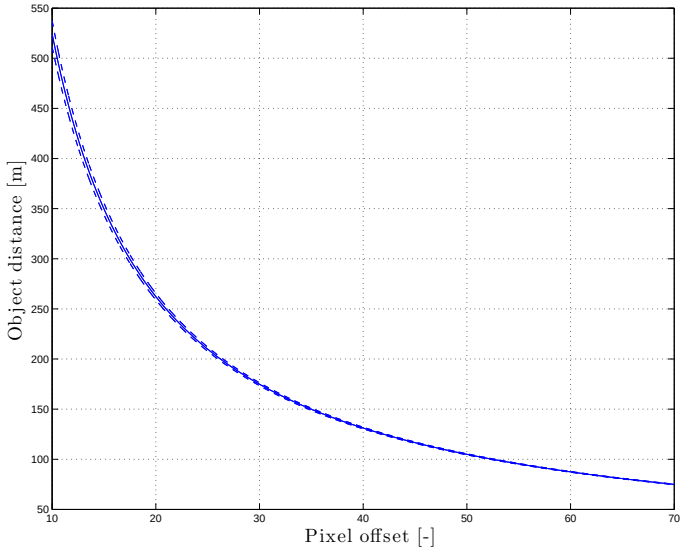

Figure I.5: Relation between obstacle distance and pixel offset, including estimated error range. Dashed lines represent the error of the estimation.

range at which the system can currently detect obstacles (a couple of hundred metres), this is regarded as acceptable.

Appendix J

Masses, centre of gravity and neutral points

A detailed overview of all the masses and centre of gravity location in the Skydowser can be found in table J.1.

Table J.1: Mass overview of the SkyDowser and centre of gravity location.

Component	**Mass [kg]**	**CoG-x position [m]**
Fuselage	1.53	1.15
Horizontal tail	0.41	1.90
Electrical power generator	0.04	0.17
Power level regulator/control	0.05	0.89
Power distribution	0.40	0.87
Wings	3.73	0.87
Propulsion generator	1.08	0.10
Rudder	0.10	1.90
Take-off system	0.10	1.90
Navigation & Guidance	0.15	0.89
Coil (1)	0.50	0.87
Coil (2)	1.00	0.87
Data storage	0.10	0.89
Battery	0.15	0.89
Fuel storage	0.10	0.87
Fuel	1.30	0.87
Nose-cone	0.20	2.20
Parachute	1.00	0.50
Vertical tail	0.22	1.90
Aileron left	0.10	0.94
Aileron right	0.10	0.94
Altimeter	0.18	0.17
Total mass	12.54	

The different centres of gravity together with their neutral points are listed in table J.2. Definitions are displayed in figure J.1.

Table J.2: Centres of gravity and neutral points.

Configuration	CoG x_{cg}	Neutral point stick fixed $x_{np_{fixed}}$	Neutral point stick free $x_{np_{free}}$
Full fuel tank	0.879	0.997	0.977
Empty fuel tank	0.881	0.998	0.978

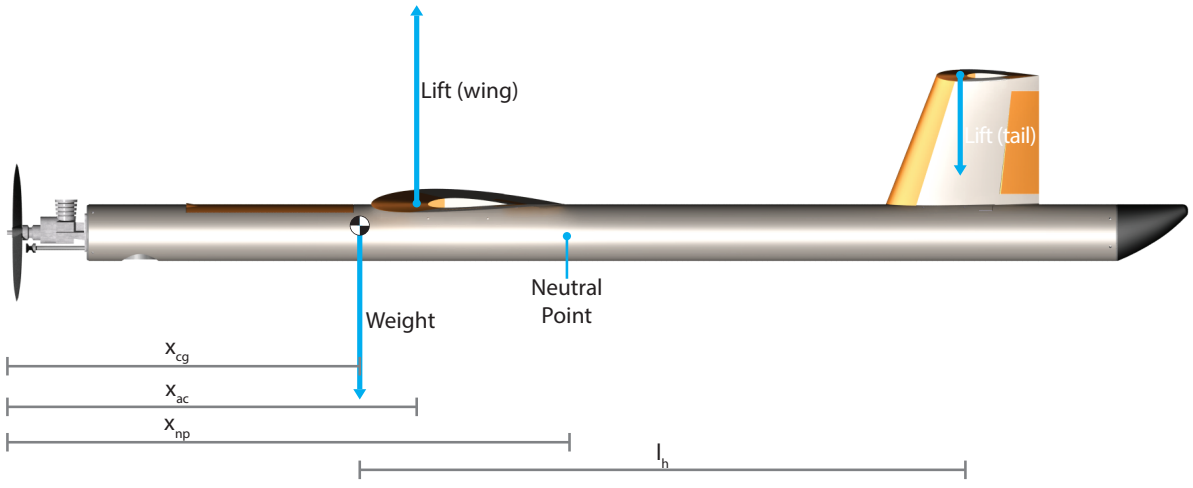

Figure J.1: Free Body Diagram of the aircraft in cruise. Forces are not to scale.

Appendix K

Electric components

In figure K.1 one can see the electrical components that are installed on the UAV. The power, mass and cost of each component can also be found. For most components an advised product has been found. In that case the power, costs and masses are accurate. In the case of some components a suitable product has not yet been found and these values are based on educated guesses or comparable equipment. Notice that for the power of the coils the average power over one second is estimated based on 6 times 4 measurements every second. Also the required power for the servos is given in the most extreme case in which the servos must be used all the time at maximum torque and velocity.

Component	*Name*	*Power total [W]*	*Power percentage [%]*	*Mass [g]*	*Price [Euro]*
Camera (2x)	Sunivision AP-IR123BW	3	10%	100	€ 100.00
Camera processor	-	8	26%	30	€ 180.00
Laser altimeter	SF03/H	0.075	2%	185	€ 513.84
Coils	FEM measurement system	4	13%	1500	€ 750.00
Measurement electronics	Compatible processor	0.15	0%	100	€ 50.00
GPS	Venus GPS with SMA Connector	0.297	1%	0.5	€ 29.33
GPS antenna	Antenna GPS Embedded SMA	0.0396	1%	18	€ 7.02
Fuel pump	-	0.1	0%	20	€ 20.00
Data link	Xbee-PRO 900	0.693	2%	3	€ 28.63
Servo's (6x)	Servo - Hitec HS-35HD (Ultra Nano Size)	7.2	24%	27	€ 16.49
Pitot tube airspeed sensor	Airspeed Kit with MPXV7002DP	0.1	0%	10	€ 29.33
Auto pilot (incl. Gyro, Magnetometer, Accelerometer)	APM 2.6 Set (With Arduino Mega)	2.685	9%	50	€ 117.44
Temperature sensors (3x)	TMP36 - Analog Temperature sensor - TMP36	0.000495	0%	0.5	€ 3.49
Engine ignition plugs	Saito FG-30B Gasoline Engine	5	16%		
Generator	A10-9L Hacker Brushless 75W 1700k/V Out Runner Motor	-	-	20	€ 29.36
Battery pack	Tenergy Li-Ion 18650 11.1V 2200mAh Rechargeable Battery Pack w/ PCB Protection	-	-	125	€ 23.63
Total		*32.02*	*100%*	*2189*	*€ 1,898.55*

Figure K.1: List of power, mass and cost budget for electrical components.

Appendix L

Risk analysis & mitigation

Table L.1: All identified risks and the corresponding risk mitigation.

Risk	Type of failure	Mitigation
Parachute failure		
Parachute gets stuck	Wind takes parachute into the tail	Parachute will be deployed when streamlines will flow over the T-tail, to take pilot chute over the tail.
Parachute does not unfold properly	Wrongly folded	Folding must be clearly described in manual and being followed at all cost. Proper training is necessary.
Hatches do not open or open too late	Servo failure	Servos are extensively tested. If servo failure does occur, transfer risk to either insurance or manufacturer of servos.
	Wind does not open hatches	Mission is designed to ensure velocity is high enough, this is tested extensively.
Hatches open too early	Servo failure	Structure can handle high loads due to parachute deployment at cruise speed.
	Wrong input signal	No safety risk.
Structural damage		
Part of wing takes impact on landing	Body rotates during landing.	Wing structure can handle impacts. Skin needs to be reinforced at wing tips (recommendation).
Mid-air collision	Bird strike	Trailing edge of wing is load bearing and will decrease impact on structure. In case of emergency parachute is deployed.
	CAS failure	Operator gets a warning from system status check and can take over by remote control. In case of emergency parachute can be deployed.
Any structural component fails during flight	Too high load factor	SkyDowser is designed on load factor 4.7. Operator must follow the manual describing the limits of the SkyDowser.
	Fatigue	SkyDowser will be tested in advance. Regular inspection and maintenance will prevent fatigue failure.
Engine failure		
Mechanical problems	Improper maintenance	Maintenance procedures will be described in manual and consist of cleaning of the engine after every flight. Engine is very accessible. In case of emergency parachute can be deployed.

Engine overheats	Too much power to be delivered	Engine does not overheat in normal operating conditions. System status check will give warning to operator in case of possible engine overheating. In case of emergency parachute can be deployed.
	Insignificant air cooling	Engine is mounted on the outside for constant air cooling. In case of emergency parachute can be deployed.
Fuel shortage	Fuel leak	System status check constantly checks fuel level and gives warning for low fuel level. UAV can glide for about 25 seconds and make semi-controlled belly landing. In case of emergency parachute can be deployed.
	Wrong flight planning	System status check constantly checks fuel level and gives warning for low fuel level. UAV can glide for about 25 seconds and make semi-controlled belly landing. In case of emergency parachute can be deployed.
Generator failure		
Mechanical problems	Improper maintenance	Battery can power electrical systems for 30 minutes. Maintenance procedures will be described in manual. In case of emergency parachute can be deployed.
Engine fails		See "Engine failure"
Battery failure		
Battery overheats	High temperatures inside UAV	A maximum operating temperature is set, this is checked before launch.
	High peak loads	A maximum operating temperature is set, this is checked before launch.
Battery too cold	Cold outside temperatures	Minimum operating temperature is set, this is checked before launch.
Leakage	Improper maintenance	Regular maintenance is performed; furthermore voltage/current of the battery is monitored throughout the flight. In case of severe/dangerous deviations, the SkyDowser will initiate a landing.
	Structural damage	Regular maintenance is performed; furthermore voltage/current of the battery is monitored throughout the flight. In case of severe/dangerous deviations, the SkyDowser will initiate a landing.
Measurement failure		
Power failure		See battery failure and generator failure
Computer failure		See On-board computer failure
Autopilot/on-board computer failure		
Software bugs	Faulty software	Extensive testing before flying and updating software regularly.
Hardware error	Wear	Maintenance procedures will be described in manual. System status check checks for errors. In case of total failure of flight computer UAV will crash and must be insured for these cases.
Altimeter failure		

No output	Dirt	The altitude can also be approximated from the GPS data and CAS. When dangerous deviations occur, landing is initiated.
Wrong output		The altitude can also be approximated from the GPS data and CAS. When dangerous deviations occur, landing is initiated.
Hostility from locals		
Lack of acceptance	Hostile appearance	The SkyDowser is painted in non-military colors to avoid this. This risk is transferred to the owner of the specific SkyDowser.
Dangerous area	War zone	It is up to the operator/local owner of the SkyDowser whether or not it is wise to deploy the SkyDowser. This risk is transferred to the owner of the specific SkyDowser.
Gyroscope failure		
No/wrong output	Internal errors	Use accelerometers and GPS to estimate position/attitude. Notify operator, and deploy parachute if attitude determination is not possible anymore.
Pitot-tube failure		
No output	Dirt	Pitot tubes are cleaned before every flight. Multiple pitot tubes are used; as redundancy.
	Internal errors	Pitot tubes are cleaned before every flight. Multiple pitot tubes are used; as redundancy.
Static port failure		
No/wrong output	Dirt	Static tubes are cleaned before every flight. Multiple pitot tubes are used; as redundancy.
	Internal errors	Multiple static tubes are used; as redundancy. Use data of other pitot tube(s).
GPS failure		
No output	Internal errors	Notify operator; location determination can be checked before launch.
	Weak coverage	Notify operator; use combination of attitude and altitude control (trajectory calculations). In worst case scenario, the operator can intervene.
Wrong output	Difficult landscape (multipath)	With the use of the CAS, one can check if the provided location is approximately correct. Also, since the mission target is to provide a preliminary scan, an error of 10 meters is not an issue. Notify operator; use combination of attitude and altitude control (trajectory calculations). In worst case scenario, the operator can intervene.
Large error		With the use of the CAS, one can check if the provided location is approximately correct. Also, since the mission target is to provide a preliminary scan, an error of 10 meters is not an issue. Notify operator; use combination of attitude and altitude control (trajectory calculations). In worst case scenario, the operator can intervene.
Camera failure		

No output	Dirt	Regular maintenance is performed. Also, manual collision avoidance by the operator is possible.
	Internal errors	A complete system check is performed before each launch. Also, manual collision avoidance by the operator is possible.
Wrong interpretation of data	Incorrect software	Perform complete software test before implementation. Worst case scenario, manual collision avoidance is performed by the operator.
Human error		
Mistake in operation	Not following the manual and operational procedures	The operator is properly trained, that sould avoid this. If not, this risk is transferred to the owner of the specific SkyDowser.
Gets hurt		The operator is properly trained, that sould avoid this. If not, this risk is transferred to the owner of the specific SkyDowser.
Wrong assembly		The operator is properly trained, that sould avoid this. Also, regular maintenance is performed. This risk is therefore completely transferred to the owner, since he/she is responsible for the correct assembly as described in the manual.
Damages UAV parts	Incautious behaviour	The operator is properly trained, that sould avoid this. If not, this risk is transferred to the owner of the specific SkyDowser.
Launch failure		
Too low exit velocity	Insufficient number of elastic bands	Before launch, the number of elastic bands is checked. Also, the designed take-off velocity is 125% of stall speed as a safety marging. The tension in the launch system can be easily checked before launch.
	Failure of elastic bands	Regular maintenance of the launch system (including scheduled replacement of the elastic bands) prevents this.
Crash into object after take-off	Insufficient take off site	The collision avoidance system is used to check the surrounding in advance, before take-off. If no object is detected when the UAV is located on the catapult, the SkyDowser is safe to take-off. In worst case scenario, the operator/owner is responsible for failure.
Damage to catapult	Too high forces on structure	The catapult is checked regularly and the catapult should be assembled using the directions from the manual. In worst case scenario, the operator/owner is responsible for failure.
	Incorrect assembly	The catapult should be assembled using the directions from the manual. In worst case scenario, the operator/owner is responsible for failure.
Control surfaces failure		
Control surfaces stuck	Servos fail	See 'servos failure'.
	Dirt	Before launch, the vehicle is cleaned and checked. In worst case scenario, the operator can intervene and a landing can be initiated.
Servos failure		

No output	Internal error	The used servos have been tested extensively. Before launch, the vehicle is checked and servos are tested once more. In case of malfunctioning, the operator is notified. In worst case scenario, the operator can intervene and a landing can be initiated.
Wrong output	Wrong input from on-board computer	See 'software failure'.
Downlink connection failure		
No connection	Out of range	The autopilot ensures the SkyDowser is within 500 meters distance of the operator. In worst case scenario, the vehicle goes into a safe mode, and initiates a landing sequence.
	Insufficient strength of signal	The autopilot ensures the SkyDowser is within 500 meters distance of the operator. In worst case scenario, the vehicle goes into a safe mode, and initiates a landing sequence.
	Component failure	The used communication link has been tested extensively. Before launch, the vehicle is checked and the communication link is tested once more. In case of malfunctioning, the operator is notified. In worst case scenario, the operator can intervene and a landing can be initiated.
Storage failure		
Not enough storage		Available storage is checked before launch.
Failure of electronics	Wear	See 'component failure', system is checked extensively before use.
Failure of on-board computer		See On-board computer failure

Appendix M

Cost analysis

M.1 Cost breakdown structure

In figure M.1 and M.2 the cost breakdown structure of the SkyDowser project is presented. The project consists of 100 UAVs that are in operation simultaneously. The duration of the project is five years, which is equal to the expected lifetime of a single UAV. In one year the SkyDowser is expected to fly a total of 180 days (almost 50% of the time). This takes into account weekends, holidays and downtime due to bad weather conditions. This project case study is based on operating in the horn of Africa. With current operations that are being set up in for instance Somalia [50], this is an interesting region to investigate the presence of groundwater. The data represented in the cost breakdown structures is based on the numbers presented in the cost table that can be seen in figures M.3 and M.3.

M.2 Cost estimation

In figures M.3 and M.4 the entire cost estimation can be found. Due to its size, the cost estimation is split into two parts. All the costs that are related to the operations, manufacturing and development of the SkyDowser is taken into account. The different large costs are separated into smaller sub-costs. For every cost a worst and best case scenario is presented. Because some costs depend on, for instance, hourly rates for labour, some variables require elaboration. Some assumptions and clarifications regarding the cost estimation:

- The operator salary for this project case study is estimated at €10 per hour.
- Approximately €10,000 is budgeted for the purchase of a jeep and its maintenance to accompany a SkyDowser throughout the entire mission.
- Petrol fuel cost is estimated by using current maximum and minimum prices of petrol in the horn of Africa [51].
- The operator needs to travel a maximum of 300 km per day with the payload to different measurement locations.
- The fuel consumption of the jeep is estimated at 1:7.
- Pilot license cost estimated from EuroUSC [52]
- Maintenance is performed locally with a salary of €10 per hour.
- The big yearly overhaul is performed by an expert that is paid €60 per hour
- All component prices are determined by choosing compatible off the shelf solutions as proposed in section K.
- The payload price is assumed to be fixed at €800.
- The engine price is based on the proposed solution as described in appendix E.
- Material cost are based on the raw material cost of fibreglass taking into account 50% waste. Other materials are budgeted since not an accurate estimation could have been made at this stage.
- Manufacturing cost is done at an hourly rate of between €50 and €60 per hour.
- Mould costs include the price of two wing molds and one fuselage mould.
- The development is estimated to be done with ten engineers working simultaneously at an hourly rate of €75 per hour.
- The wind tunnel testing is estimated at €50,000 per test day
- Certification cost is estimated with reference values from EuroUSC [52].

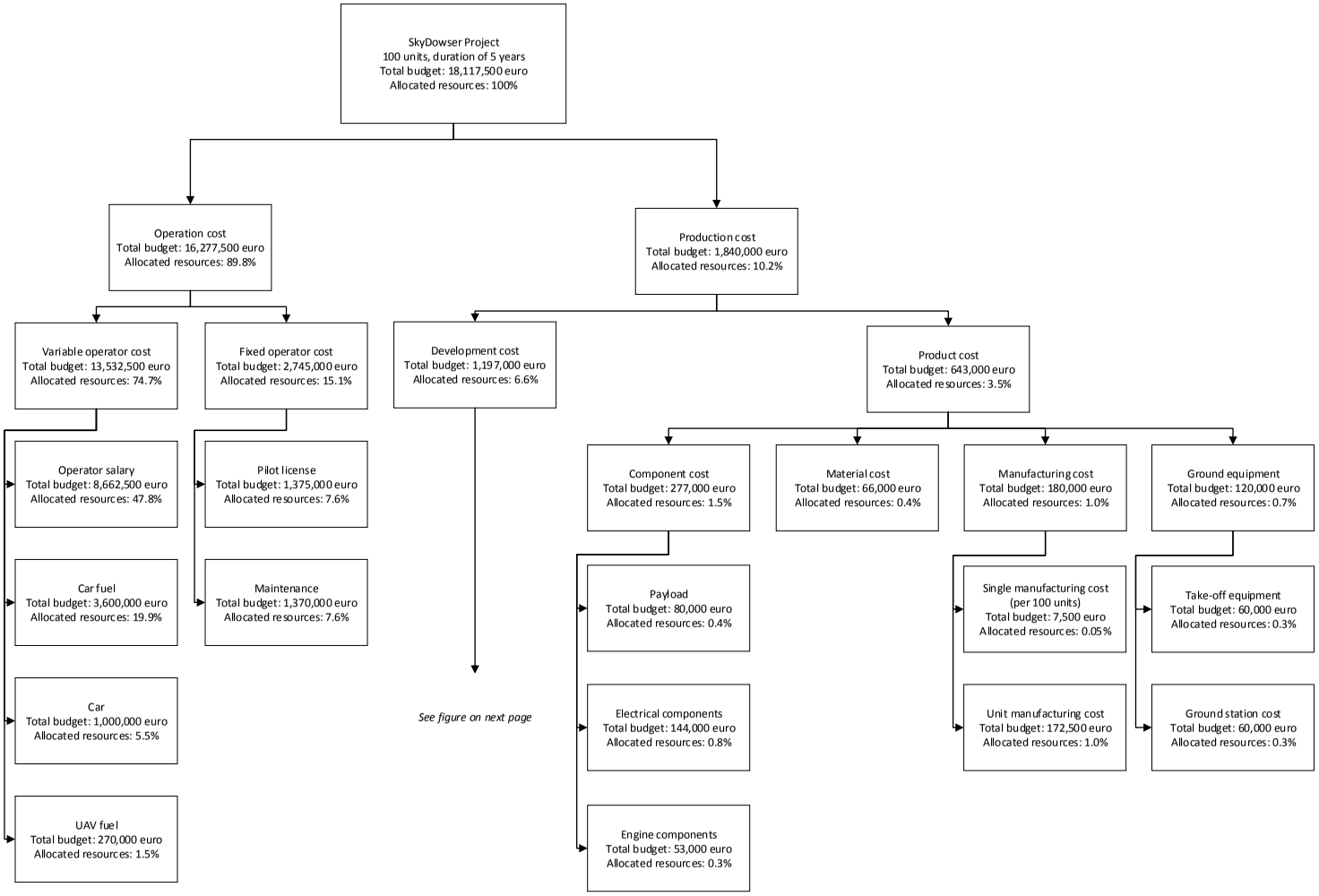

Figure M.1: Cost breakdown structure part 1.

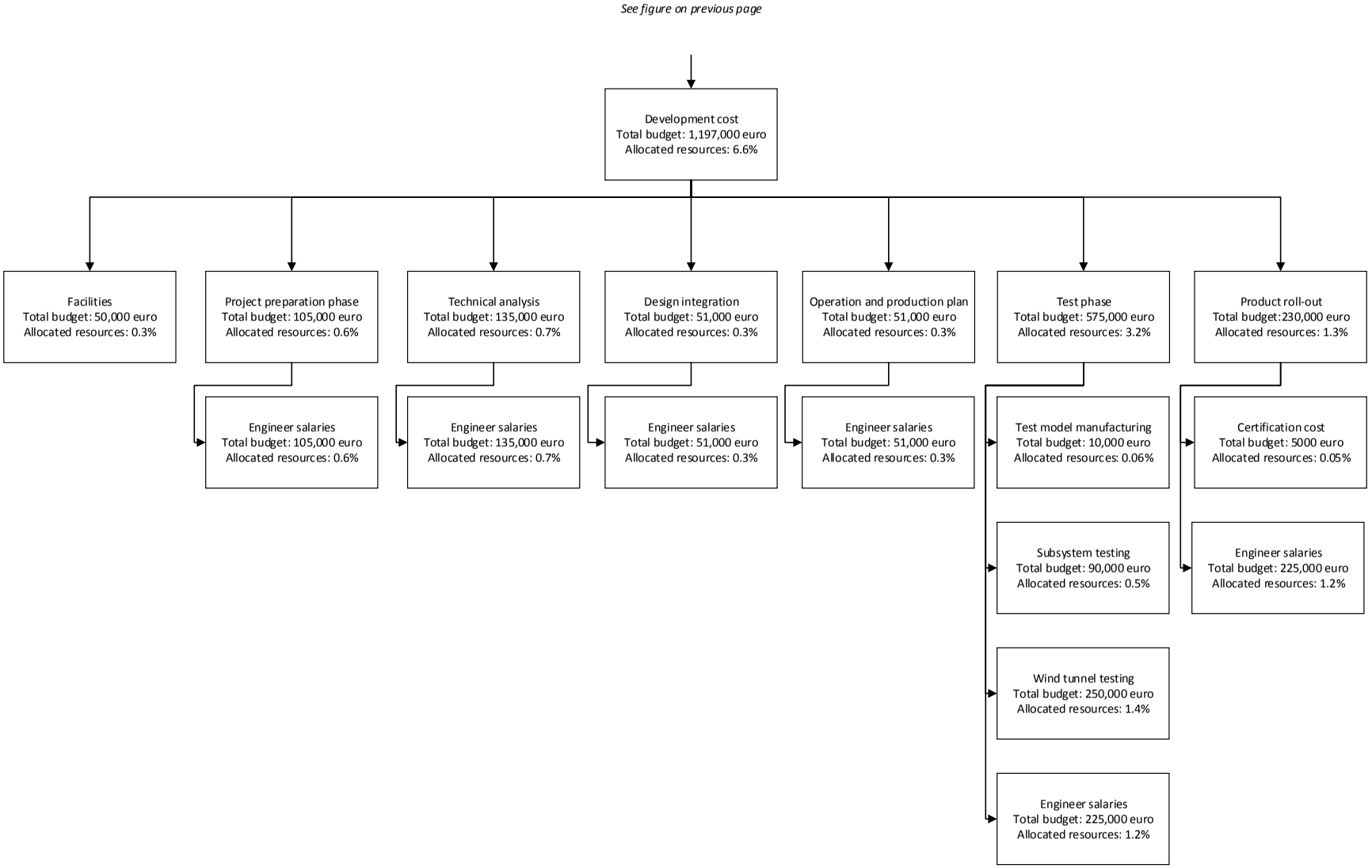

Figure M.2: Cost breakdown structure part 2.

TOTAL COSTS													
- Variable operational cost (per day)		**Worst case**			**Best case**			**Average**			**Uncertainty**		
+ Man hours per day	hours, euro	10.80	€	108.0	8.45	€	84.5	9.63	€	96.25	24%		
Startup		1.20	€	12.0	0.60	€	6.0	0.90	€	9.00	67%		
Set up vehicle		0.50	€	5.0	0.25	€	2.5	0.38	€	3.75	67%		
Set up supportive equipment		0.30	€	3.0	0.10	€	1.0	0.20	€	2.00	100%		
Fuel Vehicle		0.10	€	1.0	0.05	€	0.5	0.08	€	0.75	67%		
Set Autopilot		0.30	€	3.0	0.20	€	2.0	0.25	€	2.50	40%		
Cruise		8.00	€	80.0	7.00	€	70.0	7.50	€	75.00	13%		
Cruise time		8.00	€	80.0	7.00	€	70.0	7.50	€	75.00	13%		
Landing		1.60	€	16.0	0.85	€	8.5	1.23	€	12.25	61%		
Read data		0.50	€	5.0	0.25	€	2.5	0.38	€	3.75	67%		
Inspect for damage		0.30	€	3.0	0.20	€	2.0	0.25	€	2.50	40%		
Store vehicle		0.30	€	3.0	0.20	€	2.0	0.25	€	2.50	40%		
Store supportive equipment		0.50	€	5.0	0.20	€	2.0	0.35	€	3.50	86%		
+ Supportive Equipment (for single UAV)	€	€	1,400		€	1,000		€	1,200		33%		
Take-off		€	700		€	500		€	600		33%		
Ground station		€	700		€	500		€	600		33%		
+ Other supportive equipment (per UAV)		€	11,000		€	9,000		€	10,000		20%		
Car		€	11,000		€	9,000		€	10,000		20%		
+ Supportive Equipment (per day)	€	€	60		€	26		€	43		79%		
Electrical Energy Generation		€	1		€	0		€	0.5		196%		
Fuel car		€	55		€	25		€	40.0		75%		
Fuel UAV		€	4		€	1		€	2.5		120%		
- Operational cost (Per unit per year)													
+ Fixed operational cost		€	3,000		€	2,500		€	2,750		18%		
Pilot license (per year)		€	3,000		€	2,500		€	2,750		18%		
+ Maintenance (per unit per year)	€	€	3,500		€	1,985		€	2,743		55%		
Yearly Overhaul		€	1,100		€	900			1000		20%		
Regular check interval (x per year)			10			7			9		35%		
Man hours (per regular check)			4			3			4		29%		
Material (per regular check)		€	200		€	125		€	163		46%		
- Production cost													
+ Electric Components	€	€	1,682		€	1,194		€	1,438		34%		
Camera (2x)		€	125		€	75		€	100		50%		
Camera processor		€	300		€	150		€	225		67%		
Laser altimeter		€	550		€	450		€	500		20%		
GPS		€	35		€	25		€	30		33%		
GPS antenna		€	10		€	5		€	8		67%		
Fuel pump		€	25		€	15		€	20		50%		
Data link		€	33		€	25		€	29		26%		
Servo's (6x)		€	120		€	90		€	105		29%		
Pitot tube airspeed sensor		€	35		€	25		€	30		33%		
Auto pilot including Gyro, Magnetometer, Accelerometer		€	125		€	110		€	118		13%		
Temperature sensors (3x)		€	12		€	9		€	11		29%		
Battery		€	27		€	20		€	24		30%		
Parachute		€	225		€	175		€	200		25%		
Wiring		€	60		€	20		€	40		100%		

Figure M.3: First part of the cost estimation.

		Worst case	Best case	Average	Uncertainty
+ Payload		€ 800	€ 800	€ 800	0%
+ Engines		€ 585	€ 475	€ 530	21%
Generator		€ 35	€ 25	€ 30	33%
Engine		€ 550	€ 450	€ 500	20%
+ Materials		€ 720	€ 600	€ 660	18%
Fuel tank		€ 45	€ 30	€ 38	40%
Wings		€ 50	€ 30	€ 40	50%
Fuselage		€ 40	€ 25	€ 33	46%
Inserts, skrews, bolts		€ 350	€ 200	€ 275	55%
Epoxy/release film/ other materials		€ 350	€ 200	€ 275	55%
+ Fixed manufacturing costs per 100 units		€ 8,420	€ 6,500	€ 7,460	26%
Manhours mold production		7	5	6	33%
Molds		€ 8,000	€ 6,250	€ 7,125	25%
+ Unit Manufacturing costs	€	€ 2,100	€ 1,350	€ 1,725	43%
Man hours fuselage and wing production		7	5	6	33%
Man hours assembly and integration		11	9	10	20%
Man hours integrating electronics		11	9	10	20%
Man hours finishing		6	4	5	40%
+ Development cost	€	€ 1,335,000.00	€ 1,059,000.00	€ 1,197,000	23%
Facilities		€ 55,000.00	€ 45,000.00	€ 50,000.00	20%
Project Preparation		€ 120,000.00	€ 90,000.00	€ 105,000.00	29%
Technical analysis		€ 150,000.00	€ 120,000.00	€ 135,000.00	22%
Design integration		€ 60,000.00	€ 42,000.00	€ 51,000.00	35%
Operation and production plan		€ 60,000.00	€ 42,000.00	€ 51,000.00	35%
Test phase		€ 645,000.00	€ 505,000.00	€ 575,000.00	24%
Wind tunnel testing		€ 275,000.00	€ 225,000.00	€ 250,000.00	20%
Prelimary testing		€ 130,000.00	€ 70,000.00	€ 100,000.00	60%
Man hour cost		€ 240,000.00	€ 210,000.00	€ 225,000.00	13%
Product roll out		€ 240,000.00	€ 210,000.00	€ 225,000.00	13%
+ Certifation		€ 5,000	€ 5,000	€ 5,000.00	0%
Aircraft produced		100	100	100	
Fixed production cost		€ 1,348,420	€ 1,070,500	€ 1,209,460	23%
Manufacturing		€ 8,420.00	€ 6,500.00	€ 7,460.00	26%
Development		€ 1,335,000	€ 1,059,000	€ 1,197,000	23%
Certification		€ 5,000	€ 5,000	€ 5,000	0%
Unit cost		€ 7,287	€ 5,419	€ 6,353	29%
Aircraft cost		€ 6,487	€ 4,619	€ 5,553	34%
Payload cost		€ 800	€ 800	€ 800	0%
Price per aircraft		€ 20,771	€ 16,124	€ 18,447	25%
Total investment		€ 2,077,070	€ 1,612,400	€ 1,844,735	
Price per km^2		€ 8.25	€ 5.63	€ 6.94	

Figure M.4: Second part of the cost estimation.

Appendix N

Electrical systems

N.1 Electrical block diagram

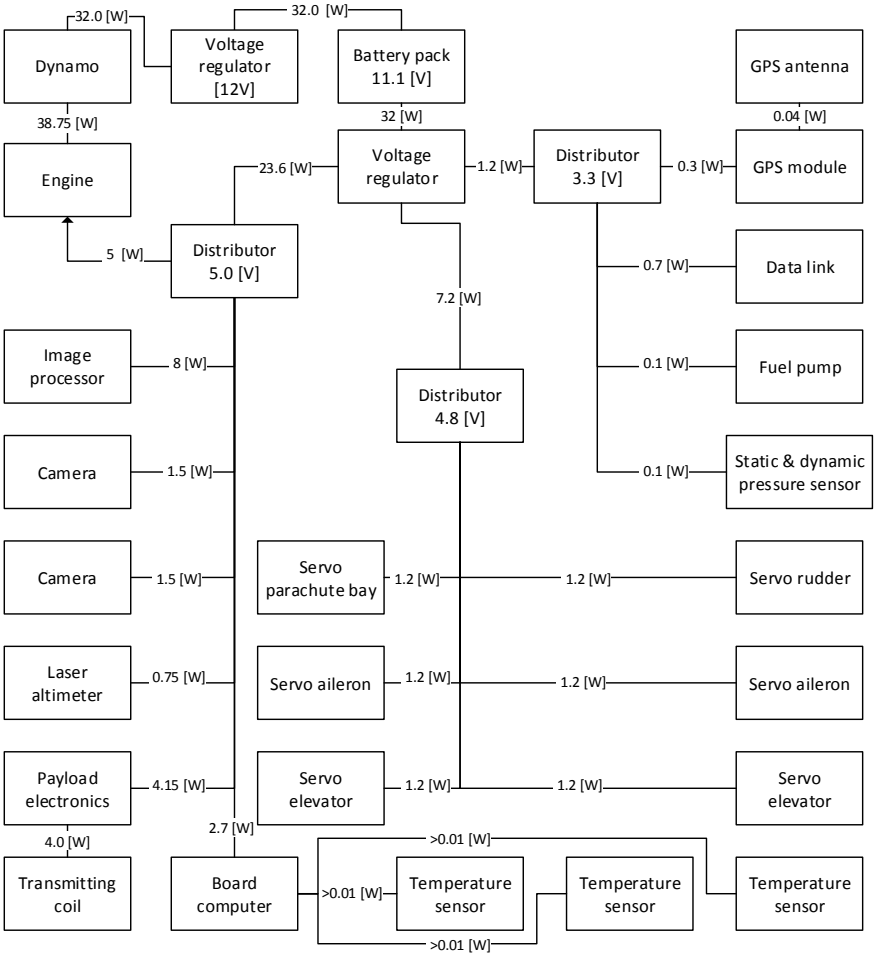

Figure N.1: The Electrical Block Diagram.

N.2 Communication flow

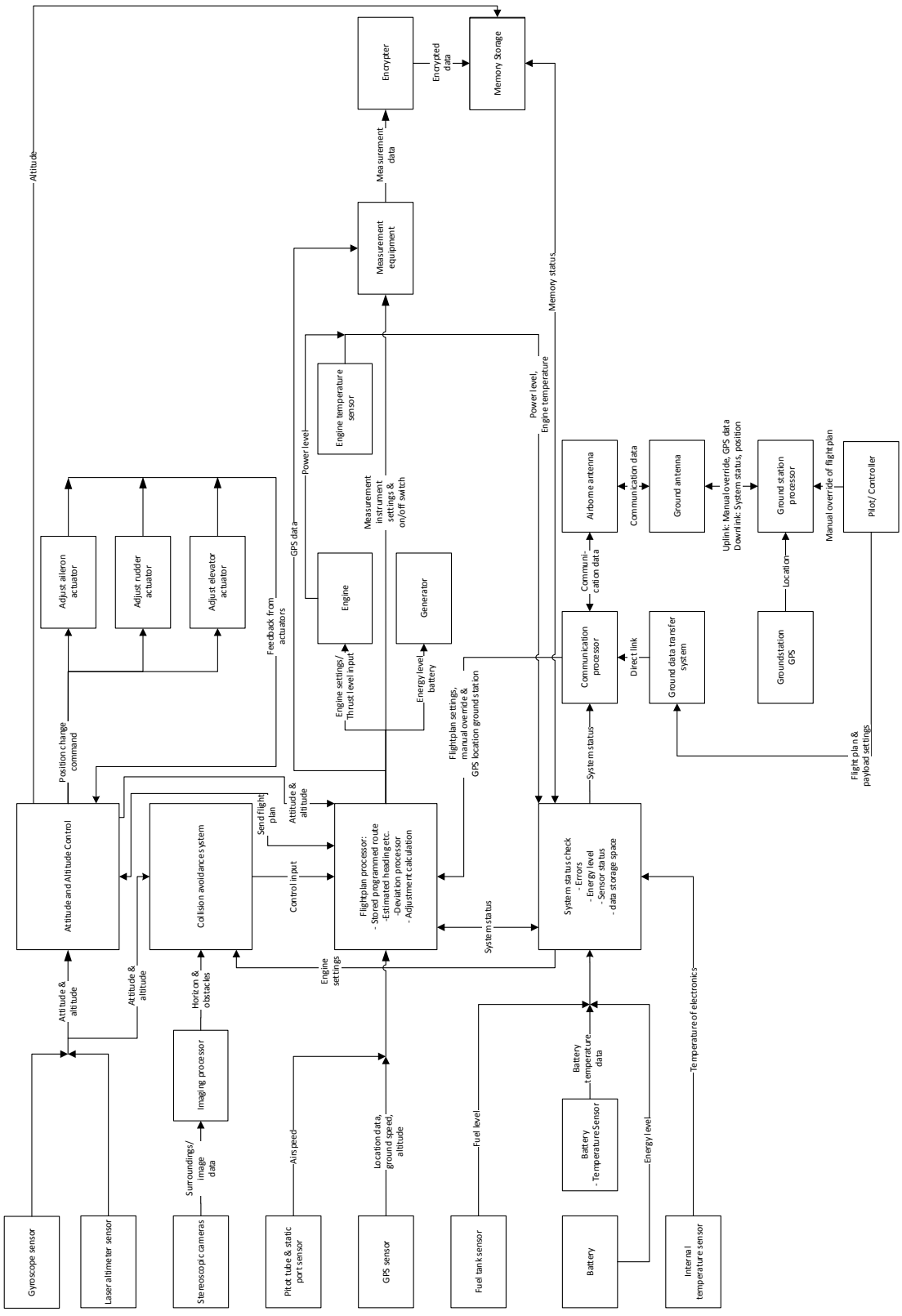

Figure N.2: Communication flow chart.

Appendix O

Project design & development logic

The steps that need to be taken in order to design and produce the final product and complete the entire project, can be found in figure O.1. This chart lists all steps, including the order and time in which they should be completed. The design and development logic breaks down the further development of the UAV into six parts, which form the top level of this breakdown. These six parts each contain several objectives, that form the second layer. The third and final layer contains the steps that need to be taken to complete the objectives. Some steps will be performed parallel. The complete structuring and scheduling can be found in the corresponding Gantt-chart. This can be found in figures O.2 and O.3.

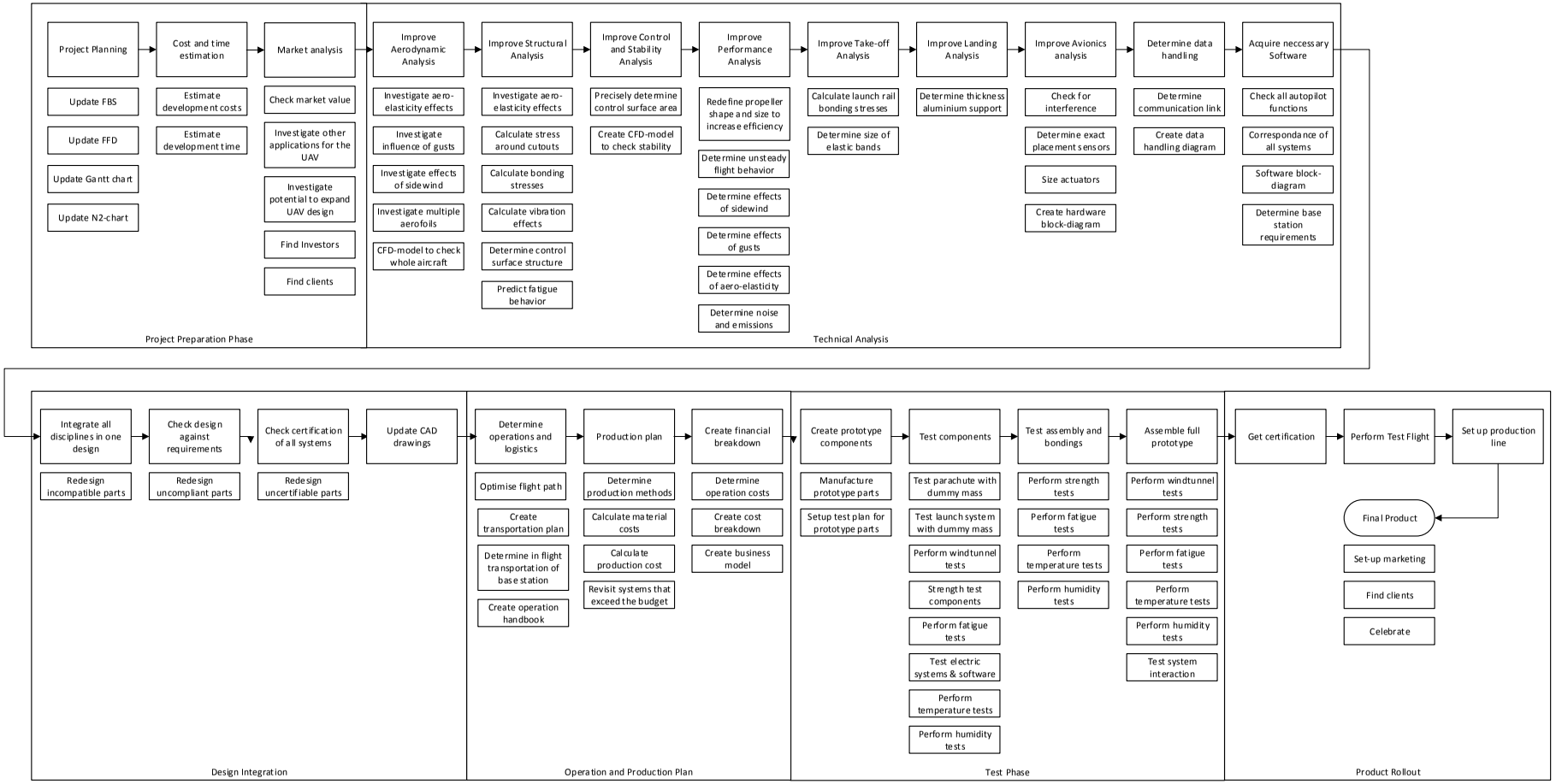

Figure O.1: Post-DSE design and development logic.

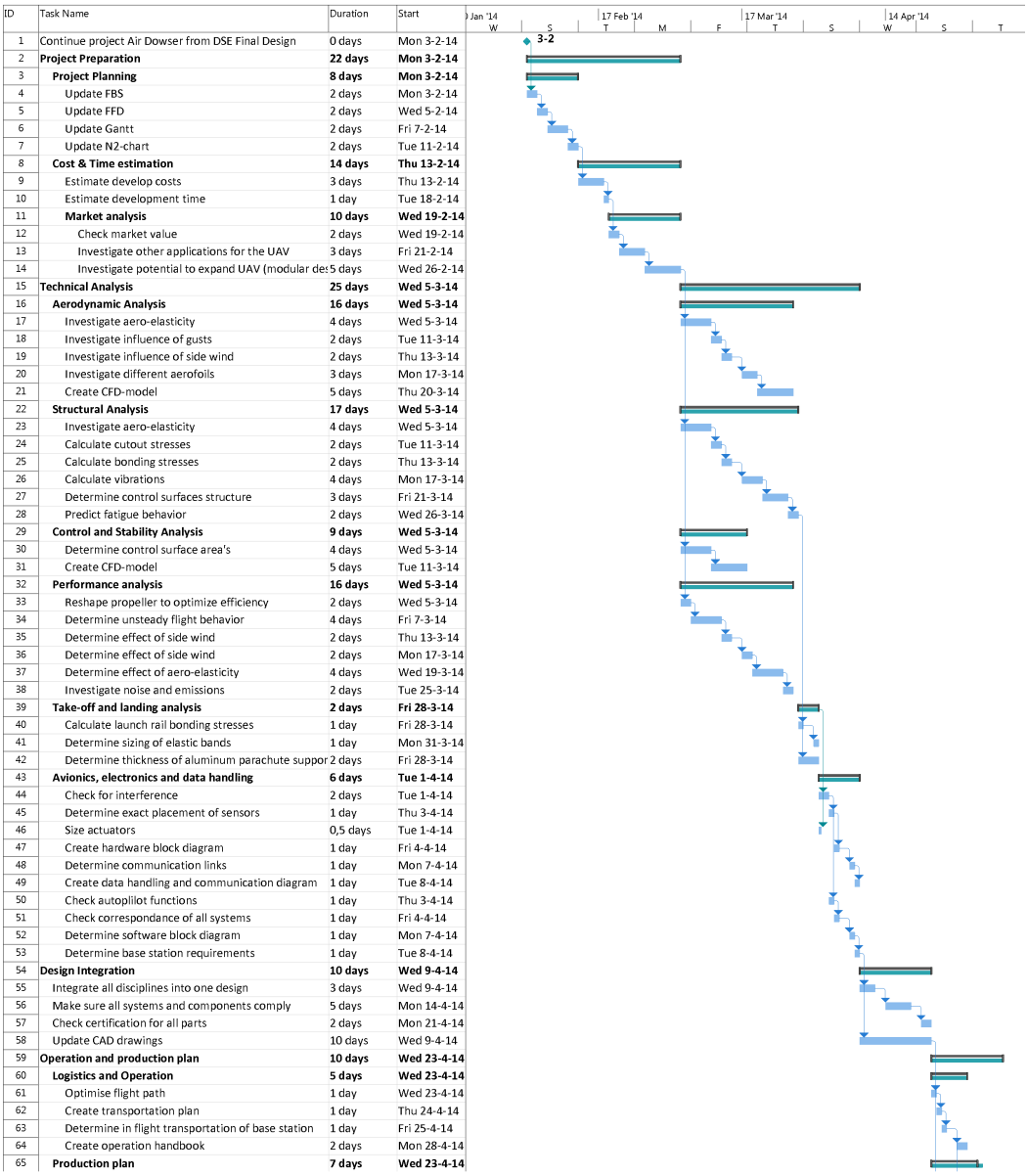

ID	Task Name	Duration	Start
1	Continue project Air Dowser from DSE Final Design	0 days	Mon 3-2-14
2	**Project Preparation**	**22 days**	**Mon 3-2-14**
3	**Project Planning**	**8 days**	**Mon 3-2-14**
4	Update FBS	2 days	Mon 3-2-14
5	Update FFD	2 days	Wed 5-2-14
6	Update Gantt	2 days	Fri 7-2-14
7	Update N2-chart	2 days	Tue 11-2-14
8	**Cost & Time estimation**	**14 days**	**Thu 13-2-14**
9	Estimate develop costs	3 days	Thu 13-2-14
10	Estimate development time	1 day	Tue 18-2-14
11	**Market analysis**	**10 days**	**Wed 19-2-14**
12	Check market value	2 days	Wed 19-2-14
13	Investigate other applications for the UAV	3 days	Fri 21-2-14
14	Investigate potential to expand UAV (modular des	5 days	Wed 26-2-14
15	**Technical Analysis**	**25 days**	**Wed 5-3-14**
16	**Aerodynamic Analysis**	**16 days**	**Wed 5-3-14**
17	Investigate aero-elasticity	4 days	Wed 5-3-14
18	Investigate influence of gusts	2 days	Tue 11-3-14
19	Investigate influence of side wind	2 days	Thu 13-3-14
20	Investigate different aerofoils	3 days	Mon 17-3-14
21	Create CFD-model	5 days	Thu 20-3-14
22	**Structural Analysis**	**17 days**	**Wed 5-3-14**
23	Investigate aero-elasticity	4 days	Wed 5-3-14
24	Calculate cutout stresses	2 days	Tue 11-3-14
25	Calculate bonding stresses	2 days	Thu 13-3-14
26	Calculate vibrations	4 days	Mon 17-3-14
27	Determine control surfaces structure	3 days	Fri 21-3-14
28	Predict fatigue behavior	2 days	Wed 26-3-14
29	**Control and Stability Analysis**	**9 days**	**Wed 5-3-14**
30	Determine control surface area's	4 days	Wed 5-3-14
31	Create CFD-model	5 days	Tue 11-3-14
32	**Performance analysis**	**16 days**	**Wed 5-3-14**
33	Reshape propeller to optimize efficiency	2 days	Wed 5-3-14
34	Determine unsteady flight behavior	4 days	Fri 7-3-14
35	Determine effect of side wind	2 days	Thu 13-3-14
36	Determine effect of side wind	2 days	Mon 17-3-14
37	Determine effect of aero-elasticity	4 days	Wed 19-3-14
38	Investigate noise and emissions	2 days	Tue 25-3-14
39	**Take-off and landing analysis**	**2 days**	**Fri 28-3-14**
40	Calculate launch rail bonding stresses	1 day	Fri 28-3-14
41	Determine sizing of elastic bands	1 day	Mon 31-3-14
42	Determine thickness of aluminum parachute suppor	2 days	Fri 28-3-14
43	**Avionics, electronics and data handling**	**6 days**	**Tue 1-4-14**
44	Check for interference	2 days	Tue 1-4-14
45	Determine exact placement of sensors	1 day	Thu 3-4-14
46	Size actuators	0,5 days	Tue 1-4-14
47	Create hardware block diagram	1 day	Fri 4-4-14
48	Determine communication links	1 day	Mon 7-4-14
49	Create data handling and communication diagram	1 day	Tue 8-4-14
50	Check autoplilot functions	1 day	Thu 3-4-14
51	Check correspondance of all systems	1 day	Fri 4-4-14
52	Determine software block diagram	1 day	Mon 7-4-14
53	Determine base station requirements	1 day	Tue 8-4-14
54	**Design Integration**	**10 days**	**Wed 9-4-14**
55	Integrate all disciplines into one design	3 days	Wed 9-4-14
56	Make sure all systems and components comply	5 days	Mon 14-4-14
57	Check certification for all parts	2 days	Mon 21-4-14
58	Update CAD drawings	10 days	Wed 9-4-14
59	**Operation and production plan**	**10 days**	**Wed 23-4-14**
60	**Logistics and Operation**	**5 days**	**Wed 23-4-14**
61	Optimise flight path	1 day	Wed 23-4-14
62	Create transportation plan	1 day	Thu 24-4-14
63	Determine in flight transportation of base station	1 day	Fri 25-4-14
64	Create operation handbook	2 days	Mon 28-4-14
65	**Production plan**	**7 days**	**Wed 23-4-14**

Figure O.2: Gantt chart for the detailed design phase.

ID	Task Name	Duration	Start
66	Determine production methods	2 days	Wed 23-4-14
67	Calculate material costs	1 day	Fri 25-4-14
68	Calculate manufacturing costs	1 day	Mon 28-4-14
69	Revisit systems that exceed budget	4 days	Tue 29-4-14
70	**Financial breakdown**	**7 days**	**Mon 28-4-14**
71	Determine operational costs	1 day	Mon 28-4-14
72	Create cost breakdown	1 day	Tue 29-4-14
73	Set up business model	5 days	Wed 30-4-14
74	**Testing Phase**	**50 days**	**Wed 7-5-14**
75	**Manufacture and test prototype parts**	**25 days**	**Wed 7-5-14**
76	Manufacture prototype parts	20 days	Wed 7-5-14
77	Create test plan for prototypes	10 days	Wed 7-5-14
78	Test parachute with dummy mass	2 days	Wed 4-6-14
79	Test launch system with dummy mass	2 days	Wed 4-6-14
80	Perform windtunnel tests	2 days	Wed 4-6-14
81	Strength test components	2 days	Wed 4-6-14
82	Test components on fatigue	5 days	Wed 4-6-14
83	Test electric systems and software	2 days	Wed 4-6-14
84	Perform temperature tests	5 days	Wed 4-6-14
85	Perform humidity tests	5 days	Wed 4-6-14
86	**Test bondings**	**5 days**	**Wed 11-6-14**
87	Strength test bondings	2 days	Wed 11-6-14
88	Test bondings on fatigue	5 days	Wed 11-6-14
89	Test bondings on temperature	5 days	Wed 11-6-14
90	Test bondings on humidity	5 days	Wed 11-6-14
91	**Test fully assembled prototype**	**20 days**	**Wed 18-6-14**
92	Assemble full prototype	5 days	Wed 18-6-14
93	Perform windtunnel tests	5 days	Wed 25-6-14
94	Perform strength tests	5 days	Wed 25-6-14
95	Perform fatigue tests	5 days	Wed 25-6-14
96	Perform temperature tests	5 days	Wed 25-6-14
97	Perform humidity tests	5 days	Wed 25-6-14
98	Test system interaction	5 days	Wed 25-6-14
99	**Final design achieved**	0 days	Wed 16-7-14
100	Confirm final design	10 days	Wed 2-7-14
101	**Product Rollout**	**50 days**	**Wed 16-7-14**
102	Certify Aircraft	10 days	Wed 16-7-14
103	Perform Test Flights	20 days	Wed 30-7-14
104	Set up production line	20 days	Wed 27-8-14
105	Set up marketing plan	5 days	Wed 27-8-14
106	**Sell to clients**	0 days	Wed 24-9-14

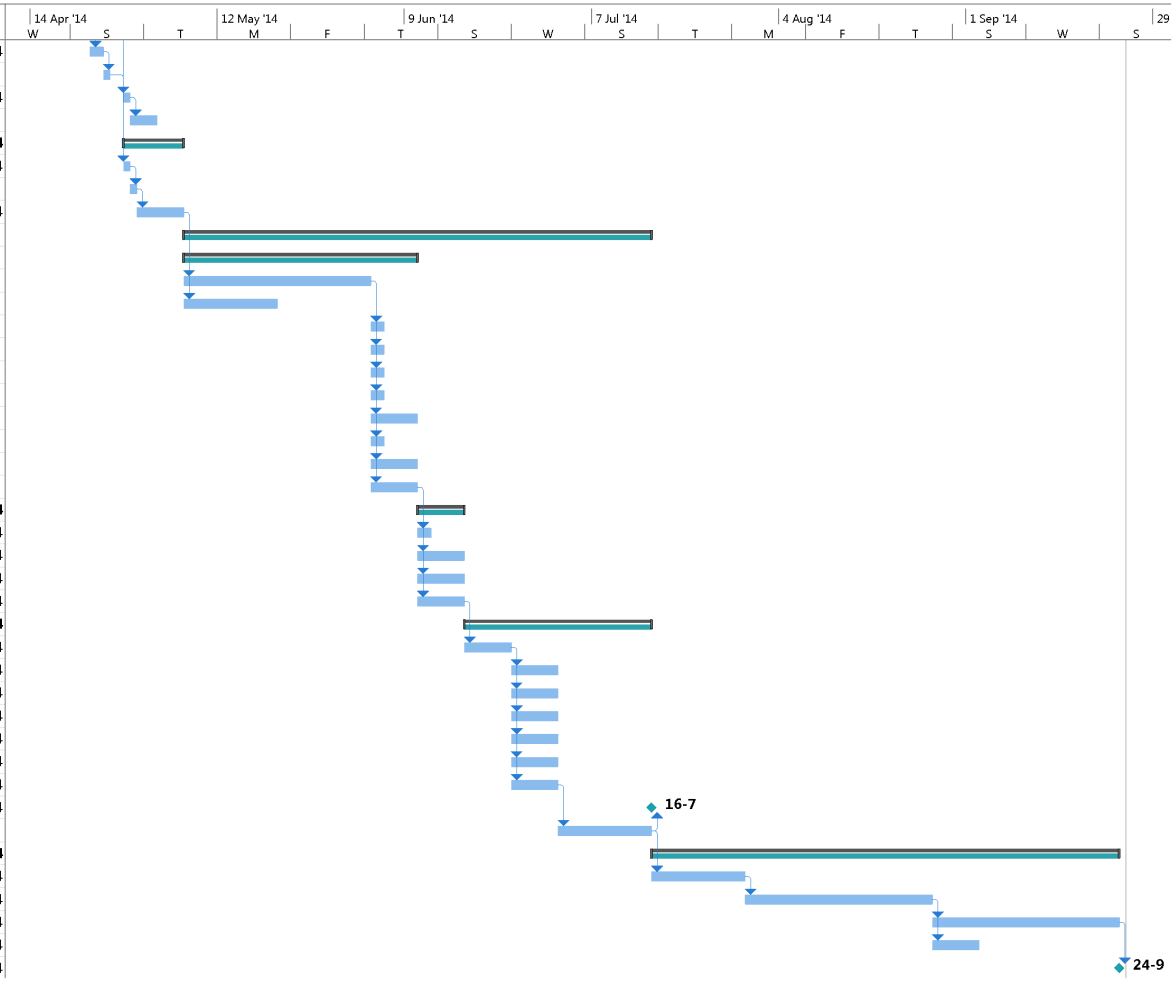

Figure O.3: Gantt chart for the detailed design phase.